TITLE:
PHYSICAL PROPERTIES OF SEMICONDUCTING AMORPHOUS SILICON CARBON ALLOY AND ITS APPLICATION TO ULTRA-THIN MULTILAYERS(Dissertation_全文)

AUTHOR(S):
Yoshimoto, Masahiro

CITATION:
Yoshimoto, Masahiro. PHYSICAL PROPERTIES OF SEMICONDUCTING AMORPHOUS SILICON CARBON ALLOY AND ITS APPLICATION TO ULTRA-THIN MULTILAYERS. 京都大学, 1988, 工学博士

ISSUE DATE:
1988-03-23

URL:
https://doi.org/10.14989/doctor.k3999

RIGHT:

京都大学学術情報リポジトリ
KURENAI 紅
Kyoto University Research Information Repository

1013 課

PHYSICAL PROPERTIES OF SEMICONDUCTING AMORPHOUS SILICON CARBON ALLOY AND ITS APPLICATION TO ULTRA-THIN MULTILAYERS

by

MASAHIRO YOSHIMOTO

December 1987

Department of Electrical Engineering
Kyoto University

PHYSICAL PROPERTIES OF SEMICONDUCTING AMORPHOUS SILICON CARBON ALLOY AND ITS APPLICATION TO ULTRA-THIN MULTILAYERS

by

MASAHIRO YOSHIMOTO

December 1987

Department of Electrical Engineering
Kyoto University

DOC
1987
7
電気系

To my family

ABSTRACT

This thesis describes the fundamental properties of hydrogenated amorphous silicon carbon alloys (a-$Si_{1-x}C_x$:H) and multilayers consisting of hydrogenated amorphous silicon (a-Si:H) and a-$Si_{1-x}C_x$:H. The main purpose of the present study is to obtain wide-gap amorphous semiconductors. The extension of the bandgap of amorphous semiconductors leads to a wide variety of electrical properties; this enables us to select optimum materials for design of amorphous semiconductor devices.

A-$Si_{1-x}C_x$:H films are deposited in a capacitive-coupling rf glow discharge chamber using SiH_4 and a hydrocarbon (mainly C_2H_4). Effects of both plasma conditions and substrate temperatures on the film formation of a-$Si_{1-x}C_x$:H are investigated using deposition rates of silicon and carbon atoms and in-situ optical emission spectroscopy (OES). The deposition rates of silicon and carbon atoms are calculated using the deposition rate, the density, and the hydrogen and carbon contents of the film. The decomposition of C_2H_4 is reduced in C_2H_4-rich gas compositions; this causes an increase in the average number of hydrogen atoms attached to a carbon atom detected by infrared absorption (IR) measurements. When the source gas is diluted with H_2 by a factor of 10, the decomposition of C_2H_4 is enhanced measured by OES, and the excess hydrogenation of carbon atoms is reduced. On the basis of these results, substitutional doping for n-type is achieved in a-$Si_{0.6}C_{0.4}$:H.

The control of the optical energy gap (E_{opt}) is the most important feature of a-$Si_{1-x}C_x$:H alloys. The value of E_{opt} is controlled over the range from 1.8 eV to 4.2 eV by changing the carbon content of the film. The wide optical energy gap is thought to be due to the excess hydrogenation of carbon atoms. Bright visible photoluminescence is observed. The luminescence mechanism is discussed with the aid of electron spin resonance measurements. Electroluminescence (EL) is observed in an AC-EL

device. The emission mechanism in the device is elucidated.

A-Si:H/a-$Si_{1-x}C_x$:H multilayers (x=0.2, 0.5 and 0.8) are fabricated by alternative deposition of the barrier layers of a-$Si_{1-x}C_x$:H (20-40 Å thick) and the well layers of a-Si:H (11-510 Å). The construction of the multilayers is confirmed by X-ray diffraction and a depth profile of Auger electron spectroscopy. Hydrogen incorporation in the well layer is investigated using IR measurements. Hydrogen atoms are incorporated as Si-H_2 dihydride bonds at the beginning of the deposition, and Si-H monohydride bonds are formed above 40 Å for the well-layer thickness. Up to 100 Å, the Si-H_2 dihydride bonds are dominant rather than the Si-H monohydride bonds. The low-packed structure of a-$Si_{1-x}C_x$:H (especially x=0.8) may cause a low-packed defective structure of very thin well layers (<20 Å) in the multilayers. The optical energy gap of the multilayers is affected by the configuration of hydrogen incorporation into the well layer.

Generation of hot electrons in the a-Si:H/a-$Si_{0.2}C_{0.8}$:H multilayer with an n-type well layer is verified using a newly devised structure. Above the applied voltage where tunneling current starts to flow through the buffer layer of a-Si:H with 50 Å thickness, hot electron injection occurs; this is important for the application of the multilayer to a wide-gap injector. In the a-Si:H/a-$Si_{0.2}C_{0.8}$:H multilayer with a p-type well layer, space charge limited conduction is dominant.

ACKNOWLEDGEMENTS

It would be impossible for me to fully express my indebtedness and gratitude to Prof. Hiroyuki Matsunami. During the six years, he has been a guiding spirit of lasting patience as well as an advisor of deep understanding. As supervisor of this thesis, he has been of constant encouragement. For all this, I am very grateful.

I am thankful to Prof. Akira Kawabata for his careful review of my manuscript and for the valuable comments that he made. I also acknowledge Prof. Akio Sasaki for his useful suggestions and criticism on the manuscript.

I am very indebted to Prof. Junji Saraie (Kyoto Institute of Technology) and Assoc. Prof. Sigehiro Nishino (Kyoto Institute of Technology), who introduced me to various aspects of semiconductor engineering. I also wish to thank Dr. Takashi Fuyuki for his advice during the experiments and discussions.

I would like to acknowledge Prof. Shoji Nitta (Gifu University) for his assistance on ESR measurements. I wish to thank Assoc. Prof. Kai-Ying Du (Sichuan University, China) for her assistance on the electrical measurements of the amorphous multilayer. Experiments in this study were also partly assisted by the use of facilities at Takagi Laboratory, Kawabata Laboratory and Sasaki Laboratory.

This work has been aided by the assistance and hard work of a number of former and recent students in Matsunami Laboratory. I wish to thank Mr. Kouji Tominaga for his assistance in fabrication of the electroluminescent cells. I wish to thank Messrs. Naotaka Kaneda, Masahiro Yamaguchi and Masanori Ochi for their collaborative work in early experiments on the multilayer. Special thanks are due to Mr. Kouichi Aizawa (Matsushita Electric Works Inc.) and Mr. Tsunenobu Kimoto for co-operation on various experiments in plasma diagnosis. I am also very thankful to Mr. Kentaro Shibahara and other colleagues for their stimulating discussions.

CONTENTS

I. Introduction

For many years it had been taken to be a fundamental fact that amorphous semiconductors could not be substitutionally doped.[1] This fact had been a serious limitation on applications of amorphous semiconductors to solid-state electronics. However, in 1975, Spear and LeComber[2,3] demonstrated that hydrogenated amorphous silicon (a-Si:H) prepared by a glow discharge method could be doped both n-type and p-type. The dark conductivity could be controlled in a remarkably wide range over ten orders of magnitude by substitutional doping in the gas phase. This work has opened up new areas of theoretical and experimental studies.[4]

Amorphous materials can be deposited very easily as a form of a thin film: Those materials are inherently free from the expense of crystal perfection. Thus, a major effort has been expended toward applications of a-Si:H to solar cells, thin-film transistors and image sensors.[5]

The controllability of the bandgap leads to a wide variety of electrical and optoelectronic properties in semiconductors; this enables investigators to select optimum materials for design of electronic devices. Multilayers fabricated by alternative deposition of a narrow-gap semiconductor and a wide-gap semiconductor are expected to exhibit unique physical properties, when the thickness of the component layer of the multilayer is less than scores times of bond lengths (less than about 100 Å).

In this thesis, hydrogenated amorphous silicon carbon (a-$Si_{1-x}C_x$:H) is taken as an example for bandgap control in amorphous semiconductors. Their structures and physical properties are investigated in connection with deposition conditions. On the basis of these results, multilayers consisting of a-$Si_{1-x}C_x$:H and hydrogenated amorphous silicon (a-Si:H) are

designed in order to examine the probability of atom-sized control of amorphous structures. Their optical and electrical properties are investigated.

Since a-$Si_{1-x}C_x$:H prepared by a glow discharge technique (GD) was first reported by Anderson and Spear,[6] it has been widely accepted that the optical energy gap (E_{opt}) of a-$Si_{1-x}C_x$:H is controlled in the visible-wavelength region by changing the carbon content of the film.[7-9] Moreover, a-$Si_{1-x}C_x$:H shows bright luminescence at 77K[10] and room temperature.[11-16] Thus, there have been considerable interests regarding wide possible applications to optoelectronic devices such as efficient solar cells[17] and large-area display devices.[18,19] In electrophotography,[5] this material is used as an insulating top layer in a photoreceptor. New experiments are now under way to make use of this material as a wide-gap emitter in a crystalline silicon transistor[20] and as a light-activated charge storage device.[21] There have also been interests in the application to protective and anti-wear coatings because of its high hardness.[22-26]

It is generally known that incorporation of hydrogen into tetrahedral amorphous semiconductors saturates dangling bonds and removes states in the gap related to them. Infrared absorption spectra (IR) of a-$Si_{1-x}C_x$:H films made by GD from SiH_4 and C_2H_4 were investigated in detail.[27] It was found that only one hydrogen atom was bonded to a silicon atom and hydrogen was bonded to carbon predominantly in CH_2 and CH_3 forms. Films deposited from SiH_4 and CH_4 was also thought to be a polymer-like material.[28] Nuclear magnetic resonance measurements (NMR) for a-$Si_{1-x}C_x$:H indicated that hydrogen was incorporated in the form of heavily hydrogenated carbon clusters embedded in a weakly hydrogenated a-Si network in the films deposited by GD or a reactive sputtering method (SP).[29] In another work, it was believed that a gathered phase of Si-H_n also existed.[30] Amounts

of incorporated hydrogen into films made by SP were first estimated using a nuclear reaction.[31,32] By combining the NMR and IR,[30] or the nuclear reaction method and IR,[33] the oscillator strength of the C-H stretching mode in IR spectra was estimated for the films deposited by GD with the aid of the known oscillator strength of the Si-H stretching mode. Since then, amounts of hydrogen attached to silicon and carbon have been evaluated separately using simple IR measurements.

Dangling bonds in unhydrogenated a-$Si_{1-x}C_x$ had already been discussed in connection with the surface of crystalline SiC.[34] The spin density measured by electron spin resonance (ESR) increased with the carbon content in films deposited by GD or SP.[35,36] The reason for the increase in the spin density was thought to be that dangling bonds were produced in order to relax a local strain owing to the difference in the covalent bond lengths between silicon (1.17 Å) and carbon (0.772 Å).[37] The relaxation of the local strain was observed by Raman spectroscopy.[38] In addition, the incorporated hydrogen in the form of the gathered phase[29,30] as mentioned above might not contribute to the decrease in the spin density.[37,39] Theoretical studies on g-values of ESR signals were also reported.[40,41]

On the basis of optical absorption and dc conductivity, Anderson et.al first suggested that a fraction of the carbon atoms in a-$Si_{1-x}C_x$:H might tend to form a three-fold coordinated graphite-like local environment.[6] The graphite-like phase was first investigated for films deposited by SP. Hitachi group[42,43] measured the quantities reflecting electronic structure averaged over several bond lengths (i.e., the atomic density detected by X-ray photoemission spectroscopy: XPS, and E_{opt}). They also measured the quantities reflecting more local environments (i.e., the chemical shifts of core-electron levels detected by XPS, and the hydrogen evolution characteristics).[42,43] The carbon-content dependences of these

properties had similar breaks at the carbon content of 0.4-0.5 in the films deposited by SP. All of these properties seemed to originate from the change in chemical-bonding structures in a-$Si_{1-x}C_x$:H, i.e., the transition from diamond-like four-fold coordination in the silicon-rich region to graphite-like tree-fold coordination in the carbon-rich region. Raman spectra[44] of carbon-rich films deposited by SP also indicated the presence of a structure similar to glassy carbon[45] composed of graphite-like microcrystals.

In a recent work,[46] graphite-like carbon was detected in a-$Si_{1-x}C_x$:H ($0.088<x<0.66$) films deposited by GD using electron energy loss spectroscopy (EELS). It was pointed out that the type of carbon bonding had a dominant effect on the electronic properties of this material even in silicon-rich samples prepared by GD.[47,48] Under plasma conditions of either high rf power or high pressure, more energetic ion bombardment against depositing films was presumed to occur,[49] which would break C-H bonds.[50] And carbon atoms came to bond in a graphite-like structure.[47]

At present, silicon-rich a-$Si_{1-x}C_x$:H ($x<0.2$) proves successful in the application to solar cells. Improvement in conversion efficiency was achieved for a p-i-n type solar cell where the p-layer was boron-doped a-$Si_{1-x}C_x$:H ($x<0.2$, $E_{opt}\simeq 1.9$ eV) in stead of p-type a-Si:H ($E_{opt}<1.8$ eV).[17,51] This result is explained that short-wavelength light can reach the active i-layer through the wide-gap a-$Si_{1-x}C_x$:H layer efficiently.[17] In this silicon-rich a-$Si_{1-x}C_x$:H, several electronic studies have been carried out. The comparison between the Fermi level detected by XPS and the activation energy of electrical conductivity showed that the hole transport in p-type a-$Si_{1-x}C_x$:H films did not take place at the valence band edge but at the band tail[52] as well in p-type a-Si:H.[53] The valence-band discontinuity at the interface between a-Si:H and a-$Si_{1-x}C_x$:H was evaluated by ultraviolet photoemission spectroscopy (UPS)[54] or XPS.[55] A

compositional-grading p-type a-$Si_{1-x}C_x$:H was fabricated in order to improve electronic characteristics at the p/i interface in a p-i-n solar cell.[56] To avoid bombardment by charged particles during deposition, a-$Si_{1-x}C_x$:H ($x<0.2$) was deposited by photochemical vapor deposition[57] and applied to solar cells.[58]

There has been an obstacle to applications of carbon-rich a-$Si_{1-x}C_x$:H ($x>0.2$) to electronic devices. Increase in the carbon content results in poor electrical properties: In carbon-rich films, substitutional doping has never been achieved. The configuration of incorporated carbon atoms in a-$Si_{1-x}C_x$:H has been thought to be not only four-fold coordinated carbon atoms with a diamond-like structure, but also the polymeric phase and the graphite-like phase as mentioned above. The absence of steric constraints in the multiphase material could allow the normal valencies of any impurity atom to be completely satisfied. Thus, the ordinary mechanism for introducing extra electrons or holes into a solid could be tremendously impeded.

The most common method for deposition of a-$Si_{1-x}C_x$:H is GD as well for a-Si:H.[59] There have also been fundamental studies on this material deposited by SP using a polysilicon-graphite target,[30,37,42,43] or a graphite target and SiH_4,[44] or a polysilicon target and CH_4.[7,31,32,60] Films which were applied to electronic devices were prepared by GD.[17,18,20,51] It should be noted that films which showed bright luminescence were deposited by GD.[10-16] In GD, an rf electric field is used to produce a plasma containing ions and other reactive species from monosilane (SiH_4) and a hydrocarbon (including organic silane): CH_4,[14,17,28,37,46,47,52,61,62] C_2H_4,[6,10,12,27,50,62] C_2H_2,[29,35] $Si(CH_3)_4$ (tetramethylsilane: TMS),[12] or $Si_2H_2(CH_3)_4$ (tetramethyldisilane :TMDS).[63] For the deposition of silicon-rich films ($x<0.2$), CH_4 is usually used.[17] These reactive species are deposited on a heated substrate (typically 200°C-300 °C) to form a-$Si_{1-x}C_x$:H. In order to obtain specific properties

of films, deposition conditions are empirically controlled by changing deposition parameters: rf power, pressure, flow rate of both a source gas and a dilution gas, and apparatus geometry. Compared with the deposition of a-Si:H, the plasma condition to be controlled becomes complicated because of the difference in the dissociation rates between silane and a hydrocarbon in an electrical discharge. At present, very little is known about the relation between film properties and deposition conditions. There has been the only study on gas-phase reactions in an rf glow discharge of CH_4-SiH_4-He atmosphere using mass spectroscopic measurements.[61] In recent works, hydrogen atmosphere plays an important role in improvement of optoelectronic properties in films[62] and microcrystallization of films.[64] In order to acquire carbon-rich a-$Si_{1-x}C_x$:H which can be substitutionally doped, it is necessary to control film structures, especially the configuration of carbon incorporation.

In recent years, there has been interest in multilayers consisting of a-Si:H and silicon based ternary alloys, e.g. a-SiN_x:H,[65-67] a-$Si_{1-x}C_x$:H,[68-70] and a-$Si_{1-x}Ge_x$:H[71,72] because of their unique optical[65-69] and electrical[65,66,70-72] properties. In multilayers with very thin layers, E_{opt} of the multilayers increased with the decreasing thickness of well layers, which was insisted to be due to a quantum size effect.[65-69] There is also information in the literature on the electrical properties along multilayer planes; the Fermi level in the a-Si:H well layers are raised by charge transfer doping of electrons from the barrier layers (a-SiN_x:H).[65,66] Regarding a-Si:H/a-$Si_{1-x}C_x$:H multilayer systems, they have already been applied to solar cells in order to improve p-type window layers.[70] In this thesis, attention is paid mainly to the generation of hot electrons in a-Si:H/a-$Si_{1-x}C_x$:H multilayers as an example of design for amorphous ultra-thin multilayers. Hot

electrons are expected to be generated by tunneling conduction through the barrier layer of wide-gap a-$Si_{1-x}C_x$:H in an a-Si:H/a-$Si_{1-x}C_x$:H multilayer as shown in Fig. 1.1. This multilayer can

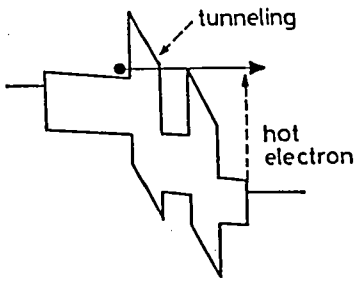

Fig. 1.1. Generation of hot electrons in a a-Si:H/a-$Si_{1-x}C_x$:H multilayer.

be used as a hot electron injector or a wide gap injector. In order to obtain multilayers with specific properties, it is important to control the structures of the component layers and the interfaces. However, very little is known about these microscopic structures in the multilayers, e.g. hydrogen incorporation in the component layers and the interfacial structures.

In the first half of this thesis, the deposition mechanism of a-$Si_{1-x}C_x$:H and a-Si:H is described. The deposition mechanism and physical properties of a-$Si_{1-x}C_x$:H are investigated over a wide-range of the carbon contents of films. In the second half of this thesis, the fabrication of a-Si:H/a-$Si_{1-x}C_x$:H multilayers is described. The atom-sized microscopic structures and physical properties of these multilayers are investigated. Finally, the conduction mechanism of electrons and holes in the multilayers are described.

In Chapter II, effects of plasma conditions, substrate temperatures, and hydrogen dilution of source gases on the film formation of a-$Si_{1-x}C_x$:H are investigated using the deposition rates of silicon and carbon atoms and in-situ optical emission spectroscopy (OES). The configuration of hydrogen incorporation in a-$Si_{1-x}C_x$:H is investigated using IR spectroscopy. The effects of hydrogen dilution in the source gases on the hydrogenation of carbon atoms are described. Under a nearly-optimum deposition condition that a hydrocarbon is efficiently decomposed, substitutional doping for n-type is successfully carried out in a-$Si_{0.6}C_{0.4}$:H. In Chapter III, the relation between the volume density of dangling bonds and deposition conditions is described on the basis of the results of ESR. The dependence of E_{opt} on deposition conditions is discussed. The relations between deposition conditions and luminescence properties are also described. Capability for the application of a-$Si_{1-x}C_x$:H to light emitting devices is proved by a fabrication of electro-luminescence devices. In Chapter IV, hydrogen incorporation into the well layer of a-Si:H/a-$Si_{1-x}C_x$:H multilayers is investigated by Fourier transform infrared measurements (FTIR). The optical energy gap of the multilayers is also discussed in connection with incorporation of hydrogen into the well layer. Chapter V describes the generation of hot electrons by tunneling conduction through the barrier layers in a-Si:H(n-type)/a-$Si_{1-x}C_x$:H multilayers, experimentally. Electrical conduction in multilayers with p-type a-Si:H layers are also discussed. Finally, conclusions of the present study are summarized in Chapter VI.

References

1) N.F.Mott: Philos.Mag. **19** (1969) 835.

2) W.E.Spear and P.G.LeComber: Solid State Commun. **17** (1975) 1193.

3) W.E.Spear and P.G.LeComber: Philos.Mag. **33** (1976) 935.

4) J.I.Pankov (editor):"Semiconductor and Semimetals: Hydrogenated Amorphous Silicon" (Academic press, New York, 1984) Part A-C.

5) Ref.4 Part D.

6) D.A.Anderson and W.E.Spear: Philos. Mag. **35** (1977) 1.

7) M.Le Contellec, J.Richard, A.Guivarc'h, E.Ligeon and J.Fontenille: Thin Solid Films **58** (1979) 407.

8) R.Sussmann and R.Ogden: Philos. Mag. **44** (1981) 137.

9) Y.Catherline, G.Turban and B.Grolleau: Thin Solid Films **76** (1981) 23.

10) D.Engemann, R.Fisher and J.Knecht: Appl.Phys.Lett. **32** (1978) 567.

11) H.Munekata, Sh. Murasato and H.Kukimoto: Appl.Phys.Lett. **37** (1980) 536.

12) R.S.Sussmann and R.Ogden: Philos. Mag. B **44** (1981) 137.

13) E.Nakazawa, H.Munekata and H.Kukimoto: Solid State Commun. **45** (1983) 925.

14) I.Watanabe, Y.Hata, A.Morimoto and T.Shimizu: Jpn. J. Appl. Phys. **21** (1982) L613.

15) B.Rauscher and B.Bullemer: Phys. Stat. Sol. **79** (1983) 161.

16) S.P.Depinna and B.C.Cavanett: Philos. Mag. B **47** (1983) L51.

17) Y.Tawada, K.Tsuge, M.Kondo, H.Okamoto and Y.Hamakawa: J.Appl.Phys. **53** (1982) 5273.

18) H.Munekata and H.Kukimoto: Appl.Phys.Lett. **42** (1983) 432.

19) D.Kruangam, T.Endo, W.Guang-Pu, H.Okamoto and Y.Hamakawa: Jpn.J.Appl.Phys. **24** (1985) L806.

20) K.Sasaki and S.Furukawa: Ext. Abs. 18th Int'l Conf. Solid State Devices & Materials, Tokyo, 1986, (Jpn.Soc.Appl. Phys., Tokyo, 1986) p.291.
21) R.Koenenkamp and S.M.Paasche: Appl. Phys. Lett. **49** (1986) 268.
22) H.Yoshihara, H.Mori and M.Kiuchi: Thin Solid Films **76** (1981) 1.
23) A.Sathyamoorthy and W.Weisweiler: Thin Solid Films **87** (1982) 33.
24) D.R.McKenzie, N.Savvides, D.R. Mills and R.C.McPhedran: Solar Energy Materials **9** (1983) 113.
25) J.P.Gerault, T.Morancho and G.Constant: Thin Solid Films **101** (1983) 83.
26) C.Y.Chang, Y.K.Fang, C.F.Huang and B.S.Wu: J. Electrochem. Soc. **132** (1985) 418.
27) H.Wieder, M.Cardona and C.R.Guarnieri: Phys. Stat. Sol. B **92** (1979) 99.
28) Y.Catherine and G.Turban: Thin Solid Films **60** (1979) 193.
29) J.A.Reimer, R.W.Vaughan, J.C.Knights and R.A.Lujan: J.Vac. Sci. Technol. **19** (1981) 53.
30) K.Nakazawa, S.Ueda, M.Kumeda, A.Morimoto and T.Shimizu: Jpn. J. Appl. Phys. **21** (1982) L176.
31) A.Guivarc'h, J.Richard, M.Le Contellec, E.Ligeon and J.Fontenille: J. Appl. Phys. **51** (1980) 2167.
32) E.Ligeon, A.Guivarc'h, J.Fontenille, M.Le Contellec, R.Danielou and J.Richard: Nuclear Instruments and Methods **168** (1980) 499.
33) F.Fujimoto, A.Ootuka, K.Komaki, Y.Iwata, I.Yamane, H.Yamashita, Y.Hashimoto, Y.Tawada, K.Nishimura, H.Okamoto and Y.Hamakawa: Jpn.J.Appl.Phys. **23** (1984) 810.
34) M.H.Brodsky and R.S.Title: Phys. Rev. Lett. **23** (1969) 581.
35) P.J.Gaczi and D.C.Booth: Solar Energy Materials **4** (1981) 279.

36) A.Morimoto, T.Miura, M.Kumeda and T.Shimizu: Jpn. J. Appl. Phys. **21** (1982) L113.

37) A.Morimoto, T.Miura, M.Kumeda and T.Shimizu: J. Appl. Phys. **53** (1982) 7299.

38) A.Morimoto, S.Oozora, M.Kumeda and T.Shimizu: Solid State Commun. **47** (1983) 773.

39) T.Shimizu: Proc. 10th Int. Conf. Amorphous & Liquid Semiconductors, Tokyo, 1983:J.Non-Cryst. Solids **59/60** (1983) 117.

40) N.Ishii, M.Kumeda and T.Shimizu: Solid State Commun. **41** (1982) 143.

41) G.Lucovsky and S.Y.Lin: AIP Conf. Proc. No.120 Optical Effects in Amorphous Semiconductors. International Topical Conference, Snowbird (USA) 1984, p.55.

42) T.Shimada, Y.Katayama and K.F.Komatsubara: J. Appl. Phys. **50** (1979) 5530.

43) Y.Katayama, T.Shimada and K.Usami: Phys. Rev. Lett. **46** (1981) 1146.

44) Y.Inoue, S.Nakashima and A.Mitsuishi: Solid State Commun. **48** (1983) 1071.

45) M.I.Nathan, J.E.Smith Jr, and K.N.Tu: J.Appl.Phys.**45** (1974) 2370.

46) D.R.McKenzie, S.D.Berger and L.M.Brown: Solid State Commun. **59** (1986) 325.

47) A.H.Mahan B.von Roedern, D.L.Williamson and A.Madan: J.Appl. Phys. **57** (1985) 2717.

48) B.G.Yacobi B.von Roedern, A.H.Mahan and K.M.Jones: Phys. Rev. B **31** (1985) 8257.

49) L.Holland and S.M.Ojha: Thin Solid Films **58** (1979) 109.

50) Y.Catherine, A.Zamouche, J.Bullot and M.Gauthier: Thin Solid Films **109** (1983) 145.

51) Y.Tawada: "Amorphous Semiconductor Technologies & Devices (JARECT Vol.10)" (OHM, Tokyo, North-Holland, Amsterdam,

1983) p.148.
52) N.Fukada, Y.Fukushima, T.Imura and A.Hiraki: Jpn. J. Appl. Phys. **22** (1983) L745.
53) B von Roedern, L.Ley, M.Cardona and F.W.Smith: Philos.Mag. B **40** (1979) 433.
54) F.Evangelisti, P.Fiorini and C.Giovannela: Appl. Phys. Lett **44** (1984) 764.
55) T.Hayashi, S.Miyazaki, and M.Hirose: Ext. Abs. 19th Conf. Solid State Devices & materials (Jpn. Soc. Appl. Phys., Tokyo, 1987) p.223.
56) K.S.Lim, M.Konagai and K.Takahashi: J.Appl.Phys. **56**(1984) 538.
57) T.Inoue, T Tanaka, M.Konagai, and K.Takahashi: Appl.Phys.Lett. **44** (1984) 871.
58) H.Takei, T.Tanaka, W.Y.Kim, M.Konagai, and K.Takahashi: J.Appl.Phys. **58** (1985) 3664.
59) E.Carlson: 'Solar Cells' in ref.5 p.7.
60) N.Saito: J. Appl. Phys. **58** (1985) 3504.
61) Y.Cahterine, G.Turban and B.Grolleau: Thin Solid Films **76** (1981) 23.
62) A.Matsuda, Y.Yamaoka, S.Wolff, M.Koyama, Y.Imanishi, H.Kataoka, H.Matsuura and K.Tanaka: J. Appl. Phys. **60** (1986) 4025.
63) H.Koinuma, M.Funabashi, K.Kishino, M.Kawasaki, T.Hirano, and K.Fueki: Jpn.J.Appl.Phys. **25** (1986) 1811.
64) Y.Fujii, A.Hatano, A.Suzuki, M.Yoshida and S.Nakajima: J. Appl. Phys. **61** (1987) 1657.
65) B.Abels and T.Tiedje : Appl. Phys. Lett. **45** (1984) 179.
66) N.Ibaraki and H.Fritzche : Phys. Rev. B **30** (1984) 5761.
67) M.Hirose an S.Miyazaki: J.Non-Cryst.Solids **66** (1984) 327.
68) H.Munekata and H.Kukimoto : Jpn. J. Appl. Phys. **22** (1983) L544.
69) T.Tiedje, B.Abels, P.D.Person, B.G.Brooks and G.D.Cody:

J.Non-Cryst.Solids **66** (1984) 345.

70) S.Tsuda, H.Tarui, T.Matsuyama, T.Takahama, S.Nakayama, Y.Hishikawa, N.Nakamura, T.Fukatsu, M.Ohnishi, S.Nakano and Y.Kuwano, Jpn.J.Appl.Phys. **26**, (1987) 28.

71) H.Shirai, A.Tanabe, S.Oda, J.Hanna, T.Nakamura and I.Shimizu: Appl.Phys. **A41** (1986) 259.

72) C.R.Wronski, P.D.Persons and B.Abels: Appl.Phys.Lett. **49** (1986) 569.

II GLOW DISCHARGE DEPOSITION OF a-$Si_{1-x}C_x$:H FILMS

2-1. Introduction

A glow-discharge technique has generally been taken to be important for the fabrication of semiconductor devices: plasma etching and deposition of passivating films.[1] In addition to these, success in device applications of hydrogenated amorphous silicon (a-Si:H) has been achieved based on this technique,[2] because the volume density of dangling bonds and the corresponding density of localized states in the gap are low compared with unhydrogenated amorphous silicon prepared by conventional sputtering or evaporation.[3]

Thin-film specimens of a-Si:H are formed by decomposing silane, generally SiH_4, in a reaction chamber (typically 0.1-1 Torr). The plasma in the reaction chamber is maintained by capacitive- or inductive-coupling of rf power into the source gas.[4] In order to obtain specific properties of a-Si:H, deposition conditions are empirically controlled by changing deposition parameters: rf power, pressure, gas flow rate of both a source gas and a dilution gas, and apparatus geometry.

It is generally known that incorporation of hydrogen into a-Si:H saturates dangling bonds and removes states in the gap related to them. It should be noted that a-Si:H with less than 10 at.% hydrogen shows excellent optoelectronic properties and has already been applied to active devices.[10] Poor electrical properties are shown in a-Si:H with more than about 10 at.% hydrogen (usually prepared at low substrate temperature[11]). When the hydrogen content comes to more than about 30 at.%, the amorphous silicon-hydrogen alloy has quite different optical and electrical properties from a-Si:H with less than 10 at.% hydrogen.[12] Large hydrogenation leads to a structural change in the amorphous silicon-hydrogen alloys. Thus, control of hydrogen

content in a-Si:H is very important in order to obtain specific properties.

Hydrogenated amorphous silicon carbon alloys ($a\text{-}Si_{1-x}C_x:H$) are obtained by introduction of a hydrocarbon gas into a reaction chamber.[5-9] In this case, the plasma condition to be controlled becomes complicated because of the difference in the dissociation rates between a silane and a hydrocarbon in glow discharge plasma. There has been little information about the deposition mechanism of $a\text{-}Si_{1-x}C_x:H$ alloys using glow discharge plasma. At this stage, carbon atoms tend to be excessively hydrogenated compared with silicon atoms. Large hydrogenation of carbon atoms presumably brings poor semiconductor properties. Thus, in carbon-rich $a\text{-}Si_{1-x}C_x:H$ ($x>0.2$), substitutional doping has never been achieved, which is an obstacle to applications of carbon-rich $a\text{-}Si_{1-x}C_x:H$ to optoelectronic devices.

The main purpose of this chapter is to clarify the deposition mechanism of $a\text{-}Si_{1-x}C_x:H$ films. A method to separate the deposition rate of the films into the deposition rates of silicon and carbon atoms is presented using the measured value of the density of the film. Dependences of the emission intensities from emissive species in glow discharge plasma of a $SiH_4\text{-}C_2H_4\text{-}H_2$ system on rf power and gas composition are discussed in relation to the deposition rates of silicon and carbon atoms. As a result, it was found that C_2H_4 was not fully decomposed in weak plasma. Schemes of hydrogen incorporation into an $a\text{-}Si_{1-x}C_x:H$ alloy system are discussed on the basis of the results on infrared absorption spectroscopy (IR). The weak decomposition of C_2H_4 causes excess hydrogenation of carbon atoms in carbon-rich films where $a\text{-}Si_{1-x}C_x:H$ shows poor electrical properties. Reduction in hydrogenation of carbon atoms is examined by means of an enhanced decomposition of a hydrocarbon: high-power decomposition and hydrogen dilution of source gases. Substitutional doping for n type in $a\text{-}Si_{0.6}C_{0.4}:H$ is achieved

under a nearly-optimized deposition condition.

2-2. Preparation

Figure 2.1 shows the glow discharge apparatus. The rf power with a frequency of 13.56 MHz is capacitively coupled. The upper electrode is electrically connected to the stainless steel chamber wall; therefore it is an anode.[13] The anode and cathode electrodes are 50 mm in diameter and they are 18 mm apart.

The source gas for the deposition of a-$Si_{1-x}C_x$:H was a mixture of SiH_4 (10 % in H_2) and a hydrocarbon. C_2H_4 (100 %) was mainly used for a hydrocarbon with the exception of a doping experiment (described in section 2-8) where C_2H_2 (10% in H_2) was

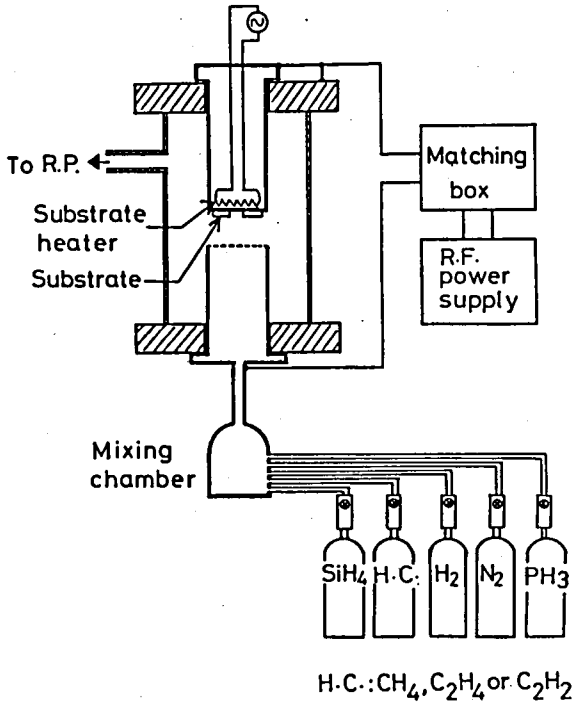

Fig. 2.1. Glow discharge apparatus.

used. CH_4 (100 %) was generally used for the deposition of silicon-rich a-$Si_{1-x}C_x$:H ($x<0.2$) as a reference. The input rf power was varied in the range of 10 W (0.51 W/cm^2)-80 W (4.1 W/cm^2). The flow rate was kept in the range from 60 to 80 sccm and the ratio of SiH_4 to a hydrocarbon was varied to change the film composition, denoted by the carbon content (x) in this work. The gas pressure in the reaction chamber was about 1.0-1.6 Torr. The substrate temperature (T_{sub}) was varied from room temperature (RT) to 260 °C. Nitrogen or argon was used as a purge gas.

Fused quartz substrates were used for fundamental absorption measurements and polished silicon wafers with high resistivity for infrared absorption measurements. Sand-blasted silicon wafers were used for photoluminescence measurements to eliminate any interference effect. For electrical measurements in section 2-8, glass (Corning 7059), NiCr-predeposited glass substrates and heavily doped crystalline silicon were used. The density of the film was evaluated from the weight and the thickness of the film deposited on a crystal quartz oscillator. The weight was determined by measuring the change in the oscillator frequency of the crystal quartz. Fused quartz and crystalline silicon substrates were cleaned by trichloroethylene, aceton and methyl alcohol. The cleaned crystalline silicon substrates were etched by diluted hydrofluoric acid. The cleaned fused quartz and glass substrates were rinsed with aqua regia (HNO_3 : HCl=3 : 1). A-$Si_{1-x}C_x$:H films of 0.5-1.0 micron thick were deposited.

The carbon content of the films was determined with the aid of an Auger electron spectroscope (AES) using crystalline SiC as the standard sample. The carbon content was controlled by changing the SiH_4 gas composition in the source gas as shown in Fig 2.2. In this figure, the SiH_4 gas composition is represented by the SiH_4 percentage (= $[SiH_4]/([SiH_4]+[hydrocarbon])$). The carbon content of the film increased with decreasing SiH_4 gas

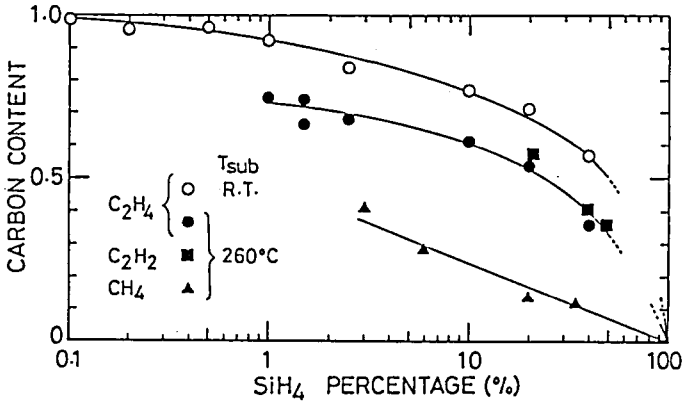

Fig. 2.2. Carbon content vs. SiH_4 percentage in the source gas. The carbon source was mainly C_2H_4. CH_4 and C_2H_2 were used for references. (Substrate temperature: room temperature and 260°C, flow rate: 78 sccm, gas pressure: 1.6 Torr, and rf power: 10 W).

composition. It should be noted that the carbon contents of the films deposited from the same gas composition decreased with increasing substrate temperature in the SiH_4-C_2H_4-H_2 system. This will be discussed in 2-5-3.

2-3. Analysis on Deposition Rate

The deposition rate of silicon (carbon) atoms is defined as the number of silicon (carbon) atoms deposited in a unit area of the films in a unit time. The rate was estimated from the carbon content, the hydrogen content and the film density. Details of calculation for this deposition rate are as follows; The numbers of silicon and carbon atoms, represented by [Si] and [C], respectively, in a unit volume of the sample can be deduced from the following formulas:

$$[Si]/[C]=(1-x)/x, \qquad (2.1)$$

and

$$(28[Si] + 12[C] + 1\,N_{Si-H} + 1\,N_{C-H})/N_A = d. \qquad (2.2)$$

Above, N_{Si-H} and N_{C-H} are the concentrations of hydrogen atoms bonding to silicon and carbon atoms, respectively, estimated from IR measurements, d the density of the film measured by the frequency change of the crystal quartz oscillator, and N_A Avogadro number. The deposition rates of silicon atoms, $D_{Si\ atom}$, and carbon atoms, $D_{C\ atom}$, can be calculated using [Si], [C] and the deposition rate D of the film by

$$D_{Si\ atom} = D\,[Si], \qquad (2.3)$$

and

$$D_{C\ atom} = D\,[C], \qquad (2.4)$$

where D is defined as the ratio of the film thickness to the deposition time.

2-4. Diagnostics by Optical Emission Spectroscopy

The emission from the glow-discharge plasma was detected by a photomultiplier through a monochromator which directly faced a viewing port made of fused quartz. The viewing port was at a distance of 8 cm from the reaction region in the chamber. No deposition on the viewing port occurred under the deposition condition as mentioned in section 2-2.

Figure 2.3 shows a typical emission spectrum from the SiH_4-C_2H_4-H_2 plasma in the wavelength region between 280 nm and 700 nm. The input rf power was 10 W (0.51 W/cm^2). The emission lines at 288.1 nm, 414.2 nm, 431.4 nm and 655.6 nm were assigned as

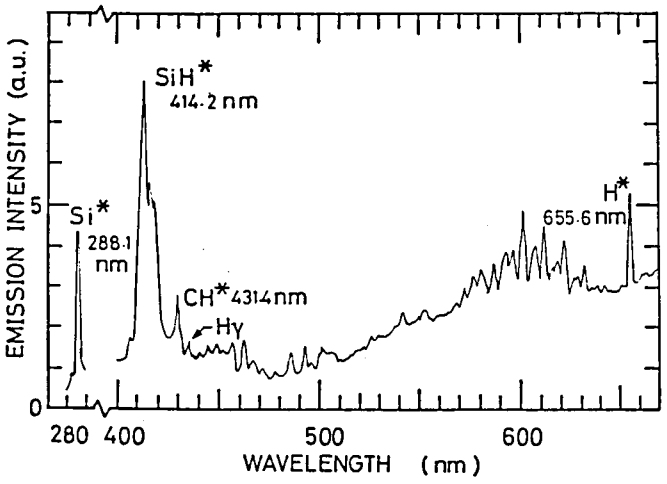

Fig. 2.3. Typical emission spectrum from SiH_4-C_2H_4-H_2 rf plasma. (Flow rate 78 sccm, gas pressure 1.6 Torr and rf power 10 W)

those from Si^*, SiH^*, CH^* and H^* (H_α), respectively.[14,15] The resolution of the monochromator was sufficient to distinguish the emission lines from CH^* (431.4 nm) and H_γ (434.0 nm). The emission lines from SiH^*, CH^* and H^* are important to elucidate the mechanism of the film formation.

2-5. Deposition Mechanism of a-$Si_{1-x}C_x$:H

2-5-1. Dependence on RF Power

In Fig.2.4, the dependences of the emission intensities from SiH^* (I_{SiH^*}), CH^* (I_{CH^*}) and H^* (I_{H^*}) on the rf power are shown. The gas compositions of SiH_4, C_2H_4 and H_2 were 7.2 %, 28.0 % and 64.8 %, respectively. The optical energy gaps (E_{opt}) of the deposited films were 2.5 eV (x=0.51) and 2.8 eV (x = 0.62), when the films were deposited at 220 °C with rf powers of 10 W and 80 W, respectively. I_{SiH^*} increases almost linearly with increasing rf power, while I_{H^*} and I_{CH^*} change in proportion to the 1.8 power of the rf power. The dependence of I_{SiH^*} on the rf power is similar to that in the SiH_4 glow discharge system.[16] From the

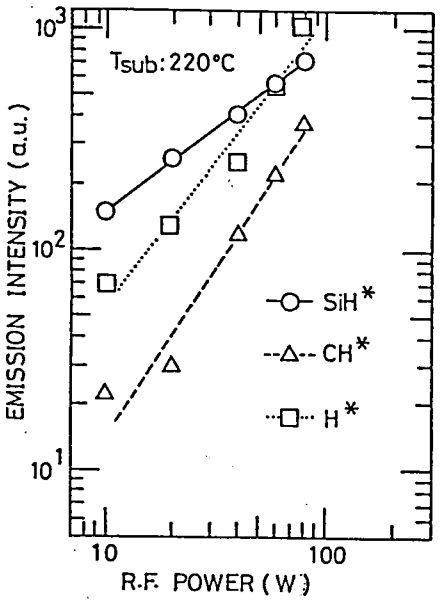

Fig. 2.4. Emission intensities of SiH^*, CH^* and H^* vs. rf power from a SiH_4 (7.2%)-C_2H_4 (28.0%)-H_2 (64.8%) plasma. (Flow rate 78sccm and gas pressure 1.6 Torr).

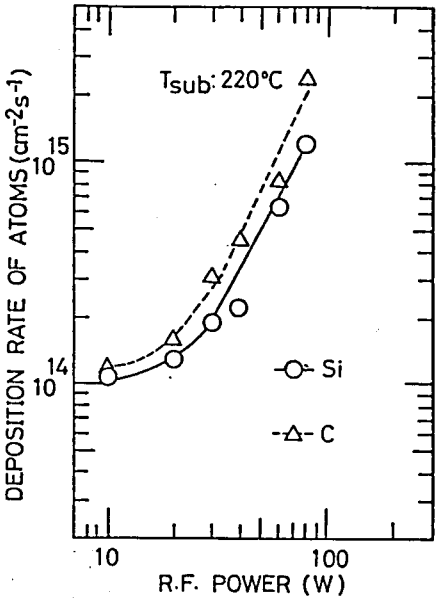

Fig. 2.5. Deposition rates of silicon and carbon atoms vs. rf power. The deposition rate of silicon (carbon) atoms was defined as the number of silicon (carbon) atoms deposited in a unit area of the film per unit time. The flow rate, gas composition and gas pressure were the same as in Fig.2.4.

dependences of I_{SiH}^*, I_{CH}^* and I_H^* upon the rf power, the SiH^* emission can be interpreted in terms of one-electron-impact excitation process and H^* and CH^* emissions in terms of two-electron-impact process following the arguments in refs.16 and 17, which indicates that the decomposition of C_2H_4 is more difficult than SiH_4.

Figure 2.5 indicates the deposition rates of silicon and carbon atoms on the rf power. The deposition rate of silicon atoms changed in proportion to the 2.3 power of the rf power. The rf power dependence of the deposition rate of silicon atoms can be interpreted by the product of I_{SiH}^* and I_H^*, as explained for the deposition of a-Si:H[14] in SiH_4-H_2 plasma. Therefore, in the SiH_4-C_2H_4-H_2 plasma, it seems that the emission intensity from SiH^* indicates the amount of SiH_4 decomposition. The presence of excited hydrogen atoms (emissive and non-emissive) may be important in the surface reaction for a-$Si_{1-x}C_x$:H deposition as well as for a-Si:H deposition.[14]

The deposition rate of carbon atoms is proportional to the 1.8 power of the rf power as shown in Fig.2.5. From the similarity of the rf power dependences (Figs.2.4 and 2.5), the deposition rate of carbon atoms is proportional to I_{CH}^*, which shows the emission intensity from CH^* is a good indicator of decomposition of C_2H_4.

2-5-2. Dependence on Gas Composition

Figure 2.6 shows I_{SiH}^*, I_{CH}^* and I_H^* vs. the gas composition in the SiH_4-C_2H_4-H_2 plasma. The total flow rate and the pressure were kept at 78 sccm and 1.6 Torr with an rf power of 10 W. Since the source gases were supplied as a mixture of SiH_4 (10 % dilution in H_2) and C_2H_4, the increase in the SiH_4 gas composition implies an increase in the H_2 gas composition as shown in the upper abscissa of Fig.2.6.

The emission intensity from SiH^* increases with increasing

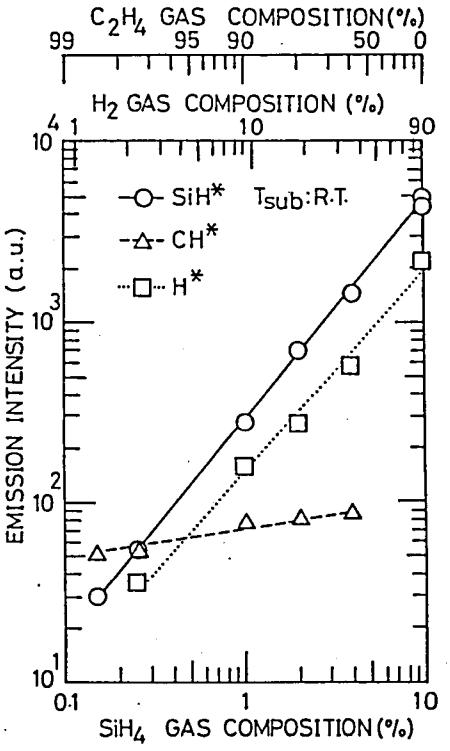

Fig. 2.6. Emission intensities of SiH^*, CH^* and H^* in a SiH_4-C_2H_4-H_2 plasma vs. gas composition. (Flow rate 78sccm, gas pressure 1.6 Torr and rf power 10 W).

SiH_4 gas composition, which is similar to the results in SiH_4-H_2 plasma for the deposition of a-Si:H.[18,19] However, the emission intensity from CH^* decreases with increasing C_2H_4 gas composition, indicating that the decomposition of C_2H_4 gas is reduced in the higher C_2H_4 gas composition.

Figure 2.7 indicates the deposition rates of silicon and carbon atoms on the SiH_4 gas composition with an rf power of 10 W without substrate heating. The deposition rate of carbon atoms decreases with increasing C_2H_4 gas composition, while the deposition rate of silicon atoms increases linearly with increasing SiH_4 gas composition. The decrease in the deposition rate of carbon atoms is related to the decrease in the emission intensity of CH^* as shown in Fig. 2.6. The weak decomposition of C_2H_4 caused the excess hydrogenation of carbon atoms in carbon-

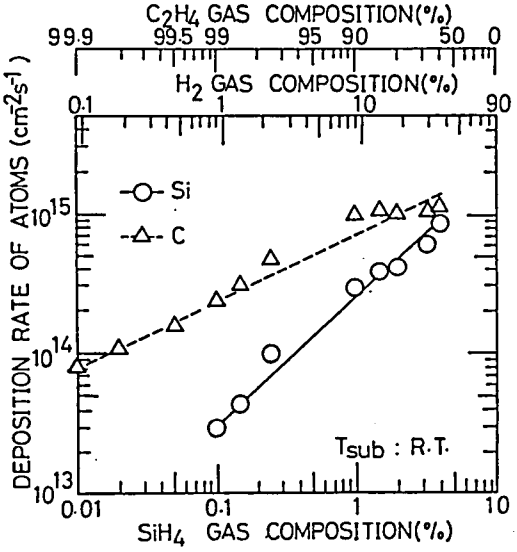

Fig. 2.7. Deposition rates of silicon and carbon atoms vs. gas composition. The flow rate, gas pressure and rf power were the same as in Fig.2.6.

rich films, which will be discussed in section 2-6.

The reason why the decomposition of C_2H_4 is hindered in the higher C_2H_4 gas composition can be interpreted as follows; (1) the dissociation rate of C_2H_4 may be much smaller than that of SiH_4 in an rf glow discharge like CH_4 in the SiH_4-CH_4 system.[20,21] The difference in the dissociation rates is due to the difference of both the collision cross-section and the threshold energy for the dissociation in the electronic collisional reaction process.[21] (2) H is important for the decomposition of C_2H_4 in an electrical discharge.[22] C_2H_4 reacts with hydrogen presumably via the following exothermic reactions:

$$C_2H_4 + H \xrightarrow{-1.68eV} C_2H_5, \qquad (2.5)$$

$$C_2H_5 + H \xrightarrow{-0.46eV} 2CH_3, \qquad (2.6)$$

while the decomposition reactions of C_2H_4, e.g. $C_2H_4 \rightarrow 2CH_2$ etc., are endothermic. Exothermic reactions may occur more easily than

endothermic reactions. However, as shown in Fig.2.6, I_H* becomes low for the higher C_2H_4 gas composition since the total flow rate is maintained constant and the high C_2H_4 gas composition gives the low H_2 gas composition. Therefore, the lack of H in the higher C_2H_4 composition may cause a hindrance of the decomposition of C_2H_4.

2-5-3. Dependence on Substrate Temperature

Figure 2.8 shows the deposition rates of silicon and carbon atoms as a function of the substrate temperature for the various gas compositions. The deposition rate of carbon atoms decreases with increasing substrate temperature, while the deposition rate of silicon atoms is constant in the range from T_{sub}=RT to T_{sub}=260 °C. This decrease in the deposition rate of carbon atoms was also observed in the deposition of a-C:H by a glow discharge.[23] The carbon content of the films deposited from the same gas composition decreased with increasing substrate

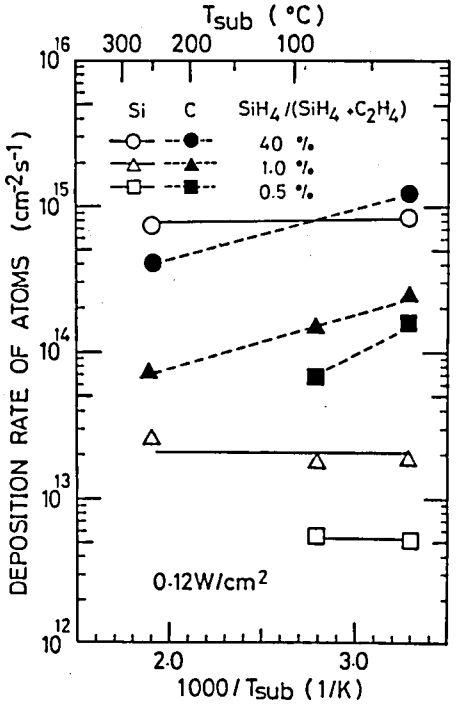

Fig. 2.8. Deposition rates of silicon and carbon atoms vs. substrate temperature for various gas compositions in a SiH_4-C_2H_4-H_2 plasma.

temperature as mentioned in section 2-2. On the basis of the discussion on IR measurements in the following section, the incorporation of carbon atoms as $C-H_3$ in the film are suppressed at higher substrate temperatures.

2-6. Hydrogen Incorporation into $a-Si_{1-x}C_x:H$

2-6-1. Infrared Absorption Measurements

Infrared absorption of $a-Si_{1-x}C_x:H$ deposited on crystalline silicon was measured by a double beam IR spectrometer, and a typical IR absorption spectrum of the film prepared at room temperature is shown in Fig. 2.9. The absorption peaks are assigned after recent works (Table 2-1).[24,25] The peak around 2000 cm^{-1} is due to the $Si-H_n$ monohydride stretching mode. The peak position of $Si-H_n$ is thought to be shifted to high wavenumbers in the environment where silicon atoms are surround by carbon atoms.[5]

From the structures of the $C-H_n$ stretching mode (2900-2800cm^{-1}), the $C-H_n$ and/or $Si-CH_2$ wagging modes (1000 cm^{-1}) and

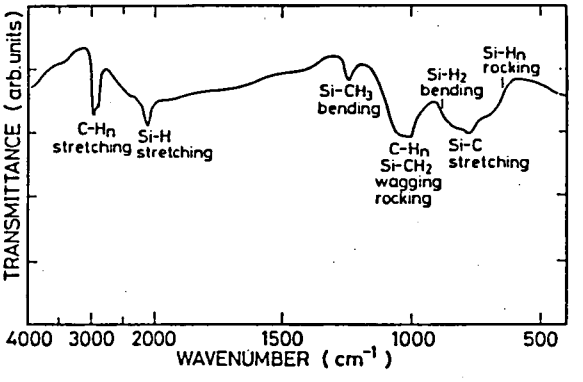

Fig. 2.9. Typical IR absorption spectrum for a sample prepared at room temperature with a carbon content of 0.82.

Type	Wavenumber (cm^{-1})	Mode
$C-H_n$	∿2900	Stretching
$Si-H_n$	∿2100	Stretching
$Si-CH_3$ or $C-CH_3$	1400∿1250	Bending
$Si-CH_2$ or $C-H_n$	1000	Wagging
$Si-CH_3$	780	Wagging
$Si-H_n$	850∿890	Bending
Si-C	670	Stretching
$Si-H_n$	640	Wagging

Table 2-1. Wave numbers of infrared absorption peaks observed and their origins.

the $Si-CH_3$ absorptions, it follows that $C-H_2$ and $C-H_3$ structures exist in the films as well as C-H structures.

In the films deposited at higher substrate temperatures, the IR absorption spectra do not change drastically except that all the absorption peaks associated with hydrogen decrease in the intensity and the $Si-H_2$ wagging mode is almost absent in the films deposited at 260 °C. The concentration ratio of the $C-H_3$ structure to the sum of the $C-H_2$ and C-H structures is less at T_{sub}=260 °C than that at T_{sub}=RT.

2-6-2. Excess Hydrogenation of Carbon Atoms

The concentration of the hydrogen atoms bonded to carbon and to silicon atoms, denoted by [C-H] and [Si-H] respectively, were estimated from the integrated intensity of the IR absorption (stretching mode vibration). The proportional constants used here are 1.0×10^{21} cm^{-1} (ref.26) and 1.39×10^{20} cm^{-1} (ref.27) for $C-H_n$ and $Si-H_n$ respectively. The number of carbon atoms, represented by [C] in Fig. 2.10(a), in a unit volume of the sample was deduced by the method described in section 2-3. In Fig. 2.10(a) the ratio [C-H]/[C] is shown as a function of the carbon content. The substrate temperatures were room temperature and 260 °C. For each T_{sub}, the value [C-H]/[C] increases with the

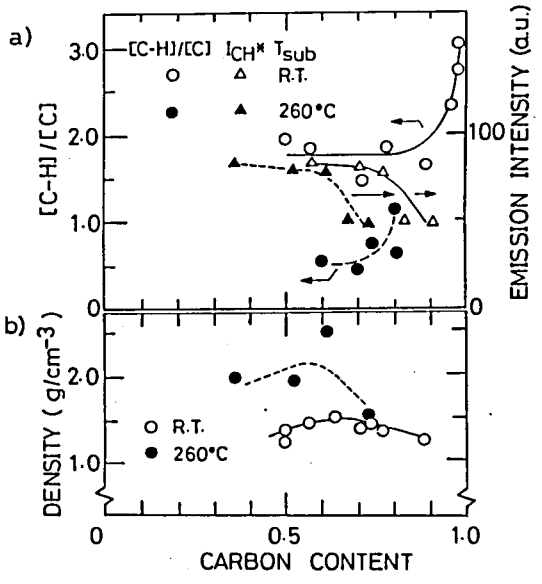

Fig. 2.10. (a) Dependence of the average number of hydrogen atoms attached to a carbon atom [C-H]/[C] on the carbon content for the films deposited at room temperature and 260 °C. Also shown is the dependence of the CH^* emission intensity on the carbon content. (b) Dependence of the density on the carbon content for the films deposited at room temperature and 260 °C.

carbon content. The value of [C-H]/[C] for T_{sub}=RT is larger than for T_{sub}=260 °C, which is the same tendency of hydrogenation of a-Si:H.[28] The increase in [C-H]/[C] with the carbon content can be attributed to the increase in the $C-H_3$ structure compared to the $C-H_2$ and C-H structures.

Roughly speaking, 1-2 hydrogen atoms bonded to one carbon atom depending on the preparation conditions. This value is very high compared with the number of hydrogen atoms attached to a silicon atom, 0.05-0.3, which is the similar value to that for a-Si:H. This result is consistent with a recent work,[25] where the number of hydrogen atoms bonding to a carbon atom was found to be greater than the number bonding to a silicon atom by a factor of

2-5 at T_{sub}=350 °C. The total hydrogen content in the films, estimated from the IR absorption coefficient, increases with the carbon content and amounts to 60-70 at.% for the films with higher carbon contents deposited at T_{sub}=RT.

Regarding Fig.2.10(a), the following results should be noticed. The carbon contents of the films deposited from the same gas composition decreases with increasing substrate temperature as mentioned in section 2-2. For a gas composition of SiH_4 5.0%, C_2H_4 45.0%, H_2 50.0%, the total hydrogen content in the film for T_{sub}=260 °C (x=0.61) is 25 %, whereas the film for T_{sub}=RT (x=0.77) has the total hydrogen content of 56 %. The hydrogen incorporation in the film becomes small with increasing substrate temperature.

The increase in hydrogen incorporation causes a decrease in the density of the deposited film(Fig.2.10(b)). From the scheme of hydrogen incorporation and the density of the film, the carbon-rich films can be considered to have bridged polymer-like structures, which are schematically shown in Fig. 2.11.

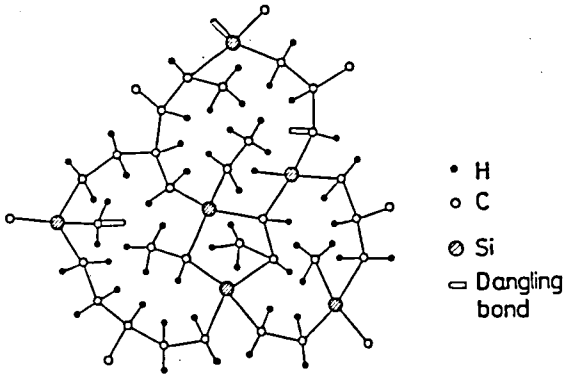

Fig. 2.11. Schematic diagram of the structure of a-$Si_{1-x}C_x$:H prepared at low substrate temperature and low rf power density. In this figure, the carbon content is about 0.8, [C-H]/[C] ≈ 2 and [Si-H]/[Si] ≈ 0.3.

The emission intensity from CH^* in Fig.2.6 was replotted against the carbon content of the film in Fig.2.10(a). In the carbon-rich films (x>0.8 for T_{sub}=RT and x>0.6 for T_{sub}=260 °C), I_{CH}^* decreases, together with an increase in the IR absorption ratio. The result also indicates that the decomposition of C_2H_4 gas is reduced in the higher C_2H_4 gas composition and that the weak decomposition of C_2H_4 causes an excess hydrogenation of carbon atoms.

The value of [C-H]/[C] mentioned above directly indicates the average number of hydrogen atoms attached to a carbon atom. However, in order to calculate the value exactly, it is necessary to evaluate many parameters as mentioned in section 2-3: the carbon content, thickness, density, IR absorption coefficients. The IR absorption pattern of the $C-H_n$ stretching mode was investigated to know the configuration of $C-H_n$ bonds through a simple procedure.

Discrepancy in the assignment for the $C-H_n$ stretching mode exists among recent works.[5,24,25,29] In Refs. 5 and 25, the absorption peaks at 2960 cm^{-1} and 2880 cm^{-1} were thought be due to the $C-H_3$ stretching mode and the $C-H_n$ (n=1 and 2) stretching modes, respectively. According to this peak assignment, the ratio of the IR absorption coefficients α_3/α_1 may correlate to the average number of hydrogen atoms attached to carbon atoms, where α_3 and α_1 are the absorption coefficients at 2960 cm^{-1} and 2880 cm^{-1}, respectively. The correlation between the ratios of α_3/α_1 and [C-H]/[C] is investigated as follows: Figure 2.12 shows the ratio α_3/α_1 as a function of the carbon content for the films deposited at T_{sub} of RT and 260 °C with an rf power of 10 W. The tendency of the IR ratio is almost the same as that of [C-H]/[C] as shown in Fig. 2.10.(a), qualitatively: The IR absorption ratio steeply increases in the carbon rich films (x> 0.8 for T_{sub}=RT and x>0.6 for T_{sub}=260 °C), and the ratio of the films deposited at RT is larger than that of T_{sub}=260 °C. Thus,

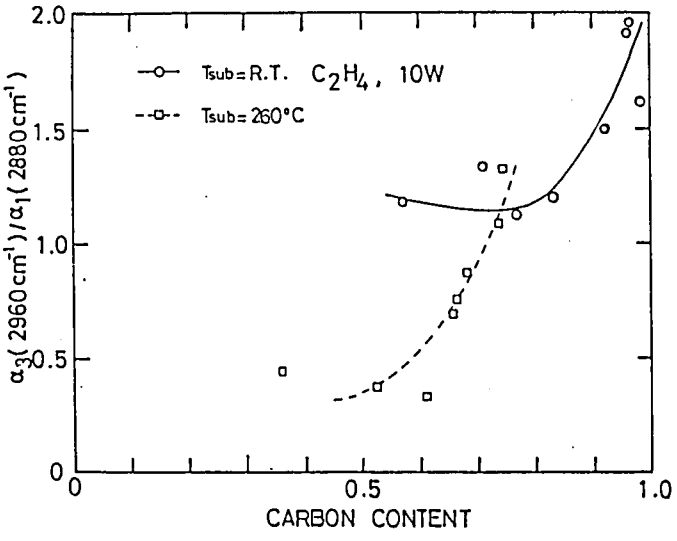

Fig. 2.12. Dependence of the infrared absorption coefficient ratio α_3/α_1 on the carbon content for the films deposited at room temperature and 260 °C.

the IR absorption ratio can be used as a convenient indicator to investigate the configuration of C-H_n, which will be used in section 2-8.

2-7. Enhanced Decomposition of Hydrocarbon

2-7-1. High Power Deposition

The deposition rate of carbon atoms and I_{CH}* increased with the rf power as shown in Figs. 2.4 and 2.5. And, the [C-H]/[C] ratio decreased with increasing rf power as shown in Fig.2.13(a). The increase in the decomposition of C_2H_4 by the increase in the rf power caused the decrease in the number of hydrogen atoms attached to carbon atoms. On the other hand, it should be noted that structural randomness of a-$Si_{1-x}C_x$:H increases with the rf power. Structural randomness is often discussed using B values in optical properties of the films. The B value is determined by

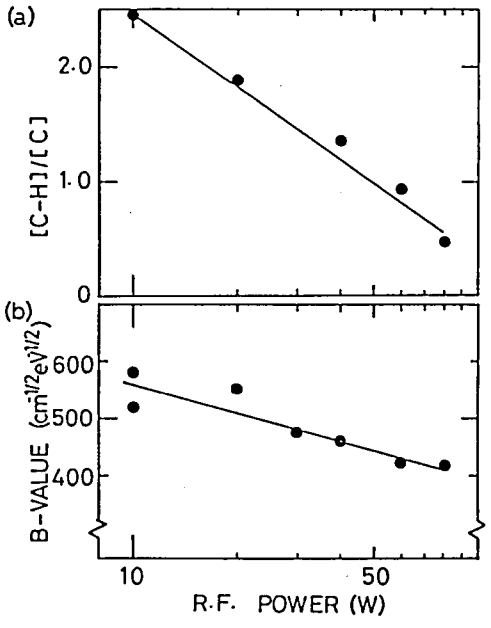

Fig. 2.13. (a) Average number of hydrogen atoms attached to a carbon atom and (b) the B value vs. the rf power.

absorption coefficients in the fundamental absorption region. Details of calculation for the B value are described in section 3-3. Decrease in the B values gives much structural randomness in films.[9] In Fig.2.13(b), the decrease in the B value indicates that structural randomness increases with the rf power. This may be due to bombardments by charged particles, which results in poor electrical properties. Hence, deposition with low rf power is required to obtain high-quality films by a glow discharge method. It is necessary to decompose C_2H_4 efficiently without an increase in the rf power.

2-7-2. Effects of Hydrogen Dilution of Source Gases

In order to enhance the decomposition of C_2H_4, the source gases of SiH_4 and C_2H_4 were diluted with H_2. The dependence of I_H^*, I_{SiH}^* and I_{CH}^* on the C_2H_4 gas composition are shown in Fig. 2.14. The flow rate of C_2H_4 was changed over the range from 1.3

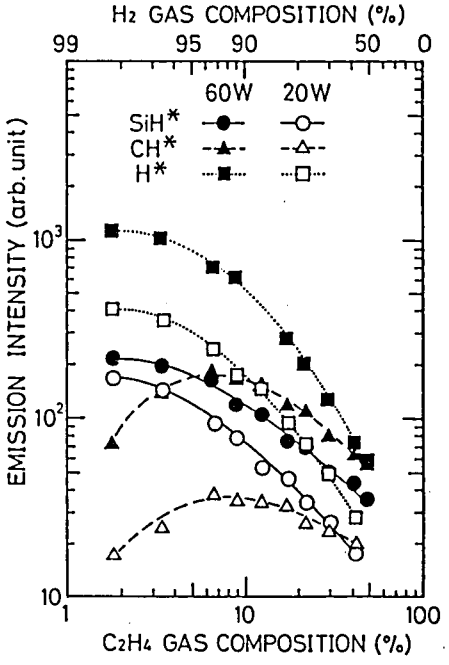

Fig. 2.14. Emission intensities of SiH^*, CH^* and H^* vs. C_2H_4 gas composition in a SiH_4-C_2H_4-H_2 plasma. The flow rate of C_2H_4 was changed over the range from 1.3 to 50 sccm. The flow rates of SiH_4 and H_2 were kept at 1 and 70 sccm, respectively.

to 50 sccm. The flow rates of SiH_4(100%) and H_2 were kept at 1 and 70 sccm, respectively. The upper abscissa of Fig. 2.14 indicates the H_2 gas composition. The substrate temperature was kept at 260 °C and the rf powers were 60 and 20 W.

The intensities of I_{SiH^*}, I_{CH^*} and I_{H^*} for the rf power of 60 W are larger than that for 20 W. In the both cases, I_{CH^*} increased with the C_2H_4 gas composition when the H_2 gas composition exceeded 90 % as shown in Fig. 2.14. This result indicates that the amount of decomposed C_2H_4 is in proportion to the amount of introduced C_2H_4 in the glow discharge plasma rich in H_2. Below 90 % for the gas composition of H_2, I_{CH^*} decreased with increasing C_2H_4 gas composition, which is due to the lack of H_2 as mentioned in section 2-5. Therefore, in order to enhance decomposition of C_2H_4, dilution of C_2H_4 with H_2 by a factor of 10 is necessary.

2-7-3. Reduction in Excess Hydrogenation

Figure 2.15 shows the average number of hydrogen atoms attached to carbon atoms on the H_2 gas composition in the films of a-$Si_{0.2}C_{0.8}$:H. The gas flow rates of C_2H_4 and SiH_4 were maintained at 8 and 1 sccm, respectively. The flow rate of H_2 was changed over the range from 9 to 84 sccm. The substrate temperature was 260°C and the rf power was 20 W. The values of [C-H]/[C] and [Si-H]/[Si] decrease with the H_2 gas composition. The dilution of source gases with H_2 causes an enhancement of the decomposition of C_2H_4, which results in the reduction in the excess hydrogenation of carbon atoms. For the H_2 gas composition of 90 %, however, the value of [C-H]/[C] is still four times as large as the value of [Si-H]/[Si]. Further reduction in the hydrogenation of carbon atoms may be necessary to improve electrical properties of the films.

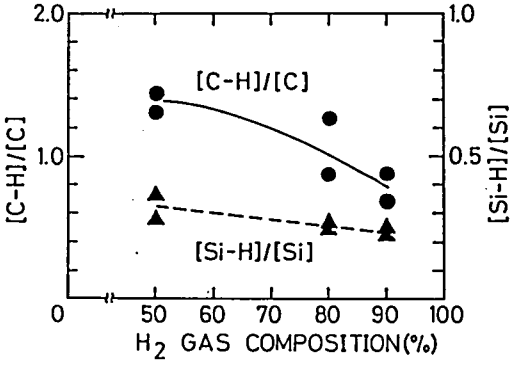

Fig. 2.15. Average number of hydrogen atoms attached to a carbon atom vs. H_2 gas composition. The flow rates of SiH_4 and C_2H_4 were maintained at 1 and 8 sccm, respectively.

2-8. Doping Effects

The excess hydrogenation of carbon atoms is an obstacle to substitutional doping in carbon-rich a-$Si_{1-x}C_x$:H ($x>0.2$). In this

section, substitutional doping of a-$Si_{0.6}C_{0.4}$:H is described. An enhanced decomposition of a hydrocarbon was achieved using C_2H_2 under a nearly-optimized deposition condition.

The ratio of the IR absorption coefficients α_3/α_1 correlates to the average number of hydrogen atoms attached to a carbon atom as mentioned in section 2-6, where α_3 and α_1 are the absorption coefficients at 2960 cm^{-1} ($C-H_3$ stretching mode) and 2880 cm^{-1} ($C-H_n$ stretching mode, n=1, 2) in IR absorption spectra, respectively.[5,6] Figure 2.16 shows the ratio α_3/α_1 as a function of the carbon content for the films deposited using CH_4, C_2H_4 or C_2H_2 as the carbon source at T_{sub}=220 °C with an rf power of 10 W. Below 0.5 for the carbon content, the absorption ratio for the films using C_2H_4 or C_2H_2 was maintained at 0.35, while the ratio for the films using CH_4 increased with the carbon content: With a low rf power, the number of $C-H_3$ bonds in a unit volume of the film using C_2H_4 or C_2H_2 is kept at a lower value,

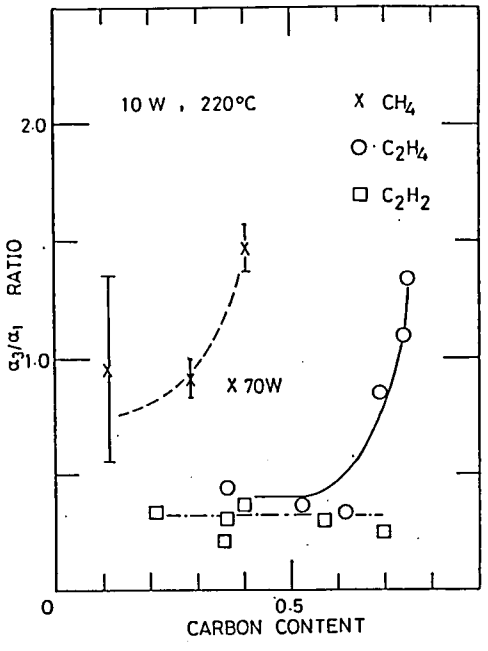

Fig. 2.16. Dependence of the IR coefficient ratio α_3/α_1 on the carbon content for the films deposited using CH_4, C_2H_4 or C_2H_2 for the carbon source.

while the number of $C-H_3$ bonds in the film using CH_4 increases drastically. On the basis of the integrated intensity of the absorption coefficient at 1250 cm^{-1} ($Si-CH_3$ bending mode), the number of $C-H_3$ bonds in a unit volume of the film using CH_4 is 20 times larger than that in the film using C_2H_4 or C_2H_2 for the carbon content of 0.4. When the rf power increased up to 70 W to enhance the decomposition of CH_4, the film with 70 W still showed a large value of the IR ratio as shown in the figure. Thus, C_2H_4 or C_2H_2 is suitable for the carbon source rather than CH_4. In this section, C_2H_2 was used for the carbon source.

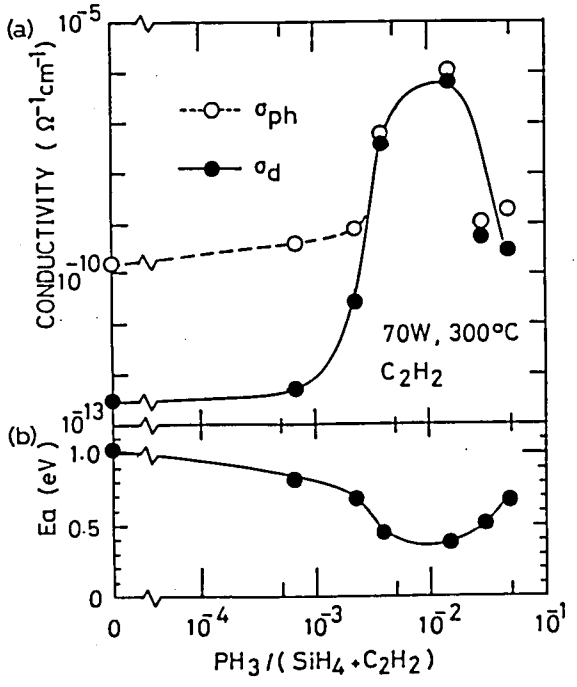

Fig. 2.17. (a) Dark and photo conductivities, (b) the activation energy of the dark conductivity and the optical energy gap as a function of the dopant gas composition for the films deposited using C_2H_2.

Figure 2.17 shows doping properties in a-$Si_{0.6}C_{0.4}$:H using C_2H_2. The substrate temperature was kept at 300 °C. In order to reduce the hydrogenation of carbon atoms in the film, the rf power increased up to 70 W and the source gases of SiH_4 and C_2H_2 were diluted with H_2 by a factor of 10. The gas composition of the dopant (PH_3), denoted by $PH_3/(SiH_4+C_2H_2)$, was varied from $7x10^{-4}$ to $5x10^{-2}$. The carbon content was maintained at 0.4 for the films mentioned below.

Figure 2.17(a) indicates dark and photo conductivities. The photo conductivity was measured under irradiation of AM1(100mW/cm^2). The dark and photo conductivities of undoped a-$Si_{0.6}C_{0.4}$:H were $2.6x10^{-13}$ and $1.5x10^{-10}$ S/cm, respectively. Above $5x10^{-3}$ for the dopant composition, the dark conductivity increased and had a maximun of $1.1x10^{-6}$ S/cm for the dopant composition of $2x10^{-2}$. The temperature dependence of the dark conductivity for any film showed the activation-type conduction over the range between 30 °C and 120 °C (Fig. 2.18). The

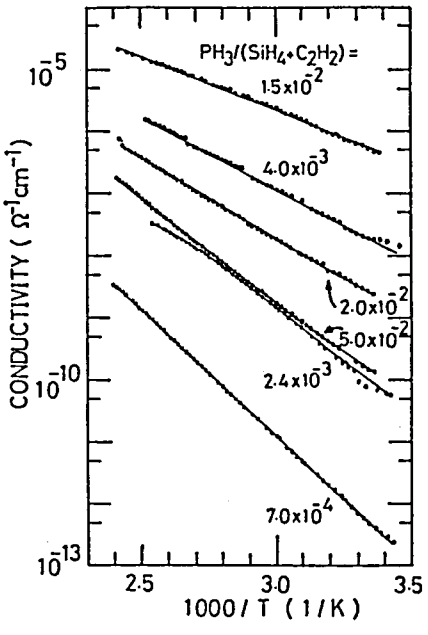

Fig. 2.18. Temperature dependence of the dark conductivity in phosphorus-doped a-$Si_{0.6}C_{0.4}$:H.

activation energy of the dark conductivity decreased with increasing dopant gas composition up to $2x10^{-2}$ as shown in Fig.2.17(b). The minimun activation energy was 0.36 eV. These results indicate that n-type impurity doping was achieved in a-$Si_{0.6}C_{0.4}$:H.

Above $2x10^{-2}$ for the dopant gas composition, the conductivity decreased and the activation energy increased with the dopant composition, while incorporated phosphorus in the film increased with the gas dopant composition on the basis of the results of AES. It can be explained that phosphorus may be incorporated in the shape of three-fold rather than four-fold as well as phosphorus in phosphorus-doped a-Si:H deposited by photo-assisted chemical vapor deposition[30] and arsenic in a Si-As binary alloy system.[31]

The dependence of the optical energy gap (E_{opt}) on the dopant gas composition is also shown in Fig.2.17(b). For undoped a-$Si_{0.6}C_{0.4}$:H, E_{opt} was 2.04 eV. Below $1x10^{-3}$ for the dopant composition, E_{opt} decreased with increasing dopant composition. For the dopant composition of $2x10^{-2}$, E_{opt} was 1.95 eV. On the basis of IR measurements, hydrogen content in the film decreased with increasing dopant gas composition. Thus, the decrease in E_{opt} is partially due to the decrease in the hydrogen content in the film.

2-9. Summary

(1) By combining an optical emission spectroscopic analysis of the SiH_4-C_2H_4-H_2 plasma and the deposition rate of films, the formation mechanism of a-$Si_{1-x}C_x$:H was elucidated.

(2) The change in the emission intensities from SiH^* with an rf power can be interpreted in terms of the one-electron-impact excitation process, whereas CH^* and H^* can be interpreted in terms of the two-electron-impact process.

(3) Using the carbon content, the density of the film and the configuration of hydrogen incorporation in the film, the deposition rate of the film was separated into the deposition rates of carbon atoms and silicon atoms. The deposition rate of carbon atoms was in proportion to the emission intensity from CH^*; this shows that CH^* is a good indicator of the decomposition of C_2H_4.

(4) The decomposition of C_2H_4 was reduced in C_2H_4-rich gas compositions; this is presumably due to either the small dissociation ratio of C_2H_4 in an electrical discharge or the lack of hydrogen. A reduction in the decomposition of C_2H_4 caused a decrease in the deposition rate of carbon atoms and an increase in the average number of hydrogen atoms attached to carbon atoms.

(5) The incorporation of carbon atoms as $C-H_3$ in films was suppressed at higher substrate temperatures.

(6) In order to enhance the decomposition of C_2H_4, it was necessary to dilute C_2H_4 with H_2 by a factor of 10, which resulted in the reduction in the excess hydrogenation of carbon atoms in films.

(7) Under a nearly-optimized deposition condition, substitutional doping for n-type was achieved in $a\text{-}Si_{0.6}C_{0.4}:H$. C_2H_2 was chosen for the carbon source. The dark conductivity and the activation energy were 1.1×10^{-6} S/cm and 0.36 eV, respectively, for a dopant gas composition of 2×10^{-2}.

References

1) S.M.Sze: "VLSI Technology" (McGraw-Hill Japan, Tokyo, 1983) Cap.3 & 8.

2) J.I.Pankov (editor):"Semiconductor and Semimetals: Hydrogenated Amorphous Silicon" (Academic press, New York, 1984) Part D.

3) E.A.Davis: "States in the Gap and Defects in Amorphous Semiconductors"; in " Amorphous Semiconductor" ed. M.H.Brodsky (Springer-Verlag, Berlin, 1979) p.46.

4) W.E.Spear and P.G.LeComber: "Fundamental and Applied Work on Glow Discharge Material"; in " The Physics of Hydrogenated Amorphous Silicon I" ed. J.D.Joannopoulos and G.Lucovsky (Springer-Verlag, Berlin, 1984) p.64.

5) H.Wieder, M.Cardona and C.R.Duarnieri: Phys. Status Solidi B **92** (1979) 99.

6) K.Nakazawa, S.Ueda, M.Kumeda, A.Morimoto and T.Shimizu: Jpn.J.Appl.Phys. **21** (1982) L176.

7) R.Sussmann and R.Ogden: Philos. Mag. **44** (1981) 137.

8) Y.Catherline, G.Turban and B.Grolleau: Thin Solid Films **76** (1981) 23.

9) D.A.Anderson and W.E.Spear: Philos. Mag. **35** (1977) 1.

10) D.E.Carlson: "Solar Cells" in ref. 2.

11) J.C.Knight, G.Lucovsky and R.J.Nemanich: Non-Cryst. Solids **32** (1979) 393.

12) D.J.Wolford, J.A.Reimer and B.A.Scott: Appl.Phys.Lett. **42** (1983)369.

13) H.R.Konig and L.I.Maissel: IBM J.Res.Develop., **14** (1970)168.

14) M.Hirose: Jpn.J.Appl.Phys. **21** (1982) suppl. 21-1, p.275.

15) D.E.Donohue, J.A.Schiavone and R.S.Freund: J.Chem.Phys. **67** (1977) 769.

16) A.Matsuda and K.Tanaka: Thin Solid Films **92** (1982) 171.

17) F.J.Kampas and R.W.Griffith: J.Appl.Phys. **52** (1981) 1285.

18) M.Hirose and T.Hamasaki: Oyo Buturi(in Japanese) **52**

(1982) 675.

19) J.P.Harbison, A.J.Williams and D.V.Lang: J.Appl.Phys.55 (1984) 946.

20) K.Tachibana, M.Nishida, H.Harima and Y.Urano: J. Phys. D: Appl. Phys. 17 (1984) 1727.

21) K. Tachibana, T.Okuyama, H.Harima, and Y.Urano: Proc. 7th Int. Sym. Plasma Chemistry, Eindhoven, 1985 p.588.

22) F.K.MacTaggart: "Plasma Chemistry in Electrical Discharge" (Elsevir, Amsterdam, 1967) p.108.

23) I.Watanabe, S.Hasegawa and Y.Kurata: Jpn.J.Appl.Phys. 21 (1982) 856.

24) Y.Tawada, K.Tsuge, M.Kondo, H.Okamoto and Y.Hamakawa: J.Appl.Phys. 53 (1983) 5273 .

25) K.Nakazawa, S.Ueda, M.Kumeda, A.Morimoto and T.Shimizu: Jpn.J.Appl.Phys. 21 (1982) L176.

26) F.Fujimoto, A.Ootuka, K.Komaki, Y.Iwata, I.Yamane, H.Yamashita, Y.Hashimoto, Y.Tawada, K.Nishimura, H.Okamoto and Y.Hamakawa: Jpn.J.Appl.Phys. 23 (1984) 810.

27) E.C. Freeman and W.Paul: Phys.Rev.B18 (1978) 4288.

28) M.Milleville, W.Fuhs, F.J.Demond, H.Mannsperger, G.Muller and S.Kalbitzer: Appl.Phys.Lett. 34 (1979) 173.

29) B.Dischler, A.Bubenzer and P.Koidl: Appl.Phys.Lett. 42 (1983) 636.

30) Y.Mishima, M.Hirose, Y.Osaka and Y.Ashida: Jpn. J.Appl.Phys. 56(1984) 2803.

31) J.C.Knights: Philos.Mag. 34 (1976) 663.

III STRUCTURES AND OPTICAL PROPERTIES OF a-$Si_{1-x}C_x$:H FILMS

3-1. Introduction

Since hydrogenated amorphous silicon carbon alloys (a-$Si_{1-x}C_x$:H) prepared by a glow discharge technique were fist reported by Anderson and Spear,[1] it has been widely accepted that one of the significant features of amorphous silicon carbon (a-$Si_{1-x}C_x$:H) is controllability of the bandgap by changing the carbon content of the material; this is linked to adaptability in design of amorphous devices including heterojunctions. Another feature is that this material shows bright visible luminescence.[2,3] Thus, it has received considerable interests regarding a possible application to light emitting devices. These optical and luminescence properties are strongly affected by film structures as well in hydrogenated amorphous silicon (a-Si:H).[4] In a-$Si_{1-x}C_x$:H, distinct discrepancy in the carbon-content dependence of the optical energy gap (E_{opt}) exists among results reported by several groups[1,5,6] owing to the differences in the hydrogen content and the structural change.

In this chapter, film structures are discussed on the basis of the results in electron spin resonance (ESR) with the aid of schemes of hydrogen incorporation in the film discussed in section 2-6. The relations between the film structures and the optical properties (E_{opt}, refractive indices and photoluminescence: PL) are described. The emission mechanisms of PL and electroluminescence (EL) are also discussed. All samples in this chapter were deposited using SiH_4 and C_2H_4.

3-2. Defect Density

A-$Si_{1-x}C_x$:H films, typically 0.5-1.0 micron in thickness, were deposited on fused quartz substrates for ESR measurements.

The substrate temperatures (T_{sub}) were mainly room temperature (RT) and 260 °C for a reference. The input rf power was 10 W (0.51 W/cm^2). The ESR signals were detected with an ESR spectrometer.

The ESR signals for the film of T_{sub}=RT have three peaks as shown in Fig. 3.1(a). The g-values of the three peaks were constant for the two, 2.040 and 1.960, and variable for peak A against the carbon content. The g-value of peak A decreased from 2.004 to 2.001 with increasing carbon content from 0.6 to 0.99 as shown in Fig.3.2. However, the film of T_{sub}=260 °C has a single peak as shown in Fig. 3.1(b). The g-value of the single peak decreased from 2.004 to 2.002 with increasing carbon content from 0.4 to 0.75 (Fig.3.2); this is consistent with other results for the film deposited at 350 °C.[7] On the basis of the similar carbon-content dependence of the g-values of peak A in the film of T_{sub}=RT to that of the single peak in the film of T_{sub}=260 °C, the origin of peak A is presumed to be dangling bonds of silicon

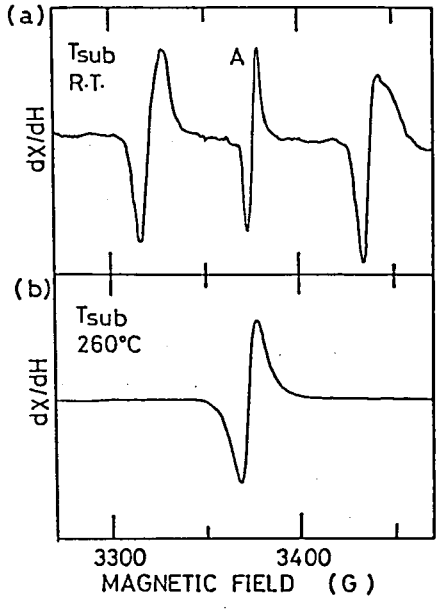

Fig. 3.1. ESR spectra of (a) a-$Si_{1-x}C_x$:H deposited at T_{sub}=RT, (b) a-$Si_{1-x}C_x$:H deposited at T_{sub}=260°C.

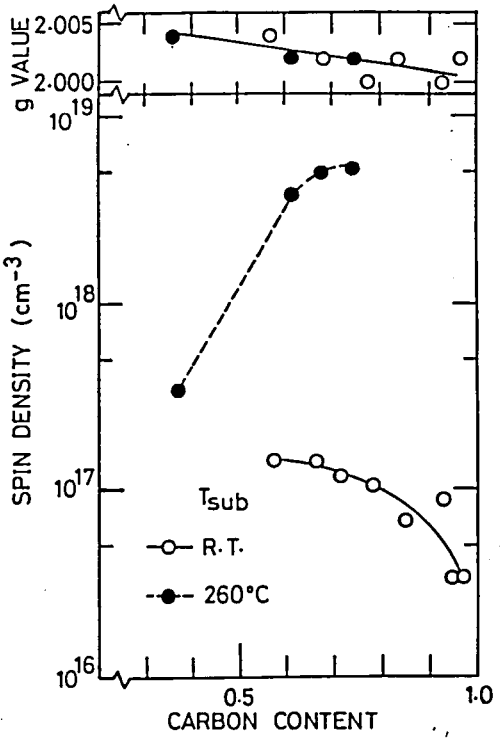

Fig. 3.2. Dependences of the spin density and g-value on the carbon content.

or carbon atoms. Here, the ESR signal from the dangling bonds of silicon atoms could not be distinguished from those of carbon atoms, because the g-value for silicon atoms shifted to a lower value near that for carbon atoms owing to the effects of surrounding carbon atoms as discussed in ref.7.

In Fig. 3.2, the change in the spin density of peak A in the film of T_{sub}=RT against the carbon content is shown together with that of T_{sub}=260 °C. In the films of T_{sub}=RT, the spin density decreased with increasing carbon content from 0.55 to 0.99. It increased with the carbon content over the range from 0.40 to 0.75 in the films of T_{sub}=260 °C, which was consistent with a recent report[7] in the films deposited at 350 °C. The increase in the spin density in the carbon-rich films was due to the increase of dangling bonds, which could be caused by either (1) the

smaller covalent bond length of carbon atoms (0.772 Å) than that of silicon (1.17 Å), (2) the tendency for the coordination number of carbon atoms to be three, or (3) the change of the incorporation scheme of hydrogen atoms.[7]

The spin density in the film of T_{sub}=RT was less than $5x10^{-2}$ of that in the film of T_{sub}=260°C in the range of the carbon content between 0.55 and 0.75. The difference in the density of the dangling bonds between the films of T_{sub}=RT and 260 °C may be due to the difference in the hydrogen contents. The average number of hydrogen atoms attached to carbon atoms in the films of T_{sub}=RT was around two, which is about twice as large as that in the films of T_{sub}=260 °C as mentioned in section 2-6. This excess hydrogenation increases the flexibility of the amorphous structure in the films of T_{sub}=RT, which may cause scarce generation of dangling bonds.

As to the anomalous two peaks (g=2.040 and 1.960) in the films of T_{sub}=RT, the spin densities were equal with each other, which implies the same origin for the two peaks. It is widely accepted that ESR signals are affected by an interaction between unpaired electrons and nuclear magnetic moments.[9] In a recent report[8] similar anomalous two peaks were explained due to the interaction between hydrogen atoms and unpaired electrons from certain centers at the interface between the film and the substrate. Thus, these anomalous two peaks are thought to be a hydrogen-related hyperfine structure of certain centers owing to enough amount of hydrogen atoms in the film of T_{sub}=RT. The separation of the two peaks was about 117 Gauss, which was around a quarter of that in a hydrogen atom (512 Gauss).[9]

3-3. Fundamental Absorption

3-3-1. Measurement

The transmissivity and reflectivity of the films on fused

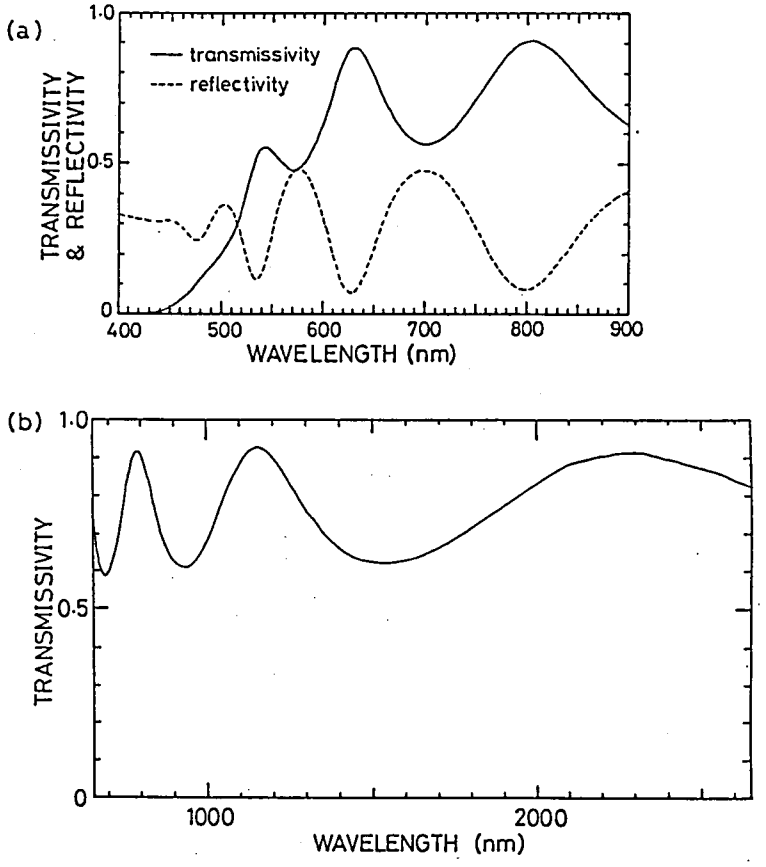

Fig. 3.3. Typical transmissivity and reflectivity spectra of a-$Si_{1-x}C_x$:H. (a) visible region, (b) near infrared region (only transmissivity spectrum).

quartz substrates were measured by a double beam spectrometer, and typical transmissivity and reflectivity spectra in the visible and near-infrared regions are shown in Fig.3.3. An interference waveform is observed in the spectra of the near-infrared region, which is due to the interference among lightwaves multireflected between the air-film and film-substrate interfaces.

The transmissivity (T) and reflectivity (R) of the film are expressed by[10)]

$$T=\frac{(1-r_1^2)(1-r_2^2)(1-r_3^2)\exp(-\alpha d)}{1+r_1^2r_2^2\exp(-2\alpha d)-2r_1r_2\exp(-\alpha d)\cos(4\pi nd/\lambda)}, \qquad (3.1)$$

and

$$R=\frac{r_1^2+r_2^2\exp(-2\alpha d)-2r_1r_2\exp(-\alpha d)\cos(4\pi nd/\lambda)}{1+r_1^2r_2^2\exp(-2\alpha d)-2r_1r_2\exp(-\alpha d)\cos(4\pi nd/\lambda)}, \qquad (3.2)$$

where $r_1=|(1-n^*)/(1+n^*)|$, $r_2=|(n_s-n^*)/(n_s+n^*)|$ and $r_3=(1-n_s)/(1+n_s)$. Above, n^* represents complex refractive index of the film, n_s refractive index of the substrate (no-absorbing), α absorption coefficient of the film, d the film thickness and λ wavelength. The value of n_s is 1.49 for the fused quartz used in this study.

In the wavelength region where $\exp(-2\alpha d)$ is nearly zero and the interference terms in Eqs.(3.1) and (3.2) are negligible, i.e., around the absorption edge, T and R are expressed by

$$T=\frac{64}{(n+1)^2+k^2}\,\frac{k^2}{(n_s+n)^2+k^2}\,\frac{n_s^2\exp(-2\alpha d)}{(1+n_s)^2}, \qquad (3.3)$$

and

$$R=\frac{(n-1)^2+k^2}{(n+1)^2+k^2}, \qquad (3.4)$$

where $n^*=n-ik$ and $\alpha=4\pi k/\lambda$. The absorption coefficient of the film is estimated using Eqs.(3.3) and (3.4).

The optical energy gap (E_{opt}) is defined as the following equation:[11]

$$\alpha h\nu=B^2\,(h\nu-E_{opt})^2, \qquad (3.5)$$

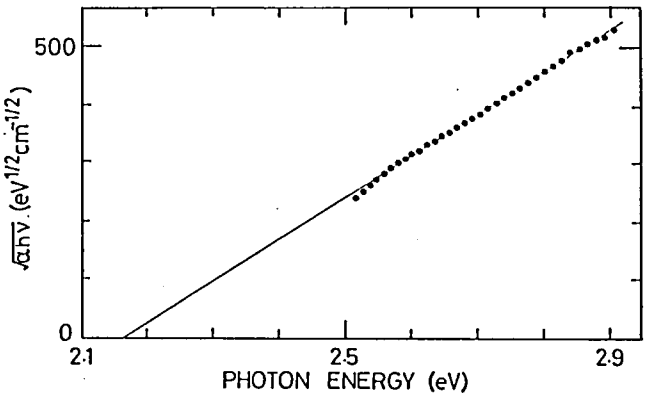

Fig. 3.4. $(\alpha h\nu)^{\frac{1}{2}}$ vs. $h\nu$ plot of absorption coefficients of $a\text{-}Si_{1-x}C_x:H$.

where $h\nu$ is photon energy. The value of E_{opt} is estimated from the intercept of a plot of $(\alpha h\nu)^{\frac{1}{2}}$ versus $h\nu$ as shown in Fig.3.4.

In the long-wavelength region where α is nearly zero, the maximum and minimum transmissions, T_{max} and T_{min}, are calculated from Eq.(3.1) as the following:

$$T_{max}=16n_s^2/(n_s+1)^4, \tag{3.6}$$

and

$$T_{min}=\frac{16n^2n_s^2}{(n^2+n_s)^2(n_s+1)^2}. \tag{3.7}$$

As shown in Fig.3.3, the measured value of T_{max} is 0.92. This value agrees with the calculated value by Eq.(3.6) using $n_s=1.49$. The refractive index of the film was estimated from Eq.(3.7).

When n is kept constant, we can evaluate the film thickness by

$$d=(1/2n)(1/\lambda_m-1/\lambda_{m+1})^{-1}, \tag{3.8}$$

where λ_m is wavelength at the minimum (maximum) transmission and λ_{m+1} is that at the minimum (maximum) transmission adjacent to λ_m ($\lambda_m < \lambda_{m+1}$).

3-3-2. Optical Energy Gap

The optical energy gap increased monotonically with the carbon content (Fig.3.5). The optical energy gap did not show a maximum in contrast with the results of others.[1,5,6] Instead,

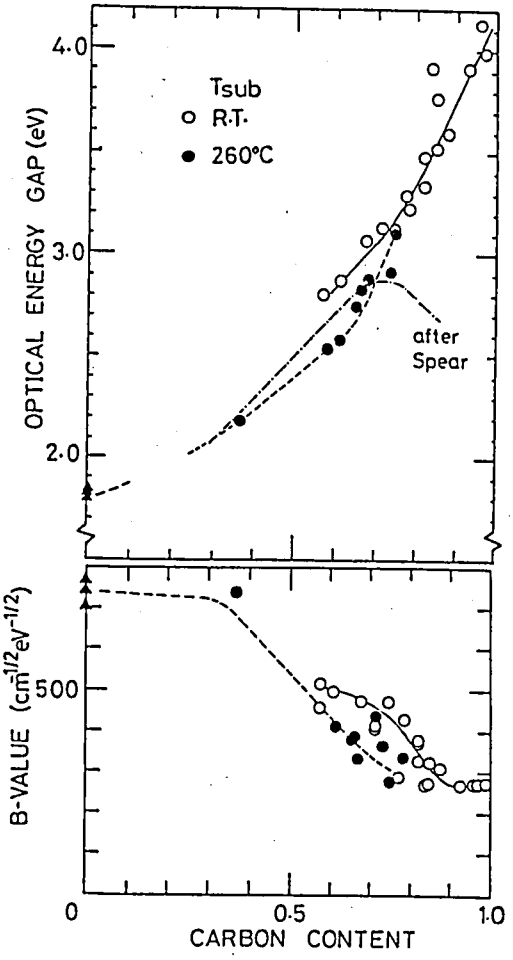

Fig. 3.5. Dependence of the optical energy gap and the B value on the carbon content for the films deposited at room temperature and 260 °C. Triangles are the results for a-Si:H. Also shown is the result from ref.1.

E_{opt} increased more steeply for the carbon contents above 0.8 for T_{sub}=RT and above 0.6 for T_{sub}=260 °C; this is due to a steep increase in the average number of hydrogen atoms attached to carbon atoms (see section 2-6). The maximum value of E_{opt} obtained was as high as 4.12 eV in the sample (T_{sub}=RT) with a carbon content of 0.97. At the same carbon content, E_{opt} for the film of T_{sub}=RT is larger than that of T_{sub}=260 °C; this is due to a larger hydrogen incorporation in the film of T_{sub}=RT.

Hydrogenated amorphous carbon has been thought to be a multi-phase material,[12,13] consisting of (1) a polymeric phase containing many C-H_n (n=2 and 3) groups, (2) a graphitic phase containing three-fold coordinated carbon atoms, and (3) a small amount of four-fold coordinated carbon atoms with a diamond-like structure. Because of the higher hydrogenation of carbon atoms and the large optical energy gap, the polymeric component of carbon atoms is dominant in the film of this work. The results of infrared absorption measurements and the density imply that the decomposition of C_2H_4 may be hindered in the case of the C_2H_4-rich gas composition (see section 2-6).

In general, E_{opt} has a maximum in the dependence on the carbon content based on the results of others,[1,5,6] which is due to the dominance of the graphitic component in carbon-rich films.[1] The difference between this work and others originates from the deposition condition; for a higher rf power or a lower pressure, ion bombardment to the surface of a film presumably breaks C-H bonds and increases the number of graphitic carbon atoms.[14] In our work, the rf power was lower (0.51 W/cm^2) and the pressure was higher (1.6 Torr) than the deposition condition where the graphitic structure was mainly formed.[15] Therefore, graphitic carbon atoms were not very dominant in our film, and E_{opt} did not decrease.

In Fig. 3.5 are also shown the B values in Eq.(3.5). A low B value compared to that in a-Si:H implies strongly disordered

amorphous structures and the existence of wide tail states in energy band structures.[1)]

3-4. Refractive Index

The refractive indices were obtained from interference fringes in optical transmission measurements over the range of wavelengths from 700 to 2500 nm (no-absorbing region for a-$Si_{1-x}C_x$:H). It decreased from 1.9 to 1.6 with the increase in the carbon content from 0.65 to 0.86. However, it can be also represented as follows. Figure 3.6 shows the relation between the refractive index n and E_{opt}, which shows a good correlation. The refractive index can be represented by the formula[16)]

$$n=1 + (h^2\omega_p^2) / (4\pi E_{av}^2), \qquad (4.9)$$

where ω_p is plasma frequency for valence electrons and E_{av} is average gap. Although E_{av} is not the same as E_{opt}, it should show a positive correlation with E_{opt} in a group of materials such as the a-$Si_{1-x}C_x$:H alloy system in which material parameters are

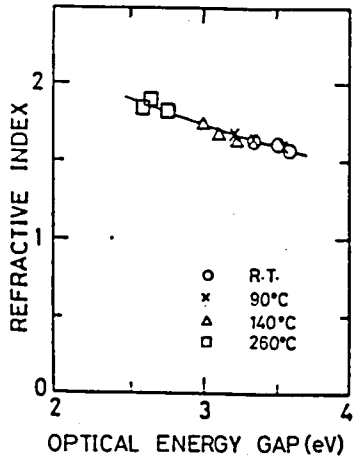

Fig. 3.6. Relation between the refractive index and the optical energy gap for various substrate temperatures.

changed systematically. Thus, the decreasing tendency of n with E_{opt} is considered to be reasonable.

3-5. Photoluminescence

3-5-1. Measurement

The photoluminescence (PL) was measured using 366nm light (3.39 eV) from an ultra-high-pressure mercury lamp or 325 nm (3.82 eV) from a He-Cd laser for excitation. Figure 3.7 shows emission spectra at room temperature. They were corrected for the

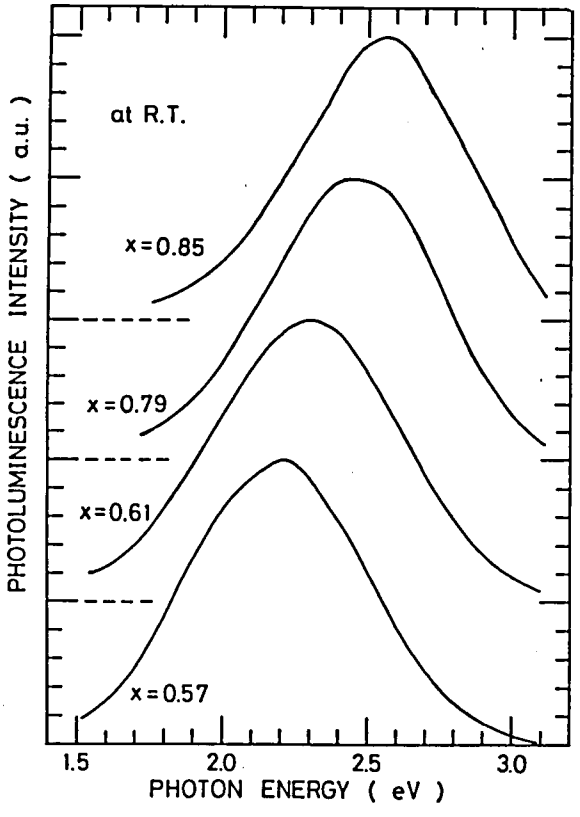

Fig. 3.7. Photoluminescence spectra measured at room temperature, corrected to the spectral response of the measuring system (each peak height normalized).

response of the measuring instruments. They are broad spectra. Although lower energy spectra were not measured, these spectra were considered to be single peaks if we compared the emission intensity at around 900 nm with that measured by Engemann et al.[17] These results are similar to those of Munekata et al.[18] and Sussmann and Ogden[5] but different from those of Engemann et al.[17] and Watanabe et al.[19]

3-5-2. Recombination Mechanism

Figure 3.8 shows the composition dependence of the emission peak energy E_{PL}. The peak energy increased with the increase in the carbon content. A bright bluish-white luminescence (E_{PL}=2.57 eV) was observed at room temperature in the sample with x=0.86. If we compared E_{PL} in the samples of similar carbon contents prepared at different T_{sub} values, E_{PL} decreased gradually with the increase in T_{sub}. The optical energy gap showed a distinct

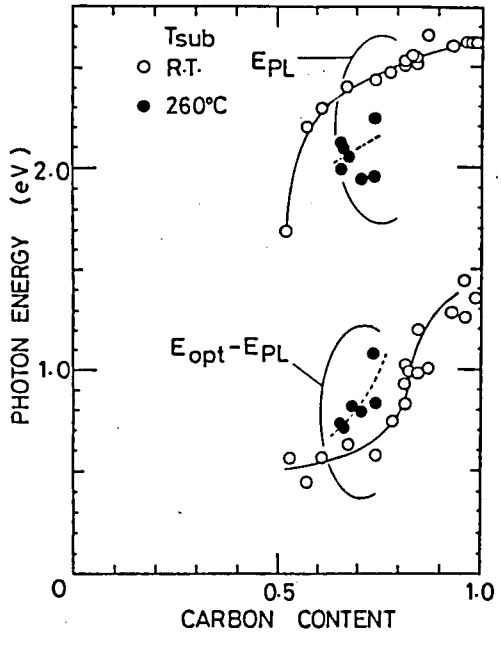

Fig. 3.8. Dependence of the emission peak energy (E_{PL}) and the difference between the optical energy gap E_{opt} and E_{PL} on the carbon content and the substrate temperature.

decrease at T_{sub}=260 °C compared with that for the room temperature deposition, as shown in Fig.3.5. Therefore, a part of the decrease in E_{PL} at 260 °C is attributed to the decrease in E_{opt}. To investigate in more details, E_{opt}-E_{PL} is plotted against the carbon content and T_{sub} in Fig. 3.8. The values of E_{opt}-E_{PL} were greater for T_{sub}=260 °C than for room temperature deposition. This increase in E_{opt}-E_{PL} is partly responsible for the decrease in E_L with T_{sub}.

The value of E_{opt}-E_{PL} increased gradually with the carbon content in the range investigated. The monotonic increase in E_{opt}-E_{PL} is thought to be due to the monotonic increase in structural randomness and the corresponding increase in the tail-state width detected by the B value (see Fig.3.5). This result is in contrast with the results of Sussmann and Ogden[5] and Engemann et al.[17], which showed a maximum in E_{opt}-E_{PL} at around the carbon content of 0.5 for samples prepared at T_{sub}=300 °C and T_{sub}=200 °C, respectively (although Engemann et al.[17] did not discuss E_{opt}-E_{PL} explicitly). According to their discussion, E_{opt}-E_{PL} could be associated with the distortion energy due to self-trapping.[20] In a configurational-coordinate model,[21] the distortion energy is in proportion to the square of electron-phonon coupling constant. Less polar nature of the network for either silicon- or carbon-rich specimens could lead to the low electron-phonon coupling constant compared with the a-$Si_{0.5}C_{0.5}$:H alloy; this results in low E_{opt}-E_{PL} in either silicon- or carbon-specimens. The discrepancy between our results and their results on E_{opt}-E_{PL} can be explained as the difference in the film structures of carbon-rich specimens as mentioned in 3-3-2.

Figure 3.9 shows the excitation intensity dependence of the PL spectrum at room temperature in the sample with a carbon content of 0.82 prepared at room temperature. Figure 3.10 shows the decay characteristics of the peak intensity. The energy shift with the excitation intensity and the t^{-n} decay characteristics

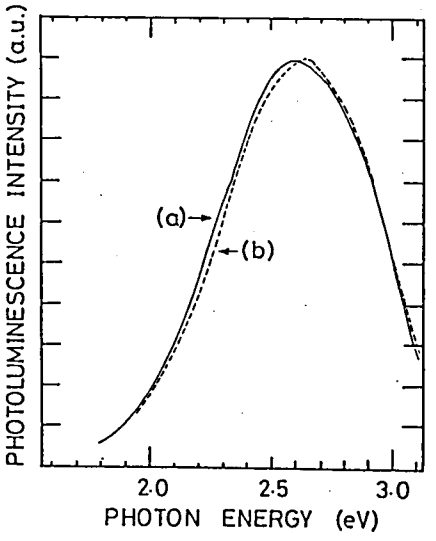

Fig. 3.9. Excitation intensity dependence of the photoluminescence spectrum at room temperature (The sample prepared at room temperature; film composition x=0.82). The sample was excited with He-Cd laser (325 nm) (a) at a power density of 7×10^{15} photons $cm^{-2}s^{-1}$ or (b) 7×10^{16} photons $cm^{-2}s^{-1}$.

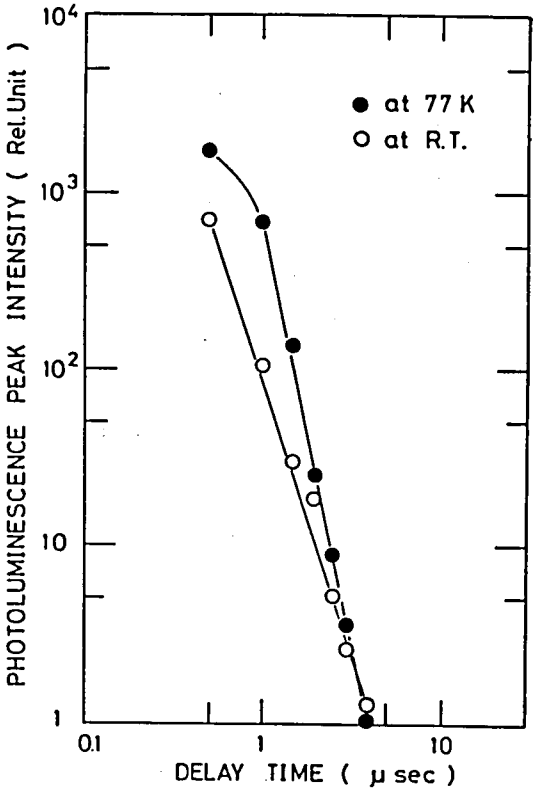

Fig. 3.10. Decay characteristics of the photoluminescence at room temperature and 77 K (sample was prepared at 90 °C; film composition x=0.86).

imply that the luminescence mechanism in the a-$Si_{1-x}C_x$:H alloy is due to pair recombination between localized centers as in a-Si:H (see for example ref.22).

Figure 3.11 shows the dependence of the photoluminescence intensity on the carbon content. The photoluminescence intensity was corrected by considering the absorption coefficient α at the excitation wavelength of 325 nm: i.e., the measured values were divided by $[1-\exp(-\alpha d)]$,[23] where d is the film thickness. In the films of T_{sub}=RT, the photoluminescence intensity increased with the carbon content, and the intensity was about one order of magnitude larger than that in the films of T_{sub}=260 °C.

Figure 3.12 indicates the relation between the PL intensity

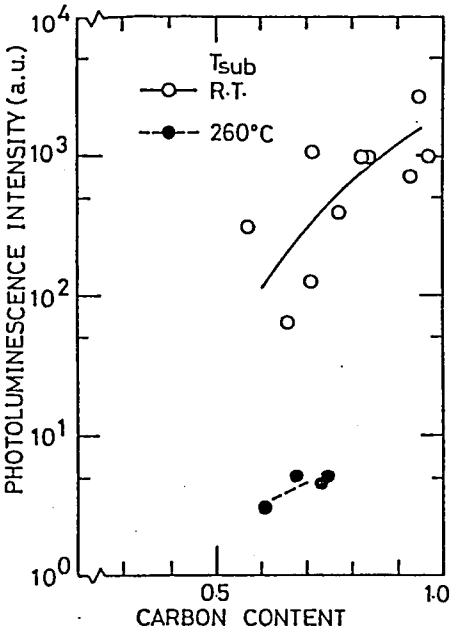

Fig. 3.11. Dependence of the photoluminescence intensity on the carbon content.

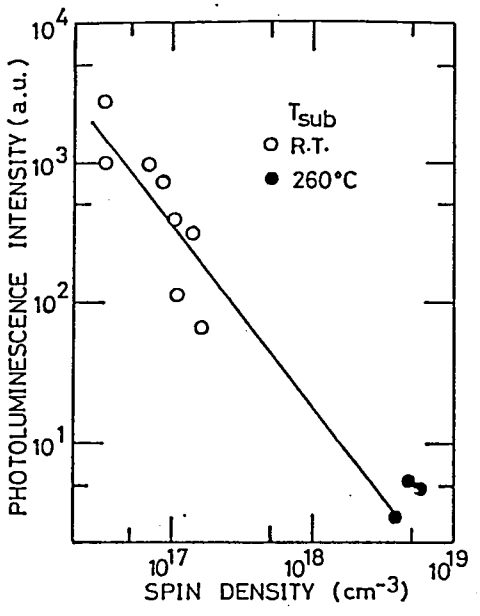

Fig. 3.12. Dependence of the photoluminescence intensity on the spin density.

and the spin density detected by ESR. For the films of T_{sub}=RT, the spin density is that for peak A (see section 3-2). The PL intensity decreased with increasing spin density in the films of T_{sub}=RT. The data for T_{sub}=260 °C are on an extrapolated line of the data for T_{sub}=RT. Therefore, the origin of peak A in the films of T_{sub}=RT is presumably the same as that of the single peak in the films of T_{sub}=260 °C from the point of the relation between the photoluminescence intensity and the spin density as well as the g-value dependence on the carbon content (see section 3-2). Since the dangling bonds in a-$Si_{1-x}C_x$:H ($0<x<0.75$) deposited at T_{sub}=300 °C were explained to work as non-radiative centers using the results of optically detected magnetic resonance (ODMR),[24] the spin density in the films of T_{sub}=260 °C in this work is thought to indicate the amount of non-radiative centers.

The lower density of non-radiative centers detected as the low spin density shown in Fig. 3.2 resulted in the intense photoluminescence in the films deposited at room temperature. In these films, the increase in the photoluminescence intensity with the carbon content was caused by the decrease in the spin density.

At 77K the emission intensity increased by a factor of 4-30. The ratio of the PL intensity at 77K to that at RT was higher for the silicon-rich samples, i.e., thermal quenching was less marked in the carbon-rich samples,[5,19] which is caused by the strong Coulomb interaction.[5] Such a strong Coulomb interaction, which was pointed out by Sussmann and Ogden,[5] Sussmann and Lauder[25] and Depinna et al.[24], arises from the low dielectric constant of carbon-rich specimens as anticipated from the low refractive index.

3-6.Electroluminescence

3-6-1. Fabrication

The EL cell structure is shown in Fig.3.13. A 2000 Å Y_2O_3 layer was first deposited onto a tin oxide (SnO_2)-coated glass substrate using an electron-beam evaporation technique with a deposition rate of 45-50 Å/s. The resistivity and the breakdown field of the Y_2O_3 layer were 1.8×10^{12} Ωcm and 5.6×10^6 V/cm, respectively. Then a 1000 Å a-$Si_{0.17}C_{0.83}$:H film was prepared onto the Y_2O_3 layer at a substrate temperature of 85 °C using SiH_4 and C_2H_4. The input rf power was 10 W. This amorphous film contains 56 at.% hydrogen, and E_{opt} is 3.34 eV. Finally, a 2000 Å Y_2O_3 layer was deposited on it and an aluminum electrode was evaporated.

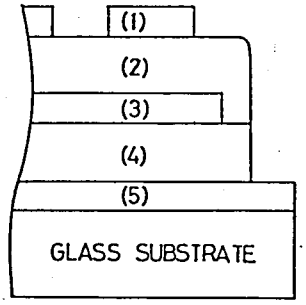

Fig. 3.13. Structure of the electroluminescence cell;
(1) electrode, Al;
(2) insulator, Y_2O_3 (2000Å);
(3) active layer, a-$Si_{0.17}C_{0.83}$:H (1000Å);
(4) insulator, Y_2O_3 (2000Å);
(5) transparent electrode, SnO_2.

3-6-2. Light Emitting Characteristics

When alternating currents with frequencies over the range from 20 Hz to 20 kHz were applied to the cell, orangeish-white electroluminescence (EL) was observed. The EL spectrum shifted to the longer wavelength side and had a narrower band compared with the PL spectrum of the same amorphous film excited by the 366 nm line from a Hg lamp as shown in Fig.3.14. The difference may be attributed to the difference of the excitation processes.

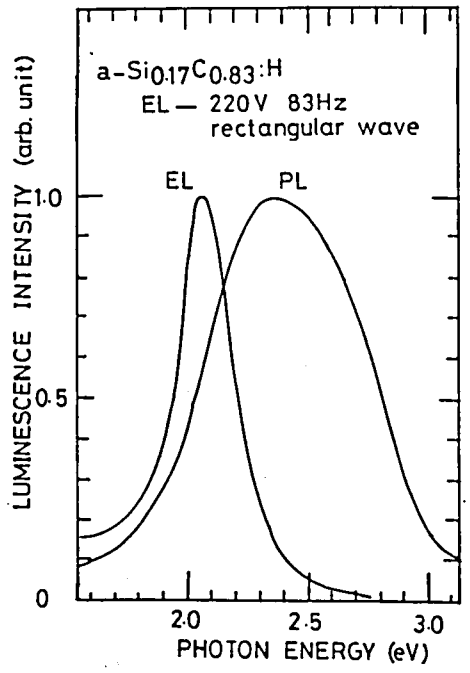

Fig. 3.14. Electroluminescence spectrum and photoluminescence spectrum measured at room temperature. (The sample was prepared at 90°C; film composition x=0.83).

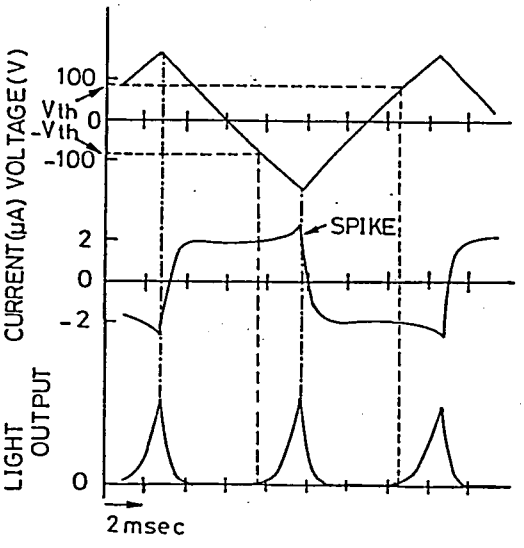

Fig. 3.15. Examples of the emission waveform and the current waveform together with the triangular applied voltage waveform.

Examples of emission waveforms detected by a photomultiplier and current waveforms together with applied-voltage waveforms are shown in Fig. 3.15. To initiate EL, the applied voltage should exceed a threshold value, which implies the association of hot carriers. Taking account of the dielectric constants of 3 and 13 for a-$Si_{0.17}C_{0.83}$:H and Y_2O_3, respectively, the effective electric field in the active amorphous layer was estimated to be 5×10^6 V/cm at a threshold voltage of 90 V. The EL intensity derived from the emission waveforms increases exponentially with the applied voltage and tends to saturate at higher voltages (Fig.3.16).

A spike-type current was observed in the current waveform, when the pulse voltage with a triangular waveform exceeded the threshold value as shown in Fig.3.15. On the assumption that the

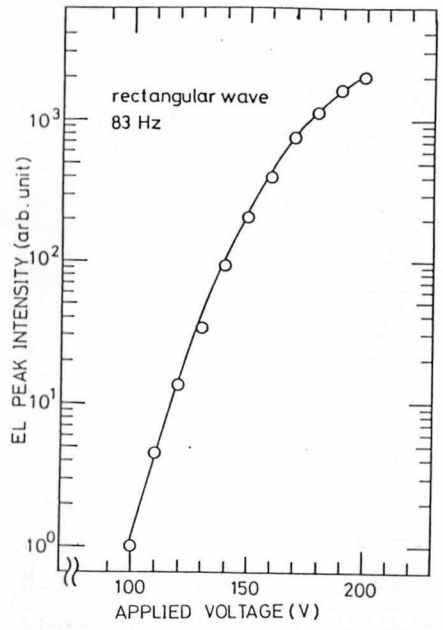

Fig. 3.16. Dependence of the electroluminescence intensity on the applied voltage.

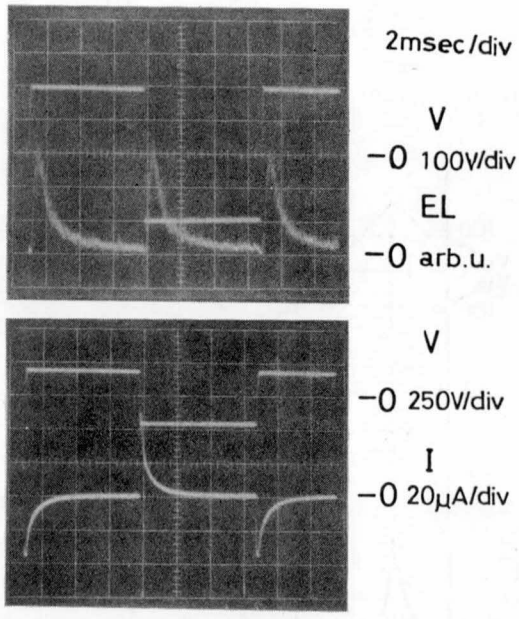

Fig. 3.17. Examples of the emission waveform and the current waveform together with the rectangular applied voltage waveform.

spike area in the current waveform is caused by the electron travelling in the active layer from one interface to another, the number of electrons is estimated to be 1×10^{12} electrons/cm^2. This value approximately agrees with that in ZnS:Mn cells of similar structures.[26] When rectangular wave pulses were applied, EL was observed at the edges of the rectangular waves where the polarity changes (Fig.3.17). The emission continued for around 10 msec under high voltages with a frequency of 85 Hz. The emission and the current decayed exponentially.

3-6-3. Emission Mechanism: Polarization Effects

When the pulses with the equal polarity were applied repeatedly to the cell, the intensity of EL was decreased with every shot. Finally, the light output vanished. Strong EL was observed by alternating the polarity of the applied voltage, which is observed as 'polarization effect' in conventional ZnS:Mn EL cells.[27] The cause of this effect can be interpreted as

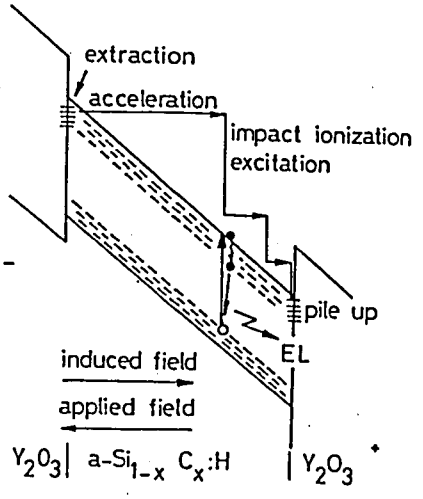

Fig. 3.18. Schematic diagram of emission mechanism in the electroluminescence cell.

follows (Fig. 3.18): Carriers trapped at the interface between the insulator and the active layer are extracted and accelerated by the applied voltage; Hot carriers thus created make an excitation stage for radiation recombination in the active layer by impact ionization; Carriers having travelled across the active layer accumulate at the interface, and make the electric field with the opposite polarity to the applied field; When the pulses of the same polarity as the former pulses are applied, the effective inner field in the active layer is depressed by the superposition of the induced opposite field by the accumulated carriers. On the assumption that the travelling carriers (1×10^{12} electrons/cm^2) contribute to make the induced field, the field becomes an order of 10^6 V/cm in our cell.

To clarify this effect, the following experiment was carried out. Several hundreds of equal polarity pulses were applied until the light output vanished. Then the pulse named as 'prior pulse' was applied with the opposite polarity to the former pulses. When the pulse with the opposite polarity was applied following the prior pulse, strong EL was observed as shown in the inset of Fig.3.19. It shows the relation between the EL peak intensity and the prior-pulse width. The EL peak intensity increased gradually with the prior-pulse width. When the period continuing the same polarity becomes long, the amount of the carriers trapped at the interface increases, and thus the EL peak intensity increases.

Figure 3.20 shows the frequency (f) dependence of the peak emission intensity (L) and the average emission intensity (Lxf). The peak intensity gradually decreased with the frequency, whereas the average intensity increased with the frequency. When the frequency increased, the pulse width of the same polarity became short. Hence, the peak intensity decreases by the similar reason as described in Fig.3.18. However, the average intensity increases proportionally to the number of applied pulses.

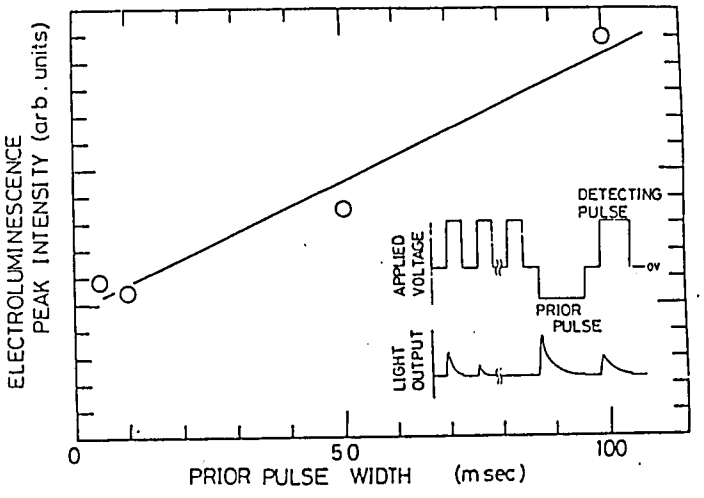

Fig. 3.19. Electroluminescence intensity versus prior pulse width. Inset shows change of light output affected by applied pulse condition.

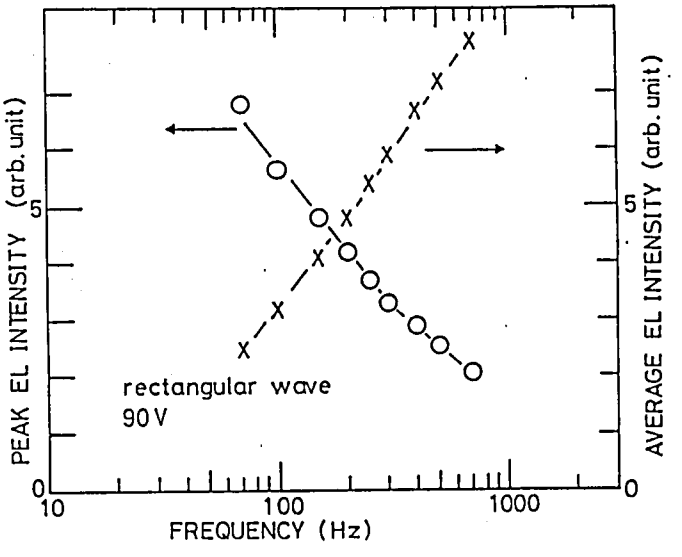

Fig. 3.20. Frequency dependence of the peak electroluminescence intensity and the average intensity.

3-7. Summary

(1) Measurements of ESR on a-$Si_{1-x}C_x$:H were carried out. The spin density increased with the carbon content in the films of T_{sub}=260 °C. The excess hydrogenation of carbon atoms in the films of T_{sub}=RT led to the lower spin density. Over the range of the carbon content above 0.55 where the sample showed intense photoluminescence, the spin density in the films of T_{sub}=RT was less than 5×10^{-2} of that for T_{sub}=260°C.

(2) The optical energy gap increased monotonically with the carbon content. The optical energy gap of the films deposited at room temperature was higher than those of films prepared at higher temperatures. This high energy gap, e.g. as high as 4.12 eV for x=0.97, and its monotonic increase are attributed to the high hydrogen content and the polymer-like structures.

(3) The films showed bright photoluminescence at room temperature, and the hue was bluish white, particularly in the carbon-rich samples (x>0.8). The difference between E_{opt} and the PL peak energy increased with the carbon content; this is thought to be due to the increase in the tail-state width with the carbon content. The PL mechanism in a-$Si_{1-x}C_x$:H is due to pair recombination between localized centers on the basis of the excitation-intensity dependence of PL and its decay characteristics. The lower spin density in the films of T_{sub}=RT than those of T_{sub}=260°C resulted in the intense PL in the films of T_{sub}=RT.

(4) AC-EL was observed in a-$Si_{0.17}C_{0.83}$:H films sandwiched with two insulating Y_2O_3 layers. Conducting electrons across the active layer were estimated to be 1×10^{12} electrons/cm^2 by the analysis of a spike-type current with the application of triangular wave pulses. The polarization effect was elucidated by changing the pulse width of the applied voltage. The frequency dependence of the EL peak intensity can be explained by the polarization effect which is similar to that in conventional

ZnS:Mn EL cells.

References

1) D.A.Anderson and W.E.Spear: Philos. Mag. 35 (1977) 1.

2) H.Munekata and H.Kukimoto: Appl.Phys.Lett. **42** (1983) 432.

3) D.Kruangam, T.Endo, W.Guang-Pu, H.Okamoto and Y.Hamakawa: Jpn.J.Appl.Phys. **24** (1985) L806.

4) C.C.Tsai and H.Fritzsche: Solar Energy Mat. **1** (1979) 29.

5) R.Sussmann and R.Ogden: Philos. Mag. **44** (1981) 137.

6) Y.Catherline, G.Turban and B.Grolleau: Thin Solid Films **76** (1981) 23.

7) A.Morimoto, T.Miura, M.Kumeda and T.Shimizu: J.Appl.Phys. **53** (1982) 7299.

8) S.Nitta, M.Sakaida, I.Murase, M.Kawai and N.Matsunami: Proc. 11th int. conf. amorphous liquid semiconductor, Rome, 1985, J. Non-Cryst.Solids **77/78** (1985) 983.

9) J.E.Wertz and J.R.Bolton: "Electron Spin Resonance" (McGrow-Hill, New York, 1972) Chap.3, p.38.

10) M.Born and E.Wolf: "Principles of Optics" (Pergamon Press, Oxford, 1970) p.61 and p.627.

11) N.F.Mott and E.A.Davis: "Electronic Processes in Non-Crystalline Materials" (Clarendon Press, Oxford, 1979) p.287.

12) B.Dischler, A.Bubenzer and P.Koidl: Solid State Commun. **48** (1983) 105.

13) F.W.Smith: J. Appl. Phys. **55** (1984) 764.

14) L.Holland and S.M.Odja: Thin Solid Films **58** (1979) 107.

15) A.H.Mahan, B. von Roedern, D.L.Williamson and A.Madan: J.Appl.Phys. **57** (1985) 2717.

16) D.Penn: Phys.Rev. **128** (1962) 2093.

17) D.Engemann, R.Fisher and J.Knecht: Appl.Phys.Lett. **32** (1978) 567.

18) H.Munekata, Sh.Murasato and H.Kukimoto: Appl.Phys.Lett. **37** (1980) 536.

19) I.Watanabe, A.Morimoto and T.Shimizu: Jpn.J.Appl.Phys.

21 (1982) L613.

20) R.A.Street, J.C.Knight and D.K.Biegelsen: Phys.Rev.B**18** (1978) 1880.

21) R.A.Street: Adv.Phys. **25** (1976) 397.

22) R.Fisher, in Brodsky(ed.), "Amorphous Semiconductor" (Springer-Verlag, Berlin, 1979) p.157.

23) R.A.Street: Adv.Phys. **30** (1981) 593.

24) S.P.Depinna, B.C.Cavenett and R.S.Sussmann: Philos. Mag. B **47** (1983) L51.

25) R.S.Sussmann and E.H.Lauder: J.Phys. (Paris) Collq. C4, **42** (1981) 1029.

26) D.H.Smith: J.Lum. **23** (1981) 209.

27) T.Inoguchi and S.Mito: "Phosphor Films", in "Electroluminescence" (ed.) J.I.Pankove (Springer-Verlag, Berlin, 1977) p.202-206.

IV FABRICATION OF a-Si:H/a-$Si_{1-x}C_x$:H ULTRA-THIN MULTILAYERS AND STRUCTURAL ANALYSIS

4-1. Introduction

In recent years, there have been interests in multilayers consisting hydrogenated amorphous silicon (a-Si:H) and silicon based ternary alloys, e.g. a-SiN_x:H,[1-3] a-$Si_{1-x}C_x$:H[4-6] and a-$Si_{1-x}Ge_x$:H[7,8] because of their unique optical[1-5] and electrical[1,2,6-8] properties. In multilayers with very thin layers, the optical energy gaps (E_{opt}) of the multilayers increase with decreasing thickness of well layers, which is insisted due to the quantum size effect.[1-5] There is also information in literatures on the electrical properties along the multilayer planes; the Fermi level in a-Si:H well layers rises by charge transfer doping of electrons from barrier layers (a-SiN_x:H) to the well layers (a-Si:H).[1,2] Regarding a-Si:H/a-$Si_{1-x}C_x$:H multilayer systems, a multilayer has already been applied to solar cells in order to improve p-type window layers.[6] We have verified the generation of hot electrons by tunneling conduction through the barrier layer of a-$Si_{0.2}C_{0.8}$:H in a multilayer, experimentally (see Chap. IV). This a-Si:H/a-$Si_{0.2}C_{0.8}$:H multilayer system can be used as a hot electron injector or a wide gap injector.

In order to investigate and obtain multilayers with specific properties, it is important to control structures of the component layers and interfaces. However, very little is known about these microscopic structures in multilayers, e.g. hydrogen incorporation in the component layers and the interfacial structures.

In this chapter, the microscopic structures of the a-Si:H/a-$Si_{1-x}C_x$:H (x=0.2, 0.5 and 0.8) ultra-thin multilayers fabricated by a glow discharge method are discussed. The scheme of hydrogen incorporation in the well layer was determined by the analysis of

infrared absorption measurements for the well-layer thickness over the range from 11 Å to 510 Å. The optical energy gap of the multilayer is also discussed in connection with the scheme of hydrogen incorporation.

4-2. Fabrication

4-2-1. Fabrication Procedure

The multilayers (a-Si:H : well, a-$Si_{1-x}C_x$:H, x=0.2, 0.5 and 0.8: barrier) were prepared by capacitive-coupled glow discharge deposition. The substrate temperature was maintained at 220°C with an rf power of 10W (0.51 W/cm^2) for all depositions. A-Si:H layers for the well layer was deposited from SiH_4 (10 % H_2 diluted). The thickness of the well layer (d_W) in the multilayer was varied from 11 Å to 510 Å by changing the deposition time. For thick a-Si:H (5000 Å), E_{opt} was 1.78 eV. The a-$Si_{1-x}C_x$:H layer for the barrier layer was deposited from a mixture of SiH_4, H_2 and C_2H_4. The thickness of the barrier layer (d_B) was kept at 20 Å in this chapter except for an experiment in 4-2-2. For thick a-$Si_{1-x}C_x$:H (around 5000 Å), the optical energy gaps were 3.18 eV, 2.40 eV and 2.18 eV for x=0.8, 0.5 and 0.2, respectively. In a-$Si_{0.2}C_{0.8}$:H, the average number of hydrogen atoms attached to a carbon atom approaches one, which results in the large optical energy gap of 3.18 eV. Neither a-Si:H nor a-$Si_{1-x}C_x$:H were doped.

To avoid carbon contamination in a-Si:H layers, the discharge was stopped at the end of each layer deposition and the source gases were completely changed. The period of the multilayer was maintained at 20, when the well layer was thinner than 100 Å. Above 100 Å, the period was kept at 7.

4-2-2. Depth Profile by Auger Electron Spectroscopy

The construction of the multilayer was confirmed by a depth profile of Auger electron spectroscopy and X-ray diffraction.

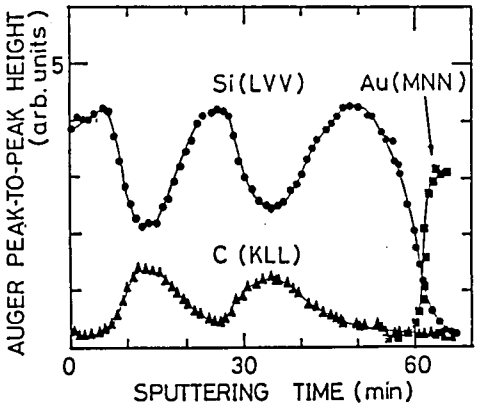

Fig. 4.1. Auger electron depth profile of a-Si:H (3 layers)/a-$Si_{0.2}C_{0.8}$:H (2 layers) on a Au-predeposited glass substrate.

Figure 4.1 gives an example of the depth profile of Auger electron spectroscopy (AES). The multilayer was deposited on a Au-predeposited glass substrate. The multilayer had 3 barrier layers (150 Å) and 4 well layers (300 Å). The signal of carbon atoms alternates with the signal of silicon atoms; this indicates that alternative deposition of two-component layers was achieved.

4-2-3. X-ray Diffraction

Figure 4.2 shows an example of an X-ray diffraction pattern in the case that the thickness of the well layer and the barrier layer were 50 and 20 Å, respectively. The multilayer showed sharp peaks in the X-ray diffraction pattern. The full width at half maximum of the first Bragg peak in the 2θ scan was 0.08°. This result indicates that stratified layers without fluctuation in the thickness of the component layers were fabricated. Figure 4.3 shows the dependence of the sum of the thickness d_W+d_B on the deposition time for the well layer in the a-Si:H/a-$Si_{0.2}C_{0.8}$:H multilayer. The thickness d_W+d_B was calculated from the X-ray diffraction peak. The deposition time for the barrier layer was kept constant. The value of d_W+d_B linearly varied with the deposition time for the well layer, which indicates that the

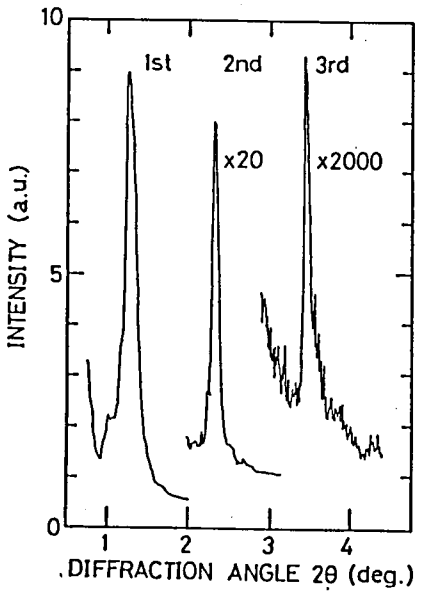

Fig. 4.2. X-ray diffraction pattern with 1st, 2nd and 3rd peaks in the case that the thickness of the well layer and the barrier layer were 50 and 20 Å, respectively. The carbon content of the barrier layer was 0.8.

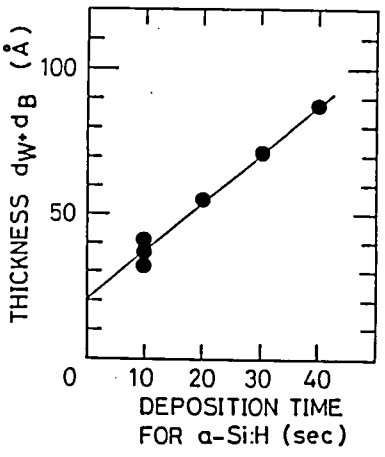

Fig. 4.3. Thickness of d_W+d_B calculated from X-ray diffraction peak as a function of the deposition time for the well layer in the a-Si:H/a-$Si_{0.2}C_{0.8}$ multilayer. Deposition time for the barrier layer was kept constant.

multilayers were fabricated controllably. The intercept with the ordinate indicates the thickness d_B (20.3 Å) and the slope shows the deposition rate of a-Si:H (1.69 Å/s).

4-3. Scheme of Hydrogen Incorporation

4-3-1. Refractive Index

In order to determine the infrared absorption in the well layer quantitatively, we used the effective medium theory[9,10] where a difference in refractive indices between the well layer and the barrier layer is taken into account. Figure 4.4 shows measured refractive indices of the multilayers when the

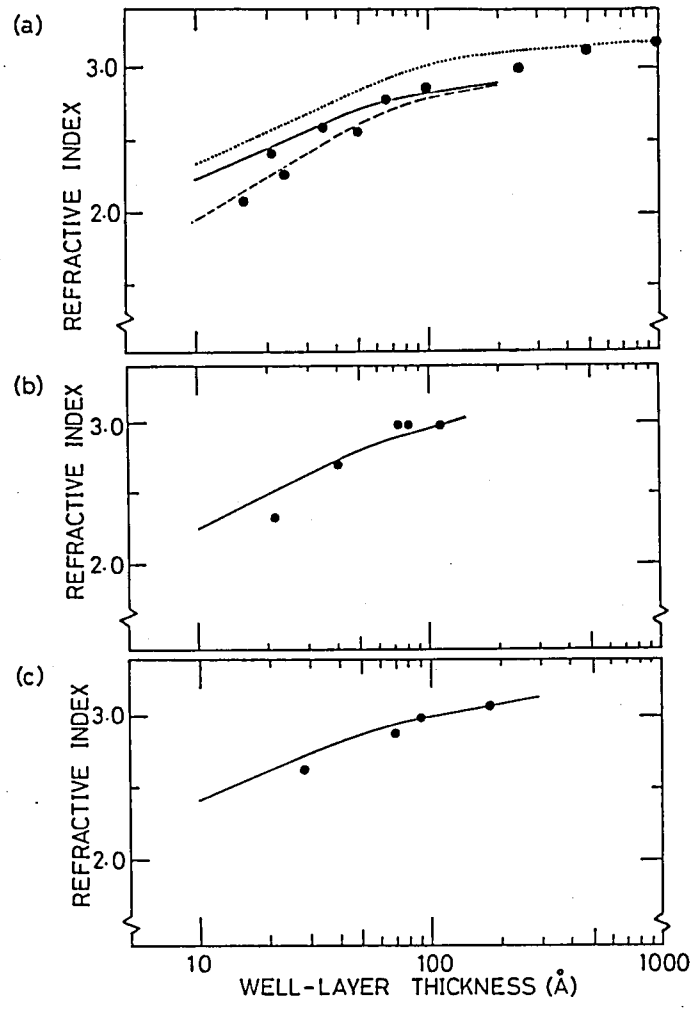

Fig. 4.4. Refractive indices n_M as a function of the well layer thickness. Solid curve, broken curve and dotted curve are predicted by Eq. (4.1) in the text. (a) the a-Si:H/ a-$Si_{0.2}C_{0.8}$:H multilayer, (b) the a-Si:H/a-$Si_{0.5}C_{0.5}$:H multilayer, and (c) the a-Si:H/a-$Si_{0.8}C_{0.2}$:H multilayer.

thickness of the well layer was changed. The refractive indices were obtained from interference fringes in optical transmittance measurements over the range of wavelengths from 7000 Å to 25000 Å (no-absorbing region for the multilayers). The measured value of the refractive index n_M for the multilayer is expressed by the following equation using the effective medium theory:[9,10]

$$n_M^2 = n_B^2 \, d_B/(d_B+d_W) + n_W^2 \, d_W/(d_B+d_W). \qquad (4.1)$$

Above, n_W and n_B are refractive indices of the well layer and the barrier layer, respectively.

In Fig. 4.4(a) for the a-Si:H/a-$Si_{0.2}C_{0.8}$:H multilayer, the value of n_W=3.2, the refractive index of thick a-Si:H, was used for the calculation of the dotted curve. The value of 1.7 for thick a-$Si_{0.2}C_{0.8}$:H was used for n_B in the calculation. The dotted curve disagrees with the measured values when the thickness of the well layer was thinner than 250 Å. Provided that the refractive index of the well layer is 3.0, the calculated curve, denoted by the solid line, agrees with measured values; this indicates that the refractive index in the well layer (n_W=3.0) is smaller than that in a-Si:H (n=3.2).

The broken curve was estimated using the value of n_W=3.0 on the assumption that a defective layer of 13 Å exists with a refractive index of 2.5 at the interface. The defective layer will be discussed in the next section. The broken curve agrees with the measured value over the range of the well-layer thickness below 30 Å, rather than the solid curve.

In Figs. 4.4(b) and (c), the measured values agree with the calculated values using (b) n_W=3.2 and n_B=1.7, and (c) n_W=3.2 and n_B=2.0, respectively.

4-3-2. Infrared Absorption

Hydrogen incorporation in the multilayer was investigated by

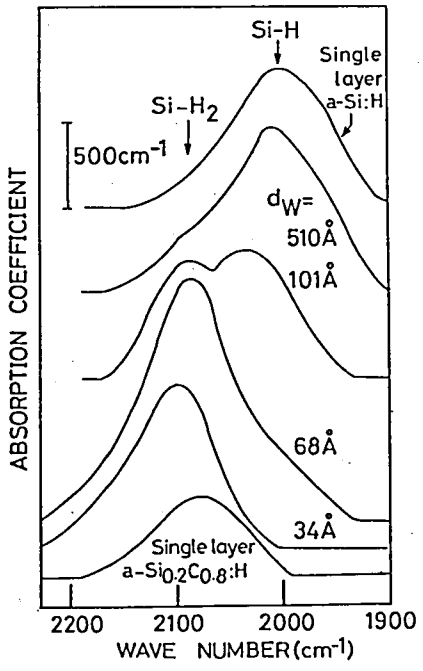

Fig. 4.5. Infrared absorption patterns of $Si-H_n$ (n=1 and 2) as a function of wave number for a-Si:H/a-$Si_{0.2}C_{0.8}$:H multilayers with various well-layer thickness; together with patterns for thick a-Si:H and a-$Si_{0.2}C_{0.8}$:H.

Fourier transform infrared absorption spectroscopy (FTIR). In Fig. 4.5, are shown examples of absorption spectra for $Si-H_n$ stretching modes (n=1 and 2) in a-Si:H/a-$Si_{0.2}C_{0.8}$:H multilayers. In the same figure, the spectra of thick a-$Si_{0.2}C_{0.8}$:H (4900 Å) and a-Si:H (5000 Å) are shown as references. The peak at 2000 cm^{-1} is due to Si-H monohydride bonds in the a-Si:H layer. The peak around 2100 cm^{-1} is a mixture of the Si-H monohydride bonds surrounded by carbon atoms in the a-$Si_{1-x}C_x$:H layer[11] and the $Si-H_2$ dihydride bonds in the a-Si:H layer.

Figure 4.6 shows the relations between the thickness of the well layer and the infrared absorption coefficient of the $Si-H_n$ stretching mode for the multilayers: (a) a-Si:H/a-$Si_{0.2}C_{0.8}$:H, (b) a-Si:H/a-$Si_{0.5}C_{0.5}$:H, (c) a-Si:H/a-$Si_{0.8}C_{0.2}$:H. In order to analyze the results quantitatively, the effective medium theory is used. The measured absorption coefficient α_M is expressed as

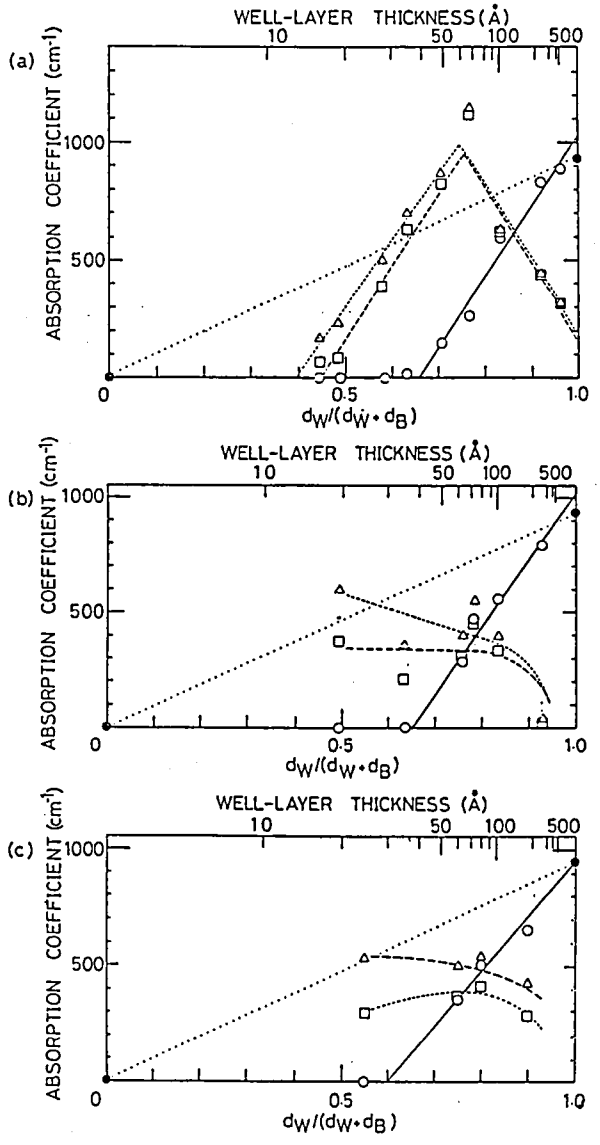

Fig. 4.6. Peak absorption coefficients of the 2000 cm^{-1} mode (open circles) and the 2100 cm^{-1} mode (squares and triangles) as a function of well-layer thickness, together with peak absorption coefficients of the 2000 cm^{-1} mode in a-Si:H and a-$Si_{1-x}C_x$:H (closed circles). Absorption coefficients were corrected by Eq.(4.2) in the text assuming α_B (see text). (a) a-Si:H/a-$Si_{0.2}C_{0.8}$:H, (b) a-Si:H/ a-$Si_{0.5}C_{0.5}$:H and (c) a-Si:H/a-$Si_{0.8}C_{0.2}$:H.

follows:[9,12]

$$\alpha_M=\alpha_W\ (n_W/n_M)\ d_W/(d_W+d_B)+\alpha_B\ (n_B/n_M)\ d_B/(d_W+d_B). \qquad (4.2)$$

Above, α_W and α_B are absorption coefficients for the well layer and the barrier layer, respectively. The peak absorption coefficients of the 2000 cm^{-1} mode for the well layer, denoted by open circles in Figs. 4.6(a)-(c), were calculated using Eq. (4.2). We supposed that the value of α_B is zero in the second term of the equation, because the 2000 cm^{-1} mode was very weak in thick a-$Si_{1-x}C_x$:H (x=0.2, 0.5 and 0.8) (for example, a-$Si_{0.2}C_{0.8}$:H in Fig. 4.5). The values of 3.0, 3.2 and 3.2 were used for n_W in Figs. 4.6 (a), (b) and (c), respectively, on the basis of the results in Fig. 4.5. Closed circles in the figures at $d_W/(d_W+d_B)$=0 and 1 are the absorption coefficients of the 2000 cm^{-1} mode for thick $Si_{1-x}C_x$:H and thick a-Si:H, respectively.

In Fig. 4.6(a) for the a-Si:H/a-$Si_{0.2}C_{0.8}$:H multilayer, if the number of the Si-H monohydride bonds in a unit volume of the well layer is the same as in thick a-Si:H, the measured values of the Si-H monohydride mode should be on the dotted line. The dotted line is calculated with Eq.(4.2), where α_B is zero (the value in thick a-$Si_{0.2}C_{0.8}$:H) and α_W is the value for thick a-Si:H. However, the measured values for the multilayer (open circle) are on the solid line, which is quite different from the dotted curve. This solid line can be extrapolated to $d_W/(d_W+d_B)$=0.66 (d_W=38 Å). This result is explained that hydrogen atoms are scarcely incorporated into the well layer in the form of the Si-H bonds, when the well-layer thickness is thinner than 38 Å. Above 38 Å for the well-layer thickness, the number of the Si-H bonds in a unit volume increases with the thickness of the well layer.

In Fig.4.6(a), are also shown the absorption coefficients of the 2090 cm^{-1} mode for the well layer. The absorption

coefficients were corrected by subtracting the contribution of the monohydride bonds in the barrier layer (a-$Si_{0.2}C_{0.8}$:H), where α_W was estimated with Eq.(4.2) using n_B=1.7. The corrected values denoted by triangles in the figure were deduced on the assumption that the number of the Si-H monohydride bonds in a unit volume of the barrier layer is the same as in thick a-$Si_{0.2}C_{0.8}$:H (i.e., α_B in the barrier layer is the same as in thick a-$Si_{0.2}C_{0.8}$:H). Squares in the figure were deduced on the assumption where the average number of the Si-H bonds in a unit volume of the barrier layer is larger by a factor of 1.6 than in thick a-$Si_{0.2}C_{0.8}$:H. The value of 1.6 is assumed from the result on hydrogenation of carbon atoms in the barrier layer detected by FTIR; the average number of hydrogen atoms attached to a carbon atom is larger by 1.6 than that in thick a-$Si_{0.2}C_{0.8}$:H on the basis of the absorption coefficients at 2900 cm^{-1} ($C-H_n$

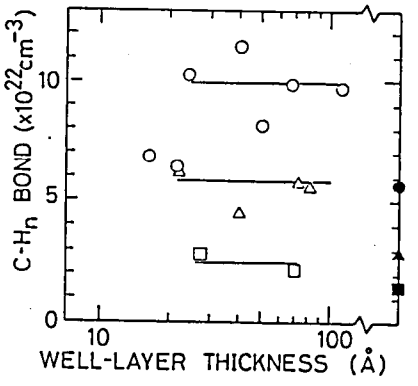

Fig. 4.7. Integrated absorption coefficients of $C-H_n$ (n=1 and 2) stretching mode around 2900 cm^{-1} in the multilayers as a function of the well-layer thickness. The integrated coefficient was calculated using the sum of the barrier-layer thickness in stead of the total thickness of the multilayer. Open circles: a-Si:H/a-$Si_{0.2}C_{0.8}$:H, open triangles: a-Si:H/a-$Si_{0.5}C_{0.5}$:H, open squares: a-Si:H/a-$Si_{0.8}C_{0.2}$:H. Closed symbols are for thick a-$Si_{1-x}C_x$:H.

stretching mode) for the multilayers (Fig. 4.7).

In the range of $d_W/(d_W+d_B)$ from 0.45 (d_W=16 Å) to 0.77 (d_W=65 Å), the squares and triangles linearly increase with $d_W/(d_W+d_B)$. The extrapolated values on the abscissa are $d_W/(d_W+d_B)$= 0.39 (d_B=13 Å) for the triangles and 0.45 (d_W=17 Å) for the squares. Above 0.77 for $d_W/(d_W+d_B)$, the absorption coefficient of the Si-H_2 mode decreases with increasing $d_W/(d_W+d_B)$. The value of the absorption coefficient can be extrapolated to nearly zero at $d_W/(d_W+d_B)$=1, which is consistent with the absorption coefficient of thick a-Si:H. This result indicates that hydrogen atoms are scarcely incorporated into the well layer in the form of the Si-H_2 bonds, when the well layer is thinner than 13-17 Å. In the range of the well-layer thickness from 17 Å to 65 Å, the number of the Si-H_2 bonds in a unit volume of the well layer increases with the well-layer thickness. Above 65 Å for the well-layer thickness, the number of the Si-H_2 bonds decreases with the well-layer thickness.

Figures 4.6(b) and (c) show the absorption coefficients for the multilayers of a-Si:H/a-$Si_{0.5}C_{0.5}$:H and a-Si:H/a-$Si_{0.8}C_{0.2}$:H, respectively. Hydrogen atoms were incorporated as the Si-H_2 dihydride bonds in the very thin well layer. When the well layer becomes thicker than 40 Å, the Si-H monohydride bonds are formed as well in the a-Si:H/a-$Si_{0.2}C_{0.8}$:H multilayers.

4-3-3. Discussion

The following schemes for hydrogen incorporation in the well layer of a-Si:H/a-$Si_{1-x}C_x$:H ($x \geq 0.2$) multilayers are predicted on the basis of the results shown in Figs. 4.6(a)-(c). Hydrogen atoms are incorporated as the Si-H_2 dihydride bonds, when the well-layer thickness is thinner than 40 Å (Fig. 4.8(b)). Above 40 Å for the well-layer thickness, the Si-H monohydride bonds are formed(Fig. 4.8(c)). This explanation is consistent with a two-dimentional nucleation process of a-Si:H observed by in-situ

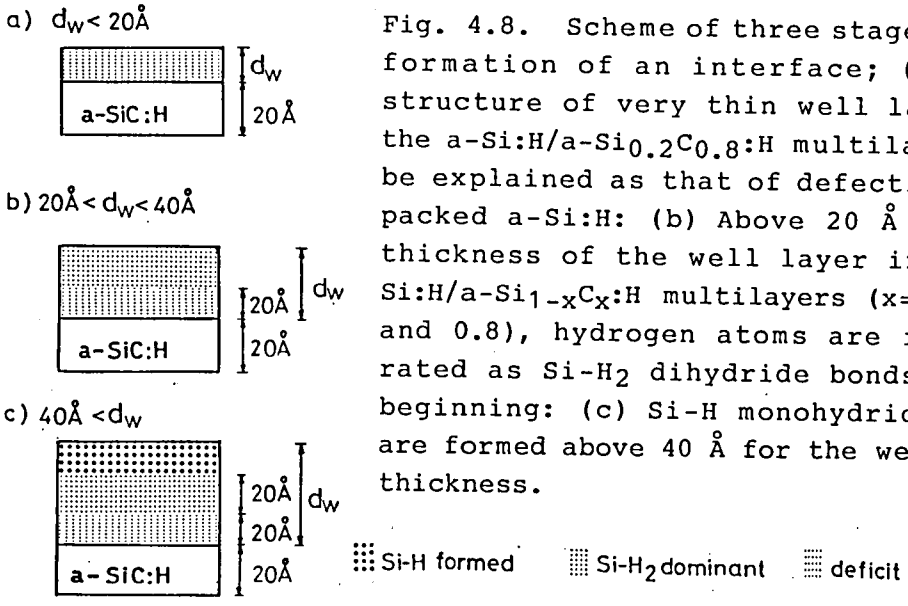

Fig. 4.8. Scheme of three stages in the formation of an interface; (a) the structure of very thin well layers in the a-Si:H/a-$Si_{0.2}C_{0.8}$:H multilayer may be explained as that of defective low-packed a-Si:H: (b) Above 20 Å for the thickness of the well layer in the a-Si:H/a-$Si_{1-x}C_x$:H multilayers (x=0.2, 0.5 and 0.8), hydrogen atoms are incorporated as Si-H_2 dihydride bonds at the beginning: (c) Si-H monohydride bonds are formed above 40 Å for the well-layer thickness.

ellipsometry measurements; islands merge on the scale of 35 Å and the properties of the growing film approach the bulk properties of a-Si:H.[13] When the well-layer thickness is thinner than 100 Å, the absorption coefficients of the 2100 cm^{-1} mode are still larger than that of the 2000 cm^{-1} mode as shown in Figs.4.6(a)-(c). Therefore, the Si-H_2 dihydride bonds are dominant rather than the Si-H monohydride bonds below d_W of 100 Å. When the well layer becomes thicker than 100 Å, the number of the Si-H_2 bonds decreases with the well-layer thickness. The dominance of the Si-H_2 dihydride bonds is consistent with the low refractive index of the well layer as shown in Fig.4.4(a).

It is difficult to evaluate the absorption intensity of the Si-H_2 dihydride mode in the very thin well layer (<20 Å) precisely, because the calculated absorption coefficient α_W is seriously affected by the uncertainty in the assumption of α_B in Eq.(4.2) below d_W=20 Å (=the constant value of d_B). For the multilayer of a-Si:H/a-$Si_{0.2}C_{0.8}$:H, however, the number of the

$Si-H_2$ bonds in a unit volume of the very thin well layer (d_W<20 Å) was less than half of that in the well layers of d_W=30-40 Å. The lack of hydrogen was not observed in the multilayers consisting a-$Si_{0.8}C_{0.2}$:H or a-$Si_{0.5}C_{0.5}$:H. Taking into account that the a-Si:H/a-$Si_{0.2}C_{0.8}$:H multilayer with the thinnest well layer (d_W=11 Å) showed a sharp peak (FWHM=0.18°) in X-ray diffraction, compositional periodicity exists even in thinner well layers. Compared with a-$Si_{0.5}C_{0.5}$:H and a-$Si_{0.8}C_{0.2}$:H, the structure of a-$Si_{0.2}C_{0.8}$:H is a low-packed structure: the lower density (see section 2-6), the higher spin density (see section 3-2) and excess hydrogenation of carbon atoms (see section 2-6). The low-packed structure of a-$Si_{0.2}C_{0.8}$:H may affect the structure of a-Si:H on it. In addition, the average covalent radii of Si and the $Si_{0.2}C_{0.8}$ alloy are 1.173 and 0.85 Å.[14] This large mismatch in the average covalent radii causes the change of structures in the very thin well layers of a-Si:H/$Si_{0.2}C_{0.8}$:H. Therefore, the very thin a-Si:H (d_W<20Å) on the a-$Si_{0.2}C_{0.8}$:H layer may be explained as defective a-Si:H owing to incompletely merged nuclei or to microvoids;[15] this may result in the small number of the $Si-H_n$ bonds in a unit volume of the well layer (Fig. 4.8(a)).

It should be noted that there is a rough-surface layer or a local-disordered layer on a scale of 10 Å in a-Si:H/a-SiN_x:H multilayer systems, deduced from Raman scattering measurements[16], in-situ ellipsometry measurements[15] and in-situ optical reflectance measurements.[10] Superficial examination of transmission microscopy (TEM) cross sections of the a-Si:H/a-SiN_x:H multilayer systems also suggests that component layers exhibit roughness on a scale of 10 Å.[17] Thus, the multilayers with the lower thickness of the component layer (a scale of 10 Å) can be expresses as a disordered system or a defective structure, rather than the stratified system with abrupt interfaces.

4-4. Optical Energy Gap

Figure 4.9(a) indicates the dependence of the optical energy gap (E_{opt}) on the well-layer thickness, together with results of a recent work.[6] The value of E_{opt} was calculated from Tauc plots expressed by Eq.(3.5). The optical energy gap increased with decreasing thickness of the well layer. The value of E_{opt} reached 2.2 eV around 20-30 Å for d_W, where hydrogen atoms are incorporated as the Si-H_2 dihydride bonds. The optical energy

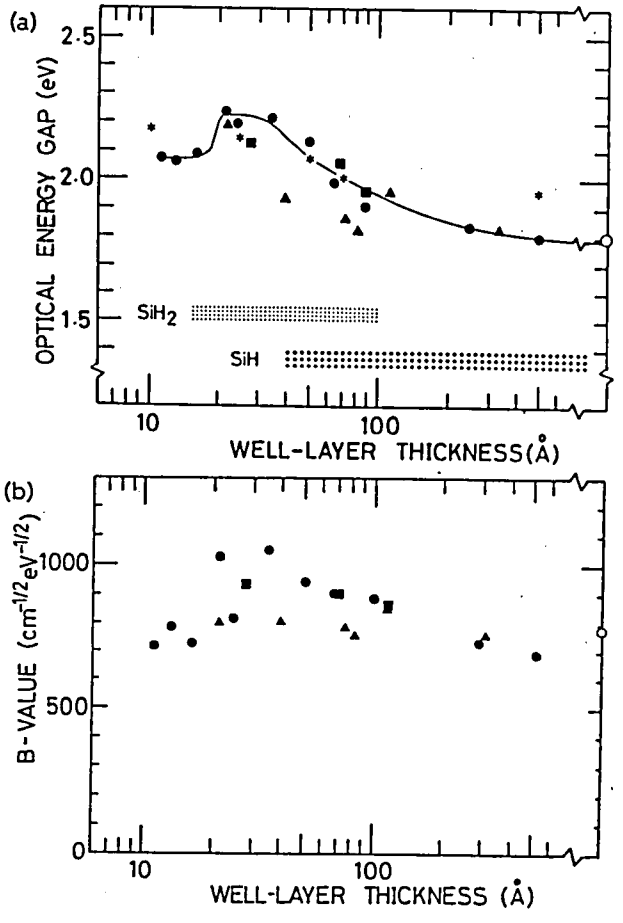

Fig. 4.9. (a) The optical energy gap as a function of the well-layer thickness. Circles: x=0.8, Squares: x=0.5, Triangles: x=0.2. Asterisks are taken from a recent work.[6] (b) The B value as a function of the well-layer thickness.

gaps of the a-Si:H/a-$Si_{1-x}C_x$:H multilayers with the various carbon contents of the barrier layer (x=0.2, 0.5 and 0.8) are almost on the same curve as shown in Fig.4.9(a), while E_{opt} of the barrier layer is changed over the range from 2.17 eV (x=0.2) to 3.17 eV (x=0.8). Taking account into that E_{opt} of the multilayer with the relatively thick well layer (65 Å) was larger by 0.2 eV than thick a-Si:H, the increase in E_{opt} is partly caused by the dominance of the $Si-H_2$ dihydride bonds over the range between 20 and 100 Å, as well as by quantum size effect.[4-6]

Below 20 Å for d_W, E_{opt} slightly dropped to 2.1 eV. The slight decrease in the B values (Fig.4.9 (b)) may lead to the slight decrease in E_{opt}. The B value in Eq.(3.5) is thought to be correlated with the Urbach-tail width. A defective layer mentioned in section 4-3 may cause an increase in the Urbach tail, and results in the decrease in E_{opt} for the multilayers below 20 Å for d_W.

In early claims,[2] an increase in the B value was observed for the multilayers with very thin well layers. We did not observe such an increase in our multilayers evidently (Fig. 4.9(b)).

4-5. Summary

(1) A-Si:H/a-$Si_{1-x}C_x$:H multilayers were fabricated by a glow discharge method. The barrier layer using a-$Si_{1-x}C_x$:H was kept at 20 Å thick. The thickness of the well layer consisting of a-Si:H was changed from 11 Å to 510 Å. The construction of the multilayer was confirmed by X-ray diffraction and a depth profile of Auger electron spectroscopy.

(2) The configuration of $Si-H_n$ (n=1 and 2) in the well layer (a-Si:H) was investigated by infrared absorption spectroscopy. Hydrogen atoms are incorporated as the $Si-H_2$ dihydride bonds when

the well-layer thickness is thinner than 40 Å. Above 40 Å for the well-layer thickness, the Si-H monohydride bonds are formed. Up to 100 Å for the thickness of the well layer, the $Si-H_2$ dihydride bonds are dominant rather than the Si-H monohydride bonds.

(3) The difference in the carbon contents of the barrier layers led to the difference in the structures of very thin well layers (<20 Å). Very thin well layers in the a-Si:H/a-$Si_{0.2}C_{0.8}$:H multilayers may be explained as defective a-Si:H.

(4) The optical energy gap of the multilayers increased with decreasing well-layer thickness. The value of E_{opt} reached 2.2 eV around 20 - 30 Å. The increase of E_{opt} is partly caused by the dominance of the $Si-H_2$ dihydride bonds over the range of the well-layer thickness between 20 and 100 Å, as well as by the quantum size effect.

(5) The slight decrease in E_{opt} was observed in the multilayer with very thin well layers (< 20 Å). This decrease may be caused by broadening of the Urbach tail owing to a defective well layer.

References

1) B.Abels and T.Tiedje : Appl. Phys. Lett. **45** (1984) 179.

2) N.Ibaraki and H.Fritzche : Phys. Rev. B **30** (1984) 5761.

3) M.Hirose an S.Miyazaki: J.Non-Cryst.Solids **66** (1984) 327.

4) H.Munekata and H.Kukimoto : Jpn.J.Appl.Phys. **22** (1983) L544.

5) T.Tiedje, B.Abels, P.D.Person, B.G.Brooks and G.D.Cody: J.Non-Cryst.Solids **66** (1984) 345.

6) S.Tsuda, H.Tarui, T.Matsuyama, T.Takahama, S.Nakayama, Y.Hishikawa, N.Nakamura, T.Fukatsu, M.Ohnishi, S.Nakano and Y.Kuwano, Jpn.J.Appl.Phys. **26** (1987) 28.

7) H.Shirai, A.Tanabe, S.Oda, J.Hanna, T.Nakamura and I.Shimizu: Appl.Phys. **A41** (1986) 259.

8) C.R.Wronski, P.D.Persons and B.Abels: Appl.Phys.Lett. **49** (1986) 569.

9) H.Ugur, R.Johanson and H.Fritzche: "Tetrahedrally-Bonded Amorphous Silicon Semiconductors" ed. D.Adler and H.Fritzche (Plenum, New York, 1985). p.425.

10) L.Yang, B.Abels and P.D.Person: Appl. Phys.Lett. **49** (1986) 631.

11) H.Wieder, M.Cardona and C.R.Duarnieri, Phys.Status Solidi **B92** (1979) 99.

12) B.Abels, L.Yang, P.D.Persons and H.S.Stasiewski and W.Lanford: Appl.Phys.Lett. **48** (1986) 168.

13) R.W.Collins and A.Pawlowski: J.Appl.Phys. **59** (1986) 1160.

14) S.Wagner: Jpn.J.Appl.Phys. **24** (1985) L155.

15) R.W.Collins: J.Appl.Phys. **60** (1986) 1377.

16) N.Maley and J.S.Lannin: Phys.Rev. B **31** (1985) 5577.

17) R.Cheng, S.Wen, J. Feng and H.Fritzche: Appl.Phys.Lett. **46** (1985) 592.

V ELECTRICAL PROPERTIES OF a-Si:H/a-$Si_{1-x}C_x$:H ULTRA-THIN MULTILAYERS

5-1. Introduction

There are several reports on the electrical properties along the multilayer plane, i.e., "charge transfer doping" as mentioned in section 4-1.[1-3] However, very little is known about the electrical properties across the amorphous multilayer plane.[4,5] New effects in the electrical conduction across the multilayer plane, e.g. resonance tunneling[6] and hot electron conduction, are expected as well in crystalline super structures. An amorphous multilayer has already been applied to a solar cell in order to improve a p-type window layer.[7]

In this chapter, we discuss the generation of hot electrons by tunneling conduction through barrier layers in an a-Si:H/a-$Si_{0.2}C_{0.8}$:H ultra-thin multilayer. In this structure, the order-of-magnitude of the tunneling current can be easily controlled by changing the optical energy gap and the thickness of the barrier layer (a-$Si_{1-x}C_x$:H). This fundamental result on hot electron conduction is important for the application of a-Si:H/a-$Si_{1-x}C_x$:H multilayers to a hot-carrier injector or a wide-gap injector.

5-2. Multilayers with n-type Well Layer

5-2-1. Current through Single Heterojunction

Current(I)-voltage(V) characteristics were measured in a single heterojunction of phosphorus-doped a-Si:H (n-type) and a-$Si_{0.2}C_{0.8}$:H as shown in Fig. 5.1. The structure of the heterojunction was a sandwiched-structure as shown in the inset of the figure. The dark conductivity of a-Si:H (n-type) was 7.4×10^{-3} S/cm and the activation energy was 0.26 eV. In the heterojunction, the I-V characteristics showed ohmic conduction as shown in Fig. 5.1. The conductivity was $2\sim4\times10^{-14}$ S/cm. This

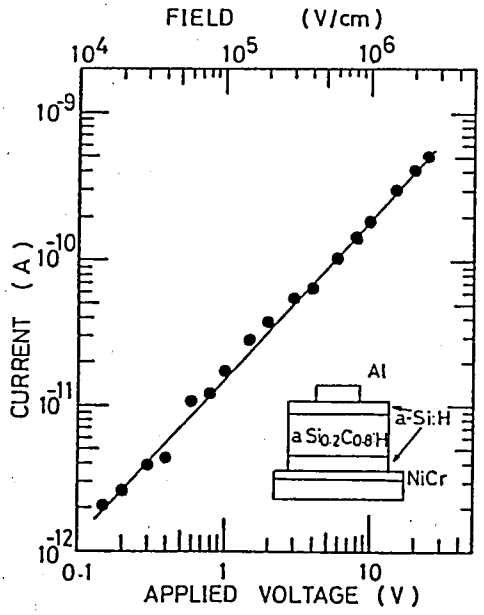

Fig. 5.1. I-V characteristics of a-Si:H(n-type)/a-$Si_{0.2}C_{0.8}$:H single heterojunction. The inset shows the schematic diagram of single heterojunction.

I-V characteristics is thought to be due to the conduction of electrons through a-$Si_{0.2}C_{0.8}$:H, because n-type a-Si:H is thought as a source of carriers. The carrier injection from a-Si:H to the conduction band of a-$Si_{0.2}C_{0.8}$:H does not occur in this single heterojunction, because there is a barrier for electrons in the conduction band as shown in Fig. 5.2.

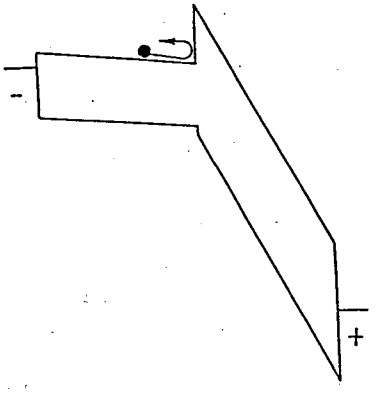

Fig. 5.2. Schematic electronic band diagram of a-Si:H (n-type)/a-$Si_{0.2}C_{0.8}$:H single heterojunction.

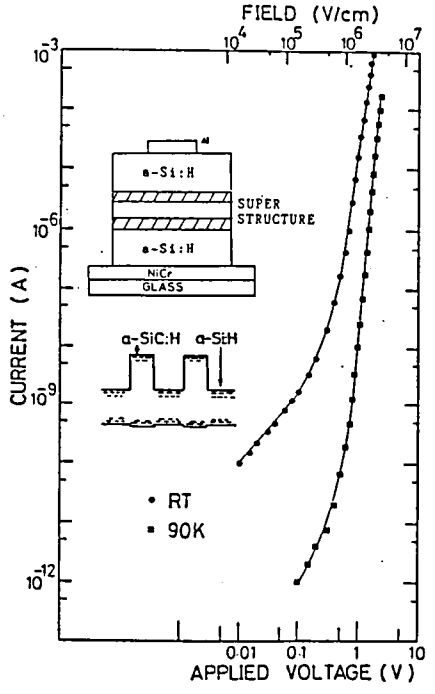

Fig. 5.3. I-V characteristics across multilayer plotted logarithmically. The well layer of the multilayer is n-type. Insets show the structure of the a-Si:H/a-$Si_{0.2}C_{0.8}$:H multilayer and its schematic electronic band diagram.

5-2-2. Current through Multi-heterojunction

Figure 5.3 shows typical I-V characteristics of the a-Si:H/a-$Si_{0.2}C_{0.8}$:H ultra-thin multilayer structure with two barrier layers. The structure shown in the inset of Fig. 5.3 was prepared on a NiCr predeposited Corning 7059 glass substrate. The a-Si:H was n-type (phosphorus-doped) with the dark conductivity of 7.4×10^{-3} S/cm and the activation energy of the conductivity of 0.26 eV. The thickness of the a-Si:H layer was 50 Å. The barrier layer of a-$Si_{0.2}C_{0.8}$:H was 30 Å thick with the conductivity of less than 10^{-13} S/cm. The ultra-thin multilayer was sandwiched between thick n-type a-Si:H layers. The upper electrode of Al was evaporated. The contact between phosphorus doped a-Si:H and the NiCr or Al electrode was verified as ohmic.

The dark conductivity was measured across the multilayer plane at room temperature and 90 K. The I-V curve was measured by

applying dc voltages. The same results described below were obtained by applying the pulse voltage of 150 msec width and 1 Hz repetition to avoid Joule heating. At room temperature, the current flows on Ohm's law with a conductivity of 2.1×10^{-12} S/cm below 0.15 V as shown in Fig. 5.3. This conductivity exceeds the value in thick a-$Si_{0.2}C_{0.8}$:H (see Fig. 5.1) by a factor of 100; this may be caused by an increase of a leak current through defect states.[8,9] Above 0.15 V, the I-V characteristic deviates from Ohm's law, and then the current increases drastically as shown in Fig. 5.3.

Using the difference in conductivities between a-Si:H and a-$Si_{0.2}C_{0.8}$:H as mentioned above, the voltage is mainly applied to the a-$Si_{0.2}C_{0.8}$:H barrier layers. The field in the a-$Si_{0.2}C_{0.8}$:H barrier layer can be estimated to be 1×10^6 V/cm at the applied voltage of 0.6 V where the current increases drastically. The I-V characteristic at 90 K is the same as at room temperature except for the decrease in the amount of current. The decrease in the current is due to a decrease in the conductivity of the a-Si:H layer at 90 K.

Figure 5.4 shows the I-V data plotted as $\log(I/V^2)$ vs. $1/V$. The value of $\log(I/V^2)$ is in proportion to the inverse of the applied voltage above 1.0 V at both room temperature and 90 K. The linear relationship of $\log(I/V^2)$ vs. $1/V$ is satisfied in the two orders-of-magnitude range. It can be concluded that the current above 1.0 V is the tunneling current through a-$Si_{1-x}C_x$:H barrier layers, because the tunneling current is expressed as:[10]

$$J \propto E^2\exp(-4\sqrt{2m^*}(2\phi_B)^{3/2}/3q\hbar E), \qquad (5.1)$$

where J is current density, E applied field, q charge of electron, $\hbar$ Planck constant, m^* effective mass of electron, ϕ_B effective barrier height for tunneling. The value of 1.0×10^6 V/cm above which the current increases drastically is comparable

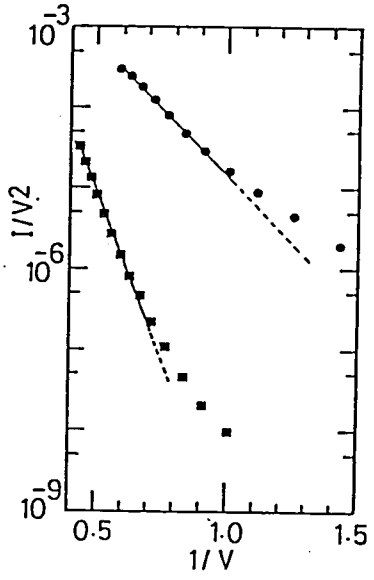

Fig. 5.4. I-V data plotted as $\log(I/V^2)$ vs. 1/V. Circles: RT, squares: 90K.

to the well-known value[11] for the onset of the tunneling current.

The effective barrier height ϕ_B can be estimated as 0.30 eV and 0.52 eV at room temperature and 90 K, respectively, from the slope of the curve in Fig. 5.4. The effective mass of an electron was assumed to equal the free-electron mass. The temperature dependence of the conductivity in a-Si:H indicated that hopping conduction is dominant at low temperature, i.e., 90 K. Thus, the energy level of the path for electrons shifted to the midgap from extended states, which resulted in the higher barrier height for the tunneling conduction.

The carbon content in a-$Si_{1-x}C_x$:H of the barrier layer was varied from 0.80 to 0.60; the energy band discontinuity ΔE in the conduction band might be changed. The effective barrier height ϕ_B decreased with decreasing carbon content as shown in Table 5-1. Thus, ϕ_B can be controlled by varying the optical energy gap of a-$Si_{1-x}C_x$:H. The tunneling current in Table 5-1 was defined as the current at a certain applied voltage above which the current

Table 5-1. Values of effective barrier height for tunneling as a function of the optical energy gap of a-$Si_{1-x}C_x$:H.

Sample	a-$Si_{1-x}C_x$:H C Content	E_{opt}	ΔE	ϕ_B	Tunnel current
#1	0.80	3.1(eV)	1.3(eV)	0.58(eV)	10^{-3}(A/cm^2)
#2	0.67	2.8	1.2	0.42	10^{-3}
#3	0.60	2.6	1.1	0.22	10^{-1}

$\Delta E=E_{opt}/2-E_a$; E_{opt}, optical energy gap of a-$Si_{1-x}C_x$:H, E_a, activation energy of dark conductivity in a-Si:H.

increased drastically. The tunneling current increased with decreasing optical energy gap as shown in Table 5-1.

5-2-3. Hot Electron Generation

The detection of hot electron generation was carried out using a newly devised structure shown in Fig. 5.5. A double-barrier multilayer was fabricated on a thick a-$Si_{0.2}C_{0.8}$:H bulk (1000 Å) with a thin buffer layer. The thickness d of the buffer layer between the multilayer and the bulk in the figure was changed. Current may flow as follows in the case where the a-$Si_{0.2}C_{0.8}$:H bulk side is positively biased to the multilayer side, namely forward bias. (a) If transferred electrons by tunneling through the multilayer do not lose kinetic energy, i.e., electrons become "hot", the electrons can be injected to a-$Si_{0.2}C_{0.8}$:H as shown in Fig. 5.5(a). (b) If transferred electrons by tunneling lose kinetic energy by scattering in the buffer layer, the electrons cannot be injected to the conduction band of a-$Si_{0.2}C_{0.8}$:H as shown in Fig. 5.5(b), because the electron injection does not occur in a a-Si:H/a-$Si_{0.2}C_{0.8}$:H single heterojunction as mentioned above. In the case where the

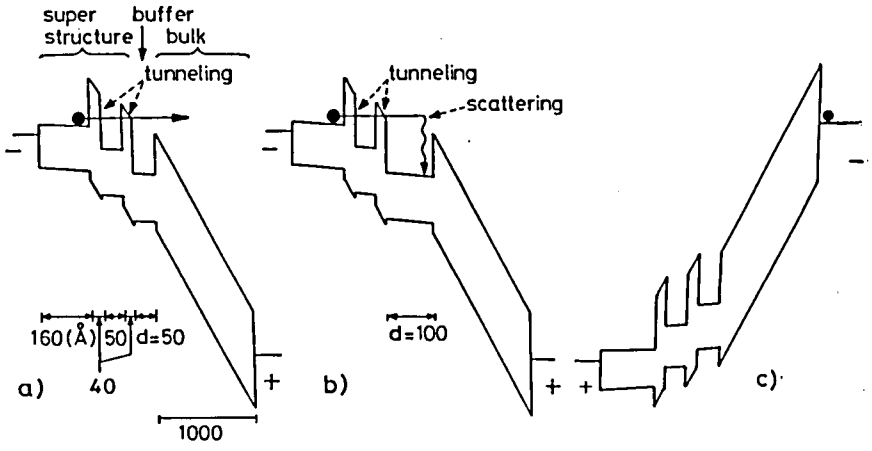

Fig. 5.5. Schematic electronic band diagram of the devised structure;
Forward biased: (a) hot electron injection (d=50 Å),
(b) non-injection (d=100 Å).
Reverse biased: (c).

a-$Si_{0.2}C_{0.8}$:H bulk side is negatively biased to the multilayer side, the I-V characteristics may be the same as in the single heterojunction because of the barrier for electrons as shown in Fig. 5.5(c).

In Fig. 5.6, the I-V curves of the devices with different d are shown with circles and triangles. In the case of d=50 Å, the current increased drastically above an applied voltage of 15 V giving an electric field of 1.4×10^6V/cm for the multilayer. The electric field corresponds to the onset of the tunneling current through the multilayer. Above the applied voltage where the tunneling current starts to flow, hot electron injection occurs as shown in Fig. 5.5(a). A drastic increase in the current was not observed when the multilayer side was positively biased to the a-$Si_{0.2}C_{0.8}$:H bulk side, i.e., reverse bias.

When the thickness d increased above 100 Å, electron injection was not observed as well in the case of the single

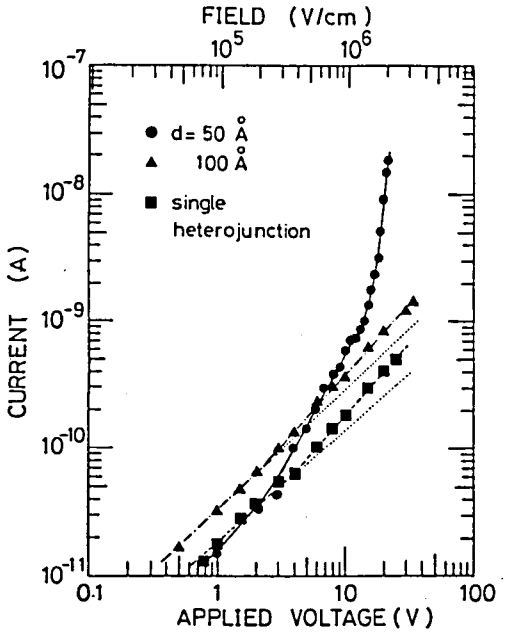

Fig. 5.6. I-V characteristics of devised structures together with I-V characteristics of single heterojunction as shown in Fig. 5.1.

heterojunction. The result implies that transferred electrons by tunneling through the multilayer are scattered in the buffer layer and lose kinetic energy for d=100 Å as shown in Fig. 5.5(b).

As a result, hot electron injection occurs through a thin a-Si:H layer (around 50 Å thick) above the applied voltage where the tunneling current starts to flow through the multilayer.

5-3. Multilayers with p-type Well Layer

5-3-1. Current through Multi-heterojunction

Figure 5.7 shows the I-V characteristics across the a-Si:H/a-$Si_{0.2}C_{0.8}$:H (d_B=40 Å, d_W=50 Å) double barrier multilayer with a p-type well layer. The current increases gradually with applied voltages; this is not due to tunneling conduction. Taking into account the values of E_{opt} in a-$Si_{0.2}C_{0.8}$:H (3.18 eV) and a-

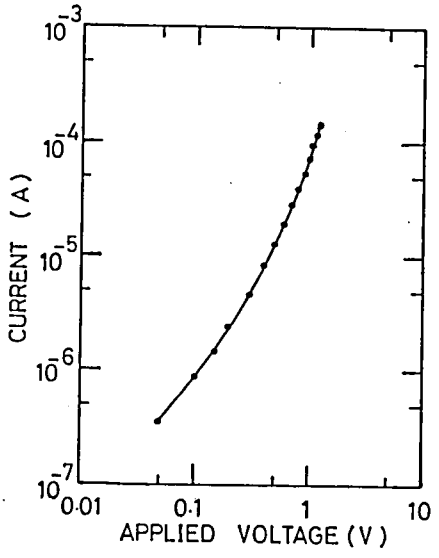

Fig. 5.7. I-V characteristics across multilayer plotted logarithmically. The well layer of the multilayer is p-type.

Si:H (1.73 eV) and the activation energy of a-Si:H (0.433 eV), the band discontinuity in the valence band in the heterojunction should be large enough to block holes. In order to clarify the conduction mechanism in multilayers with the p-type well layer, the electrical properties of a-Si:H(p-type)/a-$Si_{0.2}C_{0.8}$:H single heterojunction were examined.

5-3-2. Current through Single Heterojunction

The I-V characteristic was measured in a single heterojunction of boron-doped a-Si:H (p-type) and a-$Si_{0.2}C_{0.8}$:H as shown in Fig. 5.8. The structure of the heterojunction was a sandwiched structure of Al/a-Si:H(p-type)/a-$Si_{0.2}C_{0.8}$:H/a-Si:H(p-type)/NiCr as shown in the inset of Fig. 5.8. The thickness of a-$Si_{0.2}C_{0.8}$:H was changed over the range from 550 Å to 1650 Å. The dark conductivity (σ_d) of a-Si:H (p-type) was 2.92×10^{-6} S/cm with an activation energy (E_a) of 0.43 eV except for the 550Å-thick sample ($\sigma_d=9.70\times10^{-4}$, $E_a=0.26$ eV). The I-V characteristics showed non-linear conduction above an electric field of 1×10^5

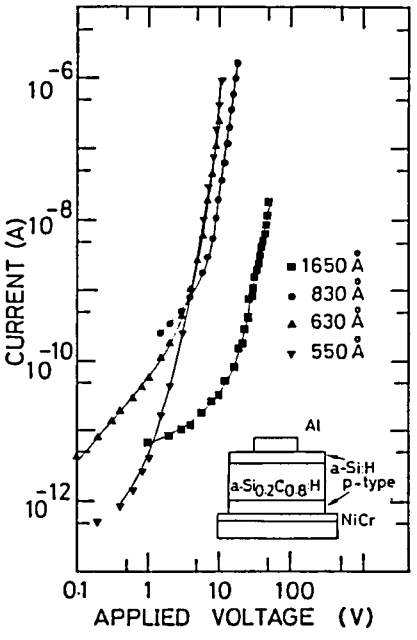

Fig. 5.8. I-V characteristics of a-Si:H(p-type)/a-$Si_{0.2}C_{0.8}$:H single heterojunction. The inset shows the schematic diagram of single heterojunction.

V/cm in all samples as shown in Fig. 5.8 in contrast to the characteristics in the a-Si:H(n-type)/a-$Si_{0.2}C_{0.8}$:H single heterojunction as mentioned in 5-2-1.

5-3-3. Space Charge Limited Current in a-$Si_{1-x}C_x$:H

The space charge limited current (SCLC) follows Eq.(5.2):[12]

$$J/d=f(V/d^2), \qquad (5.2)$$

where J is current density and d thickness of a-$Si_{0.2}C_{0.8}$:H. Figure 5.9 shows the I-V data plotted as J/d-V/d^2. The characteristics are almost on the same curve. Thus, the current flows as SCLC in a-$Si_{0.2}C_{0.8}$:H sandwiched with p-type a-Si:H. This result may be caused by the difference in transport paths of electrons and holes. Holes transfer mainly via tail states, while electrons move via extended states.[13] As shown in Fig.5.10, the

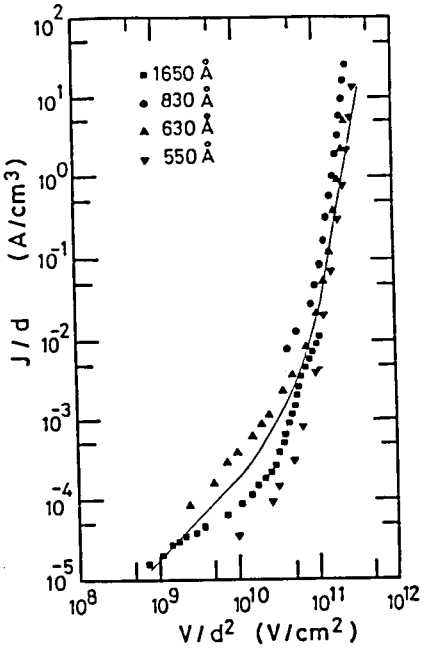

Fig. 5.9. I-V characteristics plotted as J/d-V/d^2. J: current density, d: thickness of a-$Si_{0.2}C_{0.8}$:H. The solid curve is a calculated curve of space charge limited conduction.

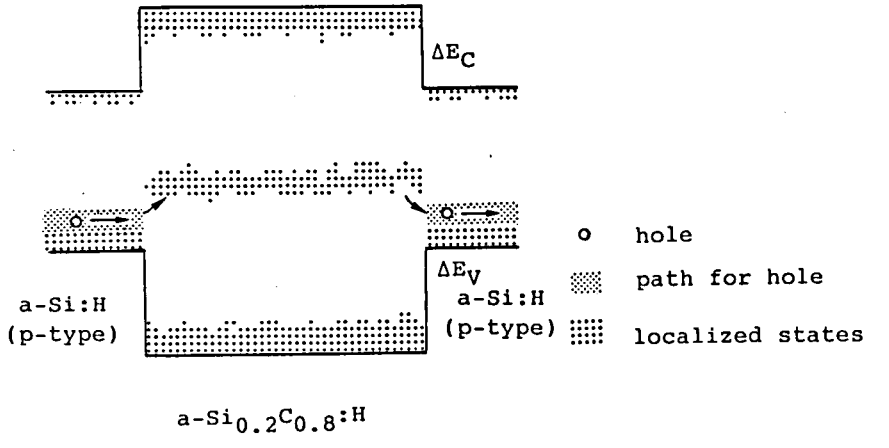

Fig. 5.10. The schematic band diagram of a-Si:H(p-type)/ a-$Si_{0.2}C_{0.8}$:H heterojunction.

energy level of the hole paths in a-Si:H (p-type) may be close to the energy level of gap states related to dangling bonds in a-$Si_{0.2}C_{0.8}$:H. Thus, it can be thought that holes are transferred via the gap states in a-$Si_{0.2}C_{0.8}$:H. As a result, the band discontinuity in the valence band does not work as a barrier for hole transport.

The solid curve in Fig. 5.9 was estimated using the method which is presented by Solomon et.al.[14] Assuming the density of the states is 3.0×10^{19} $eV^{-1}cm^{-3}$, the calculated curve fits to the measured values. In this estimation, the value of 3.35 (measured at 100 Hz) was used for the relative dielectric constant of a-$Si_{0.2}C_{0.8}$:H. The value of 3.0×10^{19} $eV^{-1}cm^{-3}$ is comparable to the defect density measured by electron spin resonance (8×10^{18} cm^{-3}, see section 3-2). For further discussion on the p-type heterojunction, it is thought to be necessary to determine the band discontinuity using photoemission spectroscopy.[15]

5-4. Summary

(1) The I-V characteristics across the amorphous multilayer were measured. The barrier layer of a-$Si_{0.2}C_{0.8}$:H with an optical energy gap of 3.18 eV was typically 30 Å thick. The thickness of the well layer consisting of doped n-type a-Si:H was changed from 50 Å to 100 Å.

(2) The tunneling current across the amorphous multilayer with the n-type well layer was demonstrated at room temperature. The effective barrier height for the tunneling and the value of the tunneling current can be varied by changing the optical energy gap of a-$Si_{1-x}C_x$:H.

(3) The I-V characteristics were measured in the newly devised structure, and the generation of hot electrons was verified in the a-Si:H/a-$Si_{0.2}C_{0.8}$:H multilayer with the n-type well layer. Above the applied voltage where the tunneling current starts to

flow through the multilayer, hot electron injection occurs through the buffer layer of 50 Å thick. This a-Si:H/a-$Si_{0.2}C_{0.8}$:H multilayer with a thin buffer layer can be used as a hot electron injector or a wide gap injector.

(4) In the a-Si:H/a-$Si_{0.2}C_{0.8}$:H multilayer with the p-type well layer, the space charge limited conduction was dominant. This result may be caused by the difference in transport paths of electrons and holes. Holes transfer mainly via tail states, while electrons move via extended states. As a result, the band discontinuity in the valence band does not work as a barrier for hole transport.

References

1) B.Abels and T.Tiedje : Appl. Phys. Lett. **45** (1984) 179.

2) N.Ibaraki and H.Fritzche : Phys. Rev. B **30** (1984) 5761.

3) M.Hirose an S.Miyazaki: J.Non-Cryst.Solids **66** (1984) 327.

4) H.Shirai, A.Tanabe, S.Oda, J.Hanna, T.Nakamura and I.Shimizu: Appl.Phys. A**41** (1986) 259.

5) C.R.Wronski, P.D.Persons and B.Abels: Appl.Phys.Lett. **49** (1986) 569.

6) S.Miyazaki, Y.Ihara and M.Hirose: Ext. Abs. 18th Int. Conf. Solid State Devices and Materials, Tokyo 1986, p.675.

7) S.Tsuda, H.Tarui, T.Matsuyama, T.Takahama, S.Nakayama, Y.Hishikawa, N.Nakamura, T.Fukatsu, M.Ohnishi, S.Nakano and Y.Kuwano, Jpn.J.Appl.Phys. **26** (1987) 28.

8) C.B.Duke: "Tunneling in Solids" (Academic Press, New York, 1969) Chap.6.

9) E.Suzuki, D.K.Shroder and Y.Hayashi: J.Appl.Phys. **60**(1986) 3616.

10) J.G.Simmons : J. Appl. Phys. **34** (1963) 1793.

11) S.M.Sze : "Physics of Semiconductor Devices" (John Wiley & Sons, New York, 1981) 2nd ed., p.402.

12) M.A.Lampert and P.Mark: "Current Injection in Solids" (Academic Press, 1970, New York) Chap.4.

13) B. von Roedern, L.Ley, M.Cardona and F.W.Smith: Philos. Mag. B**40** (1979) 433.

14) I.Solomon, R.Benferhat and H.Tran-Quoc: Phys.Rev. B**30** (1984) 3422.

15) F.Evangelisti, P.Fiorini, C.Giovannella, F.Patella, P.Perfetti, C.Quavesima and M.Capozi: Appl.Phys.Lett. **44** (1984) 764.

VI. CONCLUSION

In this thesis, the deposition mechanism, structures and physical properties of hydrogenated amorphous silicon carbon (a-$Si_{1-x}C_x$:H) films have been investigated over a wide-range of the carbon content of the film on the basis of both many characterizations on the films and plasma diagnosis on glow discharge. The bandgap of a-$Si_{1-x}C_x$:H has been controlled over a wide-range including the visible region. The possibility of atom-sized control over the structure of amorphous semiconductors has been examined using amorphous ultra-thin multilayers. The ultra-thin a-Si:H/a-$Si_{1-x}C_x$:H multilayers have been designed as a wide-gap emitter based on the investigation for a-$Si_{1-x}C_x$:H. The foundation of fabrication of the multilayers has been laid with the aid of their structural analysis. The generation of hot electrons has been demonstrated in the multilayer. This result suggests capabilities of the multilayer as a wide-gap emitter.

In Chapter II, by combining an optical emission spectroscopic analysis of the SiH_4-C_2H_4-H_2 plasma and the deposition rate of the films, the formation mechanism of a-$Si_{1-x}C_x$:H was elucidated. The change in the emission intensities from SiH^* with an rf power can be interpreted in terms of the one-electron-impact excitation process, whereas CH^* and H^* can be interpreted in terms of the two-electron-impact process. Using the carbon content, the density of the film and the configuration of hydrogen incorporation in the film, the deposition rate of the film was separated into two parts contributed by carbon atoms and silicon atoms. The deposition rate of carbon atoms was in proportion to the emission intensity from CH^*; this shows that CH^* is a good indicator of the decomposition of C_2H_4. The decomposition of C_2H_4 was reduced in C_2H_4-rich gas compositions; this is presumably due to either the small dissociation ratio of C_2H_4 in electrical discharge or the

lack of hydrogen. A reduction of the decomposition of C_2H_4 caused a decrease in the deposition rate of carbon atoms and an increase in the average number of hydrogen atoms attached to carbon atoms. The incorporation of carbon atoms as $C-H_3$ in the film was suppressed at higher substrate temperatures. In order to enhance the decomposition of C_2H_4, it was necessary to dilute C_2H_4 with H_2 by a factor of 10, which resulted in the reduction of the excess hydrogenation of carbon atoms in the film. Under a nearly-optimized deposition condition, substitutional doping for n-type was achieved in $a\text{-}Si_{0.6}C_{0.4}$:H. C_2H_2 was chosen for a carbon source. The dark conductivity and the activation energy were 1.1×10^{-6} S/cm and 0.36 eV, respectively, at a dopant gas composition of 2×10^{-2}.

In Chapter III, measurements of ESR on $a\text{-}Si_{1-x}C_x$:H were carried out. The spin density increased with the carbon content in the films of T_{sub}=260 °C. The excess hydrogenation of carbon atoms in the films of T_{sub}=RT led to the lower spin density. Over the range of the carbon content above 0.55 where the sample showed intense photoluminescence, the spin density in the films of T_{sub}=RT was less than 5×10^{-2} of that for T_{sub}=260°C. The optical energy gap increased monotonically with the carbon content. The optical energy gap for the films deposited at room temperature was higher than those for films prepared at higher temperatures. This high energy gap, e.g. as high as 4.12 eV for x =0.97, and its monotonic increase are attributed to the high hydrogen content and polymer-like structures. The films showed bright photoluminescence at room temperature, and the hue was bluish white, particularly in carbon-rich samples ($x>0.8$). The difference between E_{opt} and the PL peak energy increased with the carbon content; this is thought to be due to an increase in the tail-state width with the carbon content. The PL mechanism in $a\text{-}Si_{1-x}C_x$:H was due to pair recombination between localized centers on the basis of the excitation-intensity dependence of PL and its

decay characteristics. The lower spin density in the films for T_{sub}=RT than those of T_{sub}=260°C resulted in the intense PL in the films of T_{sub}=RT. AC-EL was observed in a-$Si_{0.17}C_{0.83}$:H films sandwiched with two insulating Y_2O_3 layers. The number of conducting electrons across the active layer were estimated to be $1x10^{12}$ cm^{-2} by the analysis of a spike-type current in application of triangular wave pulses. The polarization effect was elucidated by changing the pulse width of the applied voltage. The frequency dependence of the EL peak intensity can be explained by the polarization effect which is similar to that in conventional ZnS:Mn EL cells.

In Chapter IV, a-Si:H/a-$Si_{1-x}C_x$:H multilayers were fabricated by a glow discharge method. The barrier layer using a-$Si_{1-x}C_x$:H was kept at 20 Å thick. The thickness of the well layer consisting of a-Si:H was changed from 11 Å to 510 Å. The construction of the multilayer was confirmed by X-ray diffraction and a depth profile of Auger electron spectroscopy. The configuration of Si-H_n (n=1 and 2) in the well layer (a-Si:H) was investigated by infrared absorption spectroscopy. Hydrogen atoms were incorporated as Si-H_2 dihydride bonds when the well-layer thickness was thinner than 40 Å. Above 40 Å, the Si-H monohydride bonds were formed. Up to 100 Å for the well-layer thickness, the Si-H_2 dihydride bonds were dominant rather than the Si-H monohydride bonds. The difference in the carbon contents of the barrier layers led to the difference in the structures of a very thin well layer (<20 Å). The very thin well layers in a-Si:H/a-$Si_{0.2}C_{0.8}$:H multilayers were defective a-Si:H owing to incompletely merged nuclei or microvoids. The optical energy gap of the multilayers increased with decreasing well-layer thickness. The value of E_{opt} reached 2.2 eV around 20-30 Å. The increase of E_{opt} was partly caused by the dominance of the Si-H_2 dihydride bonds over the range of the well-layer thickness between 20 Å and 100 Å, as well as by the quantum size effect. A

slight decrease in E_{opt} was observed in the multilayer with very thin well layers (<20 Å). This decrease may be caused by broadening of the Urbach tail owing to a defective well layer.

In Chapter V, the I-V characteristics across the amorphous multilayer were measured. The barrier layer of a-$Si_{0.2}C_{0.8}$:H with an optical energy gap of 3.18 eV was typically 30 Å thick. The thickness of the well layer consisting of doped n-type a-Si:H was changed from 50 Å to 100 Å. The tunneling current across the amorphous multilayer with the n-type well layer was demonstrated at room temperature. The effective barrier height for tunneling and the value of the tunneling current can be varied by changing the optical energy gap of a-$Si_{1-x}C_x$:H. We measured the I-V characteristics in a newly devised structure and verified the generation of hot electrons in the a-Si:H/a-$Si_{0.2}C_{0.8}$:H multilayer with an n-type well layer. Above the applied voltage where the tunneling current started to flow through the multilayer, hot electron injection occurred through the buffer layer of 50 Å thick. This a-Si:H/a-$Si_{0.2}C_{0.8}$:H multilayer with a thin buffer layer can be used as a hot electron injector or a wide gap injector. In the a-Si:H/a-$Si_{0.2}C_{0.8}$:H multilayer with a p-type well layer, space charge limited conduction was dominant. This result was caused by the difference of transport paths of electrons and holes. Holes transferred mainly via tail states, while electrons moved via extended states. As a result, the band discontinuity in the valence band did not work as a barrier for hole transport.

In future, in order to obtain high-quality carbon-rich a-$Si_{1-x}C_x$:H without excess hydrogenation of carbon atoms, it will be necessary to develop a new deposition process wherein source gases are decomposed separately. Researches about semiconducting amorphous ultra-thin multilayers have just started recently. In this thesis, some unique and fundamental properties of multilayers have been clarified. In order to realize designed

properties of amorphous multilayers reproducibly, it is necessary to analyze atom-size structures of the multilayer more fully.

LIST OF PUBLICATION

I. Full Papers

(1) "Preparation of Hydrogenated Amorphous Si-C Alloy Films and Their Properties"
Junji Saraie, Yoshihisa Fujii, Masahiro Yoshimoto, Katsuhiko Yamazoe, and Hiroyuki Matsunami: Thin Solid Films **117** (1984) 59-69.

(2) Deposition of Amorphous $Si_{1-x}C_x$ Thin Films by Glow Discharge Method"
Kouichi Aizawa, Masahiro Yoshimoto, Takashi Fuyuki, and Hiroyuki Matsunami: Chem. Soc. Japan (1984) p.1661-1669 (in Japanese).

(3) "Effects of Deposition Conditions on Properties of a-$Si_{1-x}C_x$:H Diagnosed Using Optical Emission Spectroscopy"
Masahiro Yoshimoto, Kouichi Aizawa, Takashi Fuyuki, and Hiroyuki Matsunami: Jpn.J.Appl.Phys. **25** (1986) 1465-1469.

(4) "Electron Spin Resonance and Photoluminescence in a-$Si_{1-x}C_x$:H Deposited at Low temperature"
Masahiro Yoshimoto, Takashi Fuyuki, and Hiroyuki Matsunami: Jpn.J.Appl.Phys. **26** (1987) 996-998.

(5) "Hydrogen Incorporation Scheme in Hydrogenated Amorphous Silicon/Silicon Carbon Multilayers"
Masahiro Yoshimoto, Takashi Fuyuki, and Hiroyuki Matsunami: to be published.

II. Letters

(1) "Tunneling Current in a-Si:H/a-$Si_{1-x}C_x$:H Multilayer

Structures"
Masahiro Yoshimoto, Kai-Ying Du, Takashi Fuyuki, and Hiroyuki Matsunami: Jpn.J.Appl.Phys. 25 (1986) L21-L23.

(2) "Hot Electron Conduction in a-Si:H/a-$Si_{0.2}C_{0.8}$:H Super Structure"
Masahiro Yoshimoto, Takashi Fuyuki, and Hiroyuki Matsunami: 25 (1986) L922-L924.

(3) "Impurity Doping in a-$Si_{0.6}C_{0.4}$:H Using C_2H_2 for Carbon Source"
Masahiro Yoshimoto, Takashi Fuyuki, and Hiroyuki Matsunami: to be published.

(4) "Electron and Hole Transport Properties in a-Si:H/ a-$Si_{1-x}C_x$:H multilayers"
Masahiro Yoshimoto, Takashi Fuyuki, and Hiroyuki Matsunami: to be published.

III. International Conferences

(1) "Polarized Effects in AC Electroluminescence of a-$Si_{1-x}C_x$:H"
Hiroyuki Matsunami, Masahiro Yoshimoto, Yoshihisa Fujii, and Junji Saraie: Proc. 10th Int. Conf. Amorphous & Liquid Semiconductors, Tokyo, 1983 (North-Holland, Amsterdam, 1983) p569-572.

(2) "Formation Mechanism of Amorphous $Si_{1-x}C_x$:H Films in Glow Discharge Plasma"
Hiroyuki Matsunami, Masahiro Yoshimoto, and Takashi Fuyuki: Proc. 7th Int. Symposium on Plasma Chemistry, Eindhoven, 1985 (IUPAC, 1985) p154-158.

(3) "Hot Electron Generation Using Amorphous Super Structure of a-Si:H/a-$Si_{1-x}C_x$:H"
Masahiro Yoshimoto, Takashi Fuyuki, and Hiroyuki Matsunami: Ext. Abs.18th Int. Conf. Solid State Devices & Materials, Tokyo, 1986 (Bus.Center Acad.Soc.Japan, Tokyo, 1986) p679-682.

(4) "Enhanced Decomposition of Hydrocarbon for a-$Si_{1-x}C_x$:H Deposition in Plasma CVD"
Masahiro Yoshimoto, Takashi Fuyuki, and Hiroyuki Matsunami: Proc. 8th Int. Symposium on Plasma Chemistry, Tokyo, 1987 (IUPAC, 1987) p1455-1460.

(5) "Fabrication of a-Si:H/a-$Si_{0.2}C_{0.8}$:H Multilayers by Glow Discharge and Structure Analysis"
Masahiro Yoshimoto, Takashi Fuyuki, and Hiroyuki Matsunami: Proc. 8th Int. Symposium on Plasma Chemistry, Tokyo, 1987 (IUPAC, 1987) p1508-1513.

(6) "Fabrication of a-Si:H/a-SiC:H Multi-layers by Glow Discharge Method and Carrier Transport Properties"
Hiroyuki Matsunami, Masahiro Yoshimoto, and Takashi Fuyuki: Proc. 1st Int. Conf. Amorphous and Crystalline Silicon Carbide and Related Materials, Washington, D.C. 1987 (Springer-Verlag, Berlin) in press.